

Телекомуникације

Telecommunications

Power Consumption of 100GE Packet Processor Depending on a Lookup Table Size

Teodora Komazec, Aleksandra Smiljanić, Milan Bjelica, and Mihailo Vesović

Abstract—Power consumption has become a critical performance measure in the design of modern routers. In this paper, we examine power consumption of packet processor implemented on advanced Xilinx UltraScale+ chip, depending on a size of lookup table. We used SDNet to implement IPv4 lookup tables and Vivado power analysis feature to analyze the power consumption of the high-speed router ports.

Index Terms—Field Programmable Gate Arrays, Power Consumption, Lookup Tables, Routers.

I. INTRODUCTION

Internet is made of a vast number of host devices that are connected by routers. The complexity of Internet traffic puts high demands on the design of modern routers. Each Internet router maintains a routing table which is used to determine next-hop IP address for the received packet. Received IP packet contains information about final destination IP address of the packet.

Routing tables store only a portion of the destination IP address, better known as prefix. Prefix contains certain number of most significant bits of IP address. The rest of the bits are considered to be irrelevant for the lookup. The destination IP address of a packet can match more than one routing table entry, and the result of the lookup algorithm is the most specific of the matching entries. The lookup algorithms for IP routing are, for this reason, said to find the longest prefix match (LPM).

There are many reasons why implementation of different lookup algorithms is a very challenging task. Destination IP address of each incoming packet has to be compared to all entries in the routing table, while size of the routing tables can be very large. With the transition from IPv4 to IPv6 addresses, lookup algorithms take only more resources and time. Optimization of existing lookup algorithms is proposed in [1-4].

We examined power consumption [5] of packet processor

Teodora Komazec is with the School of Electrical Engineering, University of Belgrade, 73 Bulevar kralja Aleksandra, 11020 Belgrade, Serbia (e-mail: tea.k94@gmail.com).

Aleksandra Smiljanić is with the School of Electrical Engineering, University of Belgrade, 73 Bulevar kralja Aleksandra, 11020 Belgrade, Serbia (e-mail: aleksandra@efn.rs).

Milan Bjelica is with the School of Electrical Engineering, University of Belgrade, 73 Bulevar kralja Aleksandra, 11020 Belgrade, Serbia (e-mail: milan@efn.rs).

Mihailo Vesović is with the School of Electrical Engineering, University of Belgrade, 73 Bulevar kralja Aleksandra, 11020 Belgrade, Serbia (e-mail: mikives@gmail.com).

implemented on FPGA chip. FPGA chips are proven to be an appropriate solution for data plane programming. The key advantages of FPGA chips are that they are reprogrammable and reusable. This makes them adjustable to the specific needs of the customers, and adaptable over time.

Our main focus was to distinguish power consumption of lookup tables within packet processor, for a range of parameters. Xilinx developed SDNet data plane builder [6] to enable flexible packet processing while achieving high speed. SDNet can be used to implement different lookup algorithms.

Xilinx Vivado Design Suite enables implementation of designs using the UltraScale+ architecture. Xilinx UltraScale+ architecture brings many innovations to the FPGA design, such as next generation routing and enhanced logic blocks to optimize utilization of resources. In this paper, we used UltraScale+ architecture and Vivado power analysis feature to obtain power estimation results for implemented design. This feature is described in detail in [7].

The paper is structured as follows. Section II provides an overview of the Xilinx SDNet data plane builder. In this section we described basic SDNet components and their functionalities. Section III highlights the problems caused by the increased power consumption. In section IV, we analyzed the power consumption of packet processors, and their lookup modules. At the end, main conclusions are given.

II. SDNET

SDNet is a tool developed by Xilinx for the purpose of generating systems with a variety of different packet processing functions. SDNet takes modular approach of designing systems. SDNet design begins with writing SDNet functional specification. The SDNet functional specification is, then, compiled to obtain a highly efficient hardware implementation. The resulting hardware implementation can achieve processing speed in the range of 10-100 Gb/s.

SDNet employs six types of components, called engines, to create systems with desired functionalities. These engines are: parsing engine, editing engine, tuple engine, lookup engine, user engine and system engine. Engines are triggered when all of their inputs arrive. Inputs that are supported by SDNet engines are packets and tuples. Tuples represent additional information about the packets that is carried by packet headers. Ports corresponding to these inputs need to be defined.

The main task of parsing engines is to read and decode packet headers. They acquire important information from the packet headers without modifying them. Editor engines are

used to modify packet data. They can add or remove packet headers. Main task of SDNet tuple engines is to process tuple data.

Lookup engines perform lookup based on the given key. SDNet supports different types of lookup algorithm: EM (Exact Match), LPM (Longest Prefix Match), TCAM (Ternary Content Addressable Memory) and direct address lookup.

User engines enable custom IP cores to be included in the SDNet design. System engines are used to interconnect other engines.

In the SDNet functional specification, lookup tables are defined using the following parameters: type of lookup algorithm, number of entries in lookup table, key width, width of returned value, tuple format of the response, and indication whether the lookup logic is external. Each of the lookup methods has limitations in terms of the number of entries, number of bits that the key contains, and width of the returned value. In this paper, we explored LPM and direct lookup.

LPM is the algorithm which performs lookup by comparing the most significant bits of the given key to a table of prefixes. The result of LPM lookup is the longest matching prefix from the table. As the result, we get response which contains associated prefix and indication if matching indeed occurred.

Direct address match utilizes the key as the direct address to access the stored value at that location. This algorithm is the easiest to implement. However, downside of direct address match lookup is that it does not scale well for larger tables.

III. TESTING ENVIRONMENT

Power consumption has become one of the main constraints on the design of modern chips. Researchers and designers put extreme efforts to overcome problems caused by power dissipation. Shrinking the chips reduced the required power supply, which in turn reduced dynamic power. However, smaller geometries increased static power of the chips.

Device static power is the power that originates from transistor leakage. In ideal case, transistors are not drawing any current when they are in the off state. However, this is not a reality. There is a small amount of current that transistors draw even in the off state. Chips consists of millions or even billions transistors; so, the accumulated consumption can become significant. Device static power is a function of process, voltage and temperature [5]. It can be estimated by programing a blank bitstream into the device.

Dynamic power is the power that occurs as design runs. It varies with each clock cycle. Dynamic power is directly proportional to the square of the supply voltage.

Total on-chip power is calculated as a sum of device static and dynamic power. It represents the power that is consumed internally within the chip.

Characteristics of semiconductor materials are highly dependent on temperature. Ambient temperature is the air temperature of the device. Junction temperature is defined as the temperature range in which Xilinx guarantees that the device will operate according to the specification [7].

Main component of our design is the packet processor that was presented in [8]. Fig. 1 shows block diagram of the implemented component. It contains parsing, editing, lookup and tuple engines. Parsing engine extracts IP destination address from packet header, and forwards this IP address to the first lookup engine. The first lookup engine then performs LPM in the IPv4 lookup table, and provides output port number as a response. This is the port through which packet should be forwarded. The second lookup table uses direct address match to determine new source and destination MAC addresses, which will be forwarded to editing engine. At the end, editing engine performs adequate packet modifications.

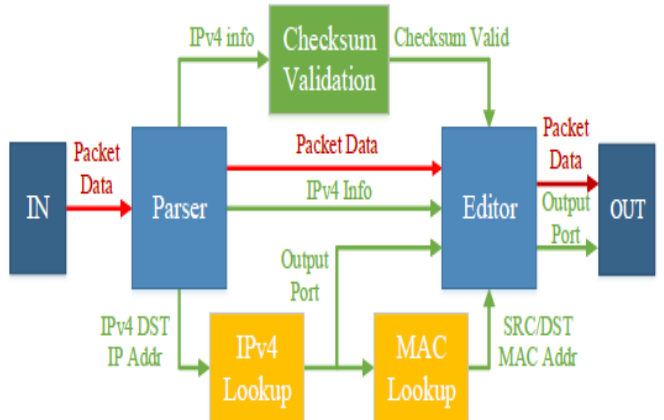


Fig. 1 SDNet packet processor – forwarding engine diagram [8]

IV. RESULTS

We used Vivado power analysis feature to generate power reports for the design of packet processor. This feature can be used to obtain power reports through all stages of the flow: post-synthesis and post-implementation. For the purpose of this paper, we performed power analysis in both post-synthesis and post-implementation stage. The results are more accurate in post-implementation stage because unused signals and blocks are not considered in that stage.

Implemented design has two packet processors. Each of the packet processors is independent and contains two lookup tables as illustrated in Fig. 1. One of the lookup tables is used for IP forwarding and it utilizes the LPM algorithm, while the other is used to change the MAC addresses. The MAC table employs direct address match algorithm. MAC table, also known as FIB (Forwarding Information Base) determines output interface to which input interface should forward a packet.

First, we observed changes in power consumption while changing the depth of the LPM lookup table. We used lookup tables with 7, 8192, 32767 and 65535 entries. In this way, we wanted to cover both minimal and maximal possible numbers of entries when calculating the power consumption of the LPM lookup table. The maximal number of lookup entries supported by SDNet is appropriate for network edge routers. Since, core routers are larger than edge routers, as they

perform centralized routing for subnetworks, they require larger lookup tables.

Fig. 2. illustrates total on-chip power consumption.

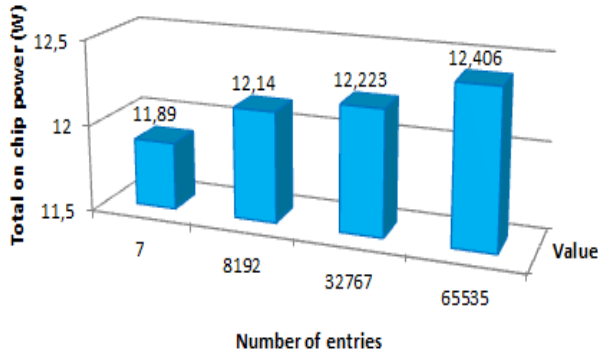


Fig. 2. Total on-chip power for longest prefix match lookup

The effect that the increase in the number of entries has on the increase of dynamic power consumption is shown in Fig. 3. Fig. 3. shows four columns. Each column has two components stacked. The bottom component represents dynamic power consumption while the top component illustrates static power consumption. We can see that the static power consumption did not change significantly. This is mainly because static power consumption primarily depends on the manufacturing process which is the same for all observed cases [9]. However, when comparing lookup table with minimal and maximal number of entries, there is an increase in dynamic power consumption for 5.5 %.

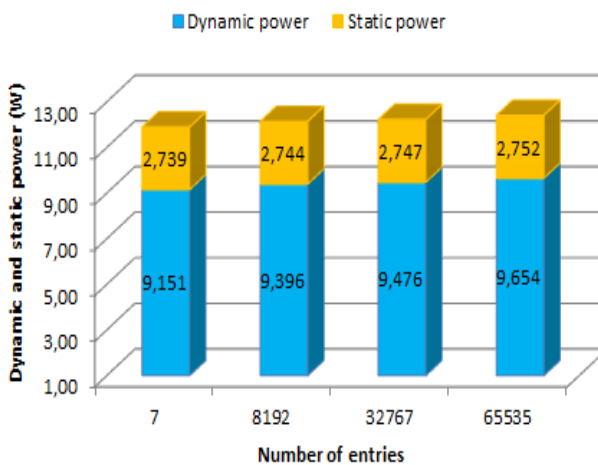


Fig. 3. Dynamic and static power for LPM lookup with respect to the number of entries

Generated power reports have a section about utilization of on-chip components. This section provides information about number of available and used components, as well as the information about power consumed by those components.

One of the on-chip components that shows significant

increase in percentage of utilized available units is Block RAM. Block RAM (Random Access Memory) components are used to store large amounts of data on FPGA chips. The FPGA has a limited number of Block RAM components, depending on its application. Fig. 4. shows how the Block RAM utilization increases with the increase of the number of entries in lookup table. Consequently, the power consumed by Block RAM components is getting higher, which is shown in Fig. 5. We can observe that there is an increase of 46.48 % in the power consumed by Block RAM components when number of entries in lookup table is maximal.

The amount of power that is consumed by Block RAM components is directly proportional to the amount of time during which they are enabled [7]. One of the ways to utilize resources more efficiently is to drive Block RAM enable low during clock cycles when Block RAM components are not used in the design.

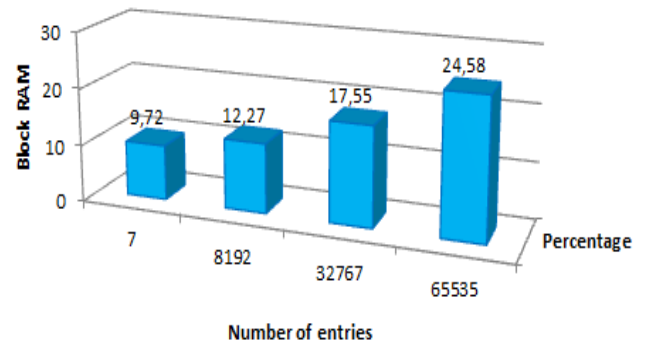


Fig. 4. The Block RAM utilization for LPM lookup with respect to the number of entries

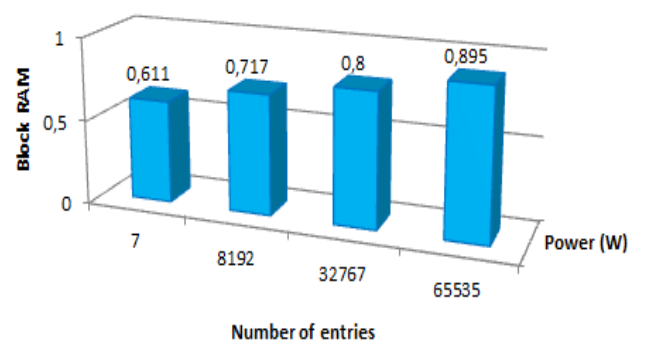


Fig. 5. Power consumed by block RAM units for LPM lookup with respect to the number of entries in lookup tables

Vivado power analysis feature gives an overview of hierarchical power consumption of a system. Fig. 6. shows increase in power consumption per packet processor with the

number of entries. It was shown that as the number of entries in lookup table increases, power consumed by both packet processors varies. The power consumed per packet processor when the number of entries of lookup table is maximal is almost 1,5 times higher than when the number of entries is minimal.

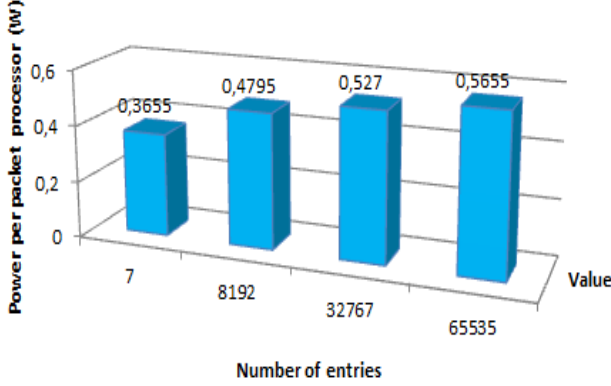


Fig. 6. Power per packet processor with respect to the number of entries in lookup tables

Once we have determined the output port through which packet should be forwarded, new source and destination MAC address have to be added to the header of the packet.

Direct address match algorithm is used for MAC lookup. MAC lookup tables usually have smaller depth. We used the following number of entries for lookup table: 128, 2048 and 4096. Fig. 7. shows increase in the total on-chip power with the number of entries in the lookup table. As in the case of LPM lookup, device static power did not change significantly with increase of the number of lookup table entries.

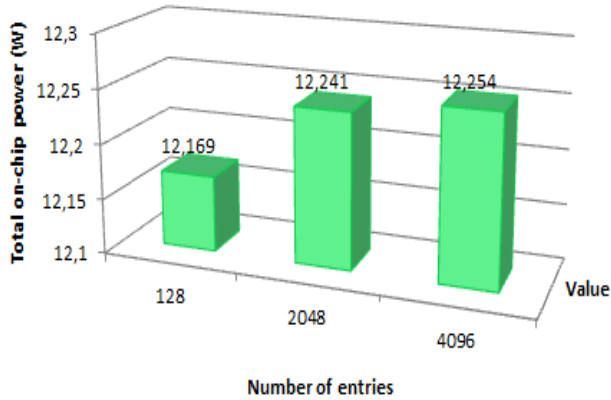


Fig. 7. Total on chip power for direct address match with respect to the number of entries

Increase in dynamic power with the change of the number of entries for direct address match lookup table is illustrated in Fig. 8. There is an increase of 0,9 % when

number of entries is 4096.

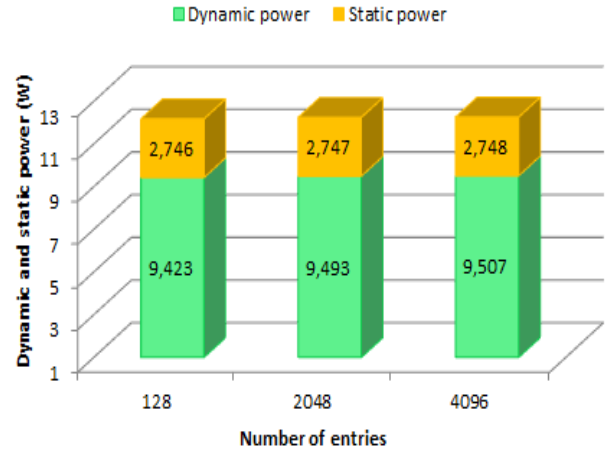


Fig. 8. Dynamic and static power for direct address match with respect to the number of entries

The percentage of available block RAM units that are utilized also records increase. This is shown in Fig. 9.

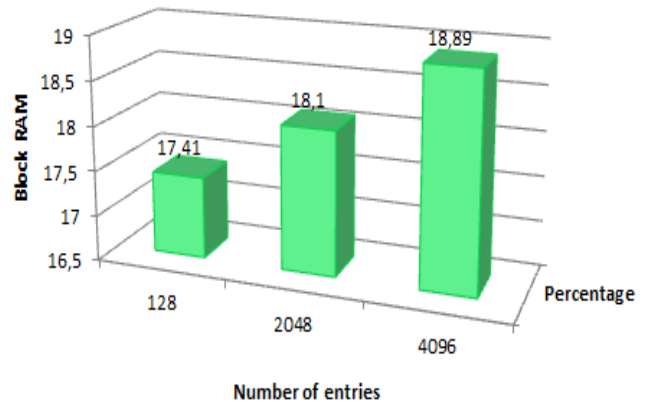


Fig. 9. Percentage of utilized block RAM units for direct address match with respect to the number of entries

V. CONCLUSION

In this paper, we examined power consumption of LPM lookup tables and direct address match lookup tables. With the increase of the number of lookup table entries, there is also an increase of the total on chip power, dynamic power of a chip, percentage of utilized RAM blocks and number of used signals.

Changes in dynamic power consumption go to 5.5 % for LPM and 0.9 % for direct address match. The estimated static power consumption stays the same because it mostly depends on a manufacturing process. Increase in the number of used signals with the number of entries in lookup tables was expected and confirmed.

REFERENCES

- [1] Levy, Gil; Kfir, Aviv, "Longest prefix match using a binary search tree with compressed hash tables," U.S. Patent Application No 16/039, 372, 2020.
- [2] Ruiz-Sanchez, Miguel A.; Biersack, Ernst W.; Dabbous, Walid, "Survey and Taxonomy of IP Address Lookup Algorithms," IEEE Network, vol. 15, no. 3, pp. 8-23, 2001.
- [3] Brown, David A, "Method and apparatus for storing sparse and dense subtrees in a longest prefix match lookup table," U.S. Patent No 6,539,369, 2003.
- [4] Huynh, Jeffrey, et al. "Chained lookups and counting in a network switch", U.S. Patent Application No 16/054, 797, 2020.
- [5] Kim, Nam Sung, et al. "Leakage current: Moore's Law meets static power computer," vol. 36, no. 12, pp. 68-75, 2003.
- [6] "SDNet Packet Processor User Guide", *Xilinx.com*, 2018. [Online]. Available: https://www.xilinx.com/support/documentation/sw_manuals/xilinx2018_2/ug1012-sdnet-packet-processor.pdf. [Accessed: 08-March-2020].
- [7] "Vivado Design Suite User Guide Power Analysis and Optimization", Xilinx.com, 2018. [Online]. Available: https://www.xilinx.com/support/documentation/sw_manuals/xilinx2019_1/ug907-vivado-power-analysis-optimization.pdf. [Accessed: 08-March-2020].
- [8] Vesović, Mihailo, Smiljanic Aleksandra, Radošević Andreja, "Evaluation of SDNet Packet Processors on Xilinx Chips", Proceedings of 5th International Conference on Electrical, Electronics and Computing Engineering, Palić, Serbia, 2018.
- [9] <https://www.sciencedirect.com/topics/computer-science/static-power> [Accessed: 08-March-2020].

Performances of RCIED Activation Signal Multisweep Jamming

Aleksandar Lebl, Vladimir Kosjer, Jovan Radivojević and Mladen Mileusnić

Abstract— In this paper we present the characteristics of RCIED activation message signal multisweep jamming. Mathematical analysis is developed for MPSK modulated signals jamming. The first contribution of the paper is that analytical expressions for *BER* calculation are developed for the whole set of amplitude ratios of RCIED activation signal to the jamming signal. The characteristics of multisweep jamming are compared to the characteristics of pure sweep jamming. The second important paper contribution is the proof that multisweep jamming implementation increases jamming reliability while in the same time decreases necessary jamming power comparing to pure sweep jamming.

Index Terms— RCIED - remote controlled improvised explosive devices; MPSK modulated signal; pure sweep jamming; multisweep jamming; jamming signal power.

I. INTRODUCTION

Security threats related to different explosive devices activating prevention constantly grow in importance. Among these threats remote controlled improvised explosive devices (RCIEDs) have the special place. Such threats are not important only in war regions, but also in the peacetime [1], [2]. The wide scope of literature related to RCIED activation prevention is presented in References [3]-[13]. The dominant technique for prevention of remote activation of improvised explosive devices is sweep jamming and it is applied to practically all available jammer solutions, like in [14]-[18]. Sweep jamming is also used in IRITEL jammer solutions [19]-[20]. Sweep jamming is popular because of its reduced emission power comparing to its alternative – barrage (or noise) jamming [21]. The problem may arise when sweep jamming is applied to the case of short RCIED activation message duration. In such a case sweep jamming rate may not be sufficient to assure coincidence of sweep signal and activation message frequencies at least once during a short time interval [22], [23]. Combined jamming (sweep and barrage in the same time) is one way to mitigate this problem, but the most important benefit of combined over pure sweep jamming is to increase jamming possibility for several dBs when RCIED activation message signal level is comparable to jamming signal level [24]. One possible method to overcome

the problem of unsufficiently high sweep rate is the use of multisweep jamming [25]. Multisweep jamming implies to cover a number of narrower frequency bands in one sweep cycle at a time in comparison to pure sweep jamming where only one wider frequency band is covered in one moment. In the Section II we present the elements for a method to calculate Bit Error Rate (*BER*) when sweep jamming is applied. The mean number of incorrectly transmitted bits in a symbol is determined as described in the Section III. Section IV presents modifications in the method for *BER* calculation when multisweep jamming is implemented instead of pure sweep jamming. The *BER* graphs for different phase modulated (PSK) signals are presented in the Section V. Implementation of multisweep jamming leads to jamming signal power save and this is illustrated by two examples also in the Section V. At the end, paper conclusions are in the Section VI.

II. METHOD FOR *BER* CALCULATION WHEN PURE SWEEP JAMMING IS USED

The *BER* calculation in this paper is performed for MPSK modulated RCIED activation signal. Specifically, the results are obtained for the cases when QPSK, 8PSK and 16PSK are applied. This means that each symbol in MPSK signal represents 2, 3 or 4 bits, respectively. The starting point in our analysis is the algorithm developed in [26], [27] and this algorithm is completed to cover all possible values of RCIED activation signal amplitude (*A*) to the jamming signal amplitude (*B*) ratio. The analysis in [26] and [27] covered only the ratio range $A/B \leq 1$ and now we consider also the range $A/B > 1$.

A. Analysis for $A/B > 1$

Let us suppose that RCIED activation signal is sinusoidal. It may be represented by a phasor whose intensity is *A* in Figure 1. The pure sweep jamming signal is also sinusoid with intensity *B* and it is represented in the Figure 1 at the moment when its frequency during sweeping is approximately the same as the frequency of RCIED activation signal. The end of the phasor *B* is on the circle with the centre in the point *Q* with radius *B* depending on the phase ratio between RCIED activation signal and jamming signal. Phasor diagram with vectors *A* and *B* is presented together with the constellation diagram for *M*-ary PSK (the corresponding value in Figure 1 is *M*=16).

The analysis according to Figure 1 is valid for $A/B > 1$. The *BER* value calculation depends on the values of *A/B* ratio within this area $A/B > 1$.

Let us start from the highest value of *A/B* ratio, i.e. from the lowest jamming signal levels. If the jamming signal amplitude

Aleksandar Lebl is with the Institute IRITEL, Batajnčki put 23, 11080 Belgrade, Serbia (e-mail: lebl@iritel.com).

Vladimir Kosjer is with the Institute IRITEL, Batajnčki put 23, 11080 Belgrade, Serbia (e-mail: vladimir.kosjer@iritel.com).

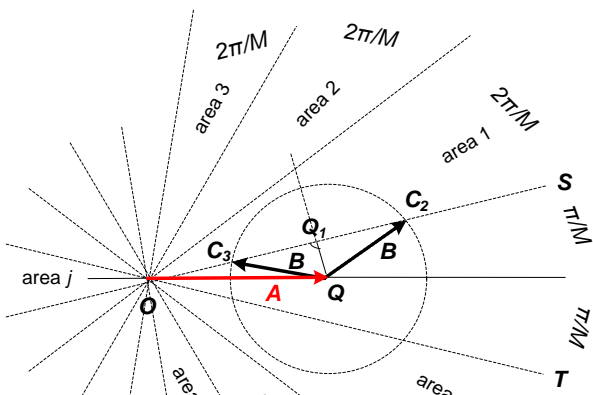
Jovan Radivojević is with the Institute IRITEL, Batajnčki put 23, 11080 Belgrade, Serbia (e-mail: jovan.radivojevic@iritel.com).

Mladen Mileusnić is with the Institute IRITEL, Batajnčki put 23, 11080 Belgrade, Serbia (e-mail: mladenmi@iritel.com).

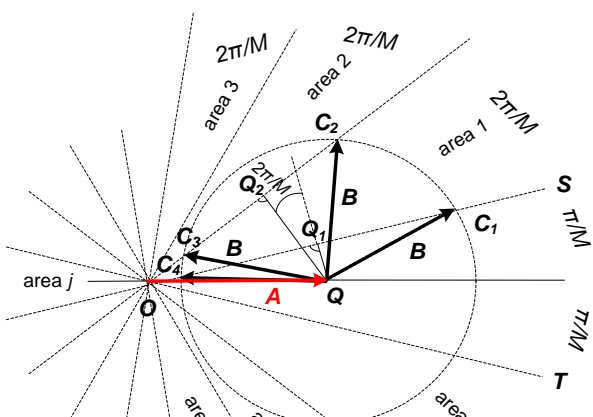
is $B < QQ_1$, i.e. $B < A \cdot \sin(\pi/M)$, the end of phasor B is in any case within the angle SOT, meaning that there is no bit errors ($BER=0$). In this case jamming is never successful.

The following possibility is that the jamming signal amplitude satisfies the condition $A \cdot \sin(\pi/M) < B < A \cdot \sin(3 \cdot \pi/M)$ where it is $QQ_1 = A \cdot \sin(\pi/M)$ (Figure 1a)). In the case that the end of B phasor is in the angle SOT, jamming is unsuccessful (no bit errors). When the B phasor end is in the adjacent area to the SOT angle (on the arc C_2C_3 in area 1), jamming becomes successful. Supposing that phase angle (\angle) between RCIED activation signal and jamming signal is uniformly distributed in the area $(0, 2\pi)$, the probability that the B phasor end is in this area equals:

$$P_{C_2C_3} = \frac{< C_2 Q C_3}{\pi} = \frac{2}{\pi} \cdot \arccos \frac{Q Q_1}{Q C_2} = \\ = \frac{2}{\pi} \cdot \arccos \frac{A \cdot \sin \frac{\pi}{M}}{B} \quad (1)$$



a)



b)

Figure 1 – Phasor and constellation diagram for MPSK signal jamming when signal amplitude ratio is $A/B>1$: a) for $A \cdot \sin(\pi/M) < B < A \cdot \sin(3 \cdot \pi/M)$; b) for $A \cdot \sin(3 \cdot \pi/M) < B < A \cdot \sin(5 \cdot \pi/M)$

If the jamming signal amplitude is further increased ($A \cdot \sin(3 \cdot \pi/M) < B < A \cdot \sin(5 \cdot \pi/M)$), the B phasor end may be also in the next one to the adjacent area (area 2 in the Figure 1b)). Jamming signal B phasor end is in the adjacent area when it is on the arc C_1C_2 or on the arc C_3C_4 (in the area 1). The probability that B phasor end is on the arc C_1C_2 is

$$\begin{aligned}
 P_{C_1 C_2} &= \frac{\angle C_1 Q C_2}{\pi} = \frac{\angle C_1 Q Q_2 - \angle C_2 Q Q_2}{\pi} = \\
 &= \frac{\angle C_1 Q Q_1 + \angle Q_1 Q Q_2 - \angle C_2 Q Q_2}{\pi} = \\
 &= \frac{1}{\pi} \cdot \left(\arccos \frac{Q Q_1}{Q C_1} + \frac{2 \cdot \pi}{M} - \arccos \frac{Q Q_2}{Q C_2} \right) = \quad (2) \\
 &= \frac{1}{\pi} \cdot \left(\arccos \frac{A \cdot \sin \frac{\pi}{M}}{B} - \arccos \frac{A \cdot \sin \frac{3 \cdot \pi}{M}}{B} \right) + \frac{2}{M}
 \end{aligned}$$

and the probability that it is on the arc C_3C_4 is

$$\begin{aligned}
 P_{C_3 C_4} &= \frac{\angle C_3 Q C_4}{\pi} = \frac{\angle C_4 Q Q_1 - \angle C_3 Q Q_1}{\pi} = \\
 &= \frac{\angle C_4 Q Q_1 - (\angle C_3 Q Q_2 + \angle Q_2 Q Q_1)}{\pi} = \\
 &= \frac{1}{\pi} \cdot \left(\arccos \frac{Q Q_1}{Q C_4} - \arccos \frac{Q Q_2}{Q C_3} - \frac{2 \cdot \pi}{M} \right) = \quad (3) \\
 &= \frac{1}{\pi} \cdot \left(\arccos \frac{A \cdot \sin \frac{\pi}{M}}{B} - \arccos \frac{A \cdot \sin \frac{3 \cdot \pi}{M}}{B} \right) - \frac{2}{M}
 \end{aligned}$$

Total probability that phasor B end is in the adjacent area (area 1) is the sum of probabilities that it is on the arc C_1C_2 and on the arc C_3C_4 , i.e.:

$$P_1 = P_{C_1 C_2} + P_{C_3 C_4} = \\ = \frac{2}{\pi} \cdot \left(\arccos \frac{A \cdot \sin \frac{\pi}{M}}{B} - \arccos \frac{A \cdot \sin \frac{3 \cdot \pi}{M}}{B} \right) \quad (4)$$

Phasor *B* end is in the area 2 when it is on the arc C_2C_3 . The probability of this event is calculated as:

$$P_{C_2 C_3} = \frac{C_2 Q C_3}{\pi} = \frac{2}{\pi} \cdot \arccos \frac{Q Q_2}{Q C_2} = \\ = \frac{2}{\pi} \cdot \arccos \frac{A \cdot \sin \frac{3 \cdot \pi}{M}}{B} \quad (5)$$

For a general case, let us suppose that area j is the most distant area of the vector B end in relation to vector A area and that 1 is the adjacent area. The probability that vector B end is in the area i may be expressed as:

$$P_j = \frac{2}{\pi} \cdot \arccos \frac{A \cdot \sin \frac{(2 \cdot j - 1) \cdot \pi}{M}}{B} \quad (6)$$

The probability that B vector end is in some other less distant area k (where $1 \leq k < j$) from vector A area is:

$$P_k = \frac{2}{\pi} \cdot \begin{cases} \arccos \frac{A \cdot \sin \frac{(2 \cdot k - 1) \cdot \pi}{M}}{B} - \\ - \arccos \frac{A \cdot \sin \frac{(2 \cdot k + 1) \cdot \pi}{M}}{B} \end{cases} \quad (7)$$

It is important to emphasize that jamming signal end may be in maximum $(M/2)+1$ areas when $A/B > 1$.

B. Analysis for $A/B < 1$

Figure 2 presents together phasor and constellation diagram for MPSK signal jamming in the case when amplitude of the jamming signal is greater than the RCIED activation signal amplitude ($A/B < 1$) [26], [27]. In this case jamming signal end may be in all M areas. The probability that B phasor end is on some arc (for example C_1C_2) in the area k distant from the area of vector A may be determined in the same way as this probability is expressed by (2):

$$P_k = \frac{1}{\pi} \cdot \left\{ \begin{aligned} & \arccos \frac{A \cdot \sin \frac{(2 \cdot k - 1) \cdot \pi}{M}}{B} - \\ & - \arccos \frac{A \cdot \sin \frac{(2 \cdot k + 1) \cdot \pi}{M}}{B} \end{aligned} \right\} + \frac{2}{M} \quad (8)$$

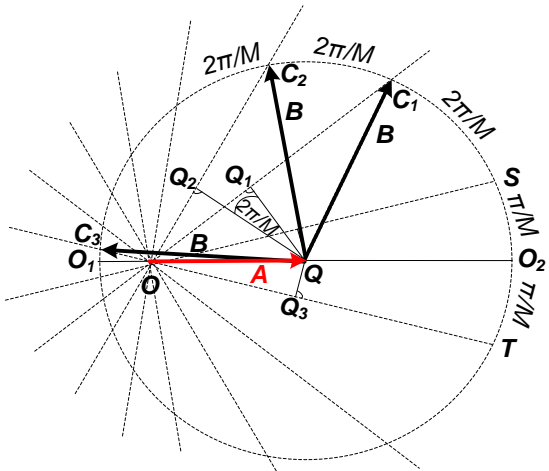


Figure 2 – Phasor and constellation diagram for MPSK signal jamming when signal amplitude ratio is $A/B < 1$

This calculation procedure may be implemented for all coding areas except the last one (area j) which corresponds to the angle C_3QO_1 . For this area, it is

$$P_j = \frac{< C_3 QO }{\pi} = \frac{< C_3 QQ_3 - < OQQ_3}{\pi} = \\ = \frac{1}{\pi} \arccos \frac{A \cdot \sin \left(2 \cdot \pi - \frac{\pi}{M} \right)}{B} - \left(\frac{1}{2} - \frac{1}{M} \right) \quad (9)$$

where the angle OQQ_3 is determined from the rectangular triangle OQQ_3 whose angle QOQ_3 is equal to π/M .

III. THE NUMBER OF ERRONEOUS BITS IN A SYMBOL

The following important element for our analysis is the mean number of incorrectly transmitted bits in a symbol for different surrounding coding areas (E_{mk}). It depends on the position of jamming signal vector end (i.e. how many areas it is distant from the position of RCIED activation signal vector). The values of this parameter are presented in the Table I for QPSK, 8PSK and 16PSK modulation according to the results from [26], [27]. In this table adjacent area to the area of RCIED activation signal position is designated as area 1 ($k=1$). The most distant area for QPSK signal is area 2 for QPSK modulated RCIED activation signal, area 4 for 8PSK and 8 for 16PSK.

TABLE I
Mean number of bit errors in a symbol (E_{mk}) when jamming is implemented for various RCIED activation signal modulation types

Modulation	Bits in symbol	Areas (k)							
		1	2	3	4	5	6	7	8
QPSK	2	1	2						
8PSK	3	1	2	2	2				
16PSK	4	1	2	2	2	2.5	3	2.5	2

The total number of incorrectly transmitted bits in a symbol of RCIED activation message is now determined considering probability that resultant vector is in each of surrounding coding areas (P_k) and the mean number of incorrectly transmitted bits (E_{mk}) for the considered area:

$$N_{EB} = \sum_{k=1}^j P_k \cdot E_{mk} \quad (10)$$

Here j is the most distant coding area from the position of RCIED activation message signal vector as already stated. The value of BER for our further analysis is now calculated dividing the value in (10) by the number of bits forming a symbol or $\log_2 M$.

IV. INFLUENCE OF MULTISWEEP JAMMING ON *BER* CALCULATION

Figure 3 presents example of RCIED activation message signal jamming by pure sweep signal (Figure 3a)) and by multisweep signal (Figure 3b)). The presentation is in the field signal frequency as a function of time. The complete jamming frequency band is $f_2-f_1=W$. RCIED activation signal is in the frequency band $C(1)$ and in $C(2)$. Message duration is T_{mess} and in the case of pure sweep jamming this duration is lower than the sweep period T_{sw} . As a consequence the message in the band $C(1)$ may be successfully jammed (according to Figure 1a)), but the message in the band $C(2)$ will not be jammed.

Multisweep jamming is realized in such way that frequency range W is divided into four equally wide parts (W_{MS}). Jamming is performed simultaneously in all four parts. In this case both RCIED activation message signals are successfully jammed.

jammed during time intervals designated by T_c . Jamming is more reliable, because in this example both message signal frequencies coincide with the jamming signal frequency two times.

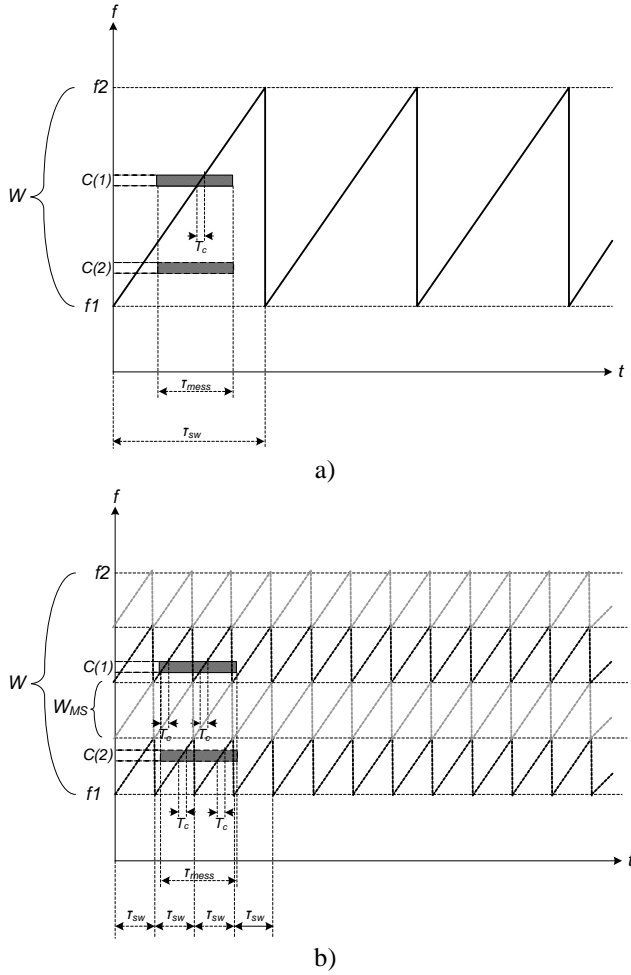


Figure 3 – RCIED activation message signal jamming by: a) pure sweep jamming; b) multisweep jamming

Let us suppose that K_{MS} is the number of different simultaneous sweep signals in a multisweep signal ($K_{MS}=4$ in the Figure 3b)). The frequency band which is swept equals

$$W_{MS} = \frac{W}{K_{MS}} \quad (11)$$

for each one of sweep components in multisweep signal. On the base of (11) the sweeping period of multisweep signal (Figure 3b)) may be expressed as

$$T_{sw} = \frac{W_{MS}}{v_{sw}} = \frac{W}{v_{sw} \cdot K_{MS}} \quad (12)$$

where v_{sw} is the speed of sweeping. Then the number of coincidences between frequency of RCIED activation message signal and the jamming signal frequency is

$$n = \left\lfloor \frac{T_{mess}}{T_{sw}} \right\rfloor = \left\lfloor \frac{T_{mess} \cdot v_{sw} \cdot K_{MS}}{W} \right\rfloor \quad (13)$$

where $\lfloor \cdot \rfloor$ means rounding to lower integer value.

It is considered that a symbol in RCIED activation message may be incorrectly transmitted when there is coincidence

between two signal frequencies. In such case the real *BER* is determined by the method explained by equations (1)-(9). To simplify our analysis, we suppose that only one symbol is altered during each coincidence event. This approximation is „on the safe side“, because alterations on more symbols lead to higher successful jamming probabilities. The total number of incorrectly transmitted bits may be determined as

$$N_{EBMS} = N_{EB} \cdot n \quad (14)$$

V. BER RESULTS FOR VARIOUS MPSK SIGNALS

Figure 4 presents *BER* as a function of the RCIED activation message signal amplitude to the jamming signal amplitude ratio (A/B). The results are related to three modulation types of RCIED activation signal: QPSK, 8PSK and 16PSK. For the amplitudes ratio $A/B \leq 1$ ($A/B \leq 0$ in dB) the derived formulas are (8) and (9) and for the amplitudes ratio $A/B > 1$ ($A/B > 0$ in dB) the obtained formulas are (1) - (7). The breakpoint (which is at $A/B=0.7$ dB for 8PSK modulated RCIED activation signal and at $A/B=5.1$ dB for 16PSK signal), is the consequence of the fact that at these signal levels the mean number of erroneous bits in a symbol changes from one to two (or vice versa). In other words, at A/B ratios higher than the emphasized ones only one bit in a symbol may be in error and for lower ratios it is possible to have more than one erroneous bit in a symbol.

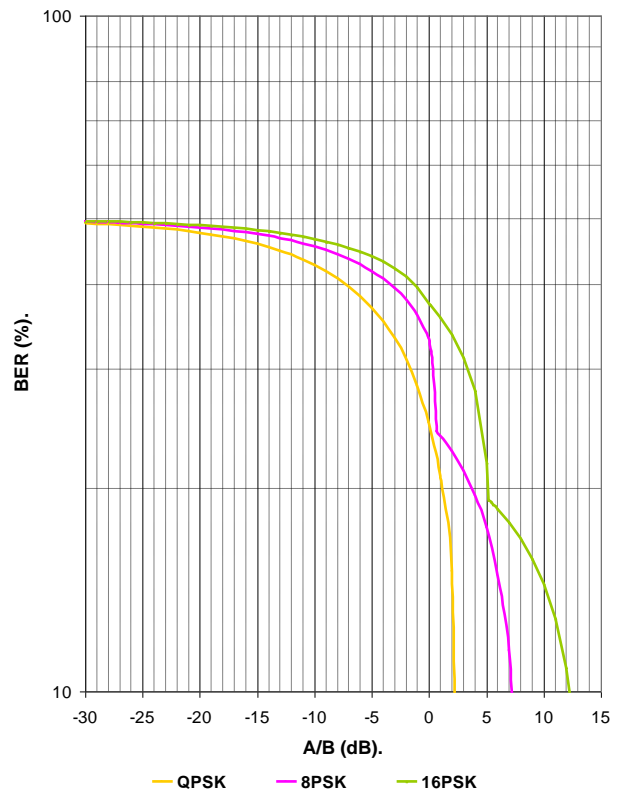


Figure 4 – *BER* as a function of amplitude ratio RCIED activation to the jamming signal for QPSK, 8PSK and 16PSK modulated RCIED activation message signals

Two practical examples related to the calculation applications and solutions will be given in further text.

Example 1: RCIED activation message is transmitted as 16PSK signal of $T_{mess}=6\text{ms}$ duration. Jamming of this message is considered to be successful (RCIED is not activated) when at least 4 bits in its content are received incorrectly. What speed of sweeping and what jamming signal power are necessary to be applied to achieve such a result with pure sweep signal? In which way will jamming signal power be changed if pure sweep signal is replaced by multisweep signal with four simultaneous sweep signals at the same sweep speed?

Solution: Let us first suppose that it is necessary to achieve signal frequencies coincidence two times during the RCIED activation message lifecycle. In this way 2 symbols (or 8 bits as 16PSK is implemented) would be hit by jamming. As 4 bits have to be altered, *BER* value should be at least 0.5. This value of *BER* may not be achieved by limited jamming power according to the graph in the Figure 4. Two frequencies should be equal at least 3 times during the activation message, or sweep period should be 2ms or less according to (13). It means that the number of incorrectly transmitted bits per symbol should be $4/3=1.333$ or $BER=1.333/4=0.333$. This value of *BER* is achieved when power ratio between RCIED activation signal and jamming signal is $A/B=2\text{dB}$ according to the graph in Figure 4 for 16PSK signal.

When multisweep signal with 4 simultaneous sweep signals is implemented, frequencies of RCIED activation signal and sweep signal coincide 12 times as a consequence of (13) (48bits total are hit by jamming). The corresponding value of $BER=4/48=0.0833$. The value $A/B=12.5\text{dB}$ may be determined again from the Figure 4. As there are 4 simultaneous signals of equal power in multisweep signal, the total power ratio is decreased for 6dB comparing to A/B ($A/B_f=6.5\text{dB}$). It means that multisweep signal implementation in this case caused power saving of 4.5dB.

Example 2: RCIED activation message is transmitted as 16PSK signal of $T_{mess}=1\text{ms}$ duration. The sweep signal period is $T_{sw}=2\text{ms}$. Jamming of the activation message is considered to be successful (RCIED is not activated) when at least 3 bits in its content are received incorrectly. What jamming signal power is necessary to be applied to achieve such a result with pure sweep signal? How will jamming signal power change if pure sweep signal is replaced by multisweep signal with four simultaneous sweep signals at the same sweep speed?

Solution: In this case the possibility to realize jamming for pure sweep jamming is 0.5 because $T_{mess}/T_{sw}=0.5$. The goal to change the content of 3 bits may be only considered for 50% cases when frequencies coincidence exists. This coincidence happens only once during the message lifecycle. According to the graph in the Figure 4, *BER* values are always less than 0.5, so maximum 2 of 4 bits in 16PSK signal may be altered. The conclusion of this complete analysis is that the request to achieve 3 erroneous bits is never reached. On the contrary, the request may be always satisfied by multisweep jamming. According to (13), frequencies coincidence exists two times during the message lifecycle. It means that total 8 bits are hit by jamming and it should be $BER=0.375$ (3 of 8 erroneous

bits). The defined goal is achieved when $A/B=0\text{dB}$ according to the Figure 4. The total power for 4 simultaneous signals in multisweep signal is increased for 6dB meaning that $A/B_f=-6\text{dB}$. The conclusion of this example is that the goal, which couldn't be satisfied by pure sweep jamming, is realized by multisweep jamming with not so high jamming signal power.

VI. CONCLUSIONS

In this paper the characteristics of multisweep signal jamming are presented comparing to pure sweep jamming. The *BER* values are determined for the complete set of amplitude ratios RCIED activation signal level to the jamming signal level. Multisweep jamming implementation is specially justified in the case when RCIED activation message duration is comparable or lower than the pure sweep signal period. Multisweep jamming increases jamming reliability and decreases necessary jamming power for such signals timing relations. The conclusions are practically illustrated by two examples with the emphasis on the example 2 where jamming requests even may not be satisfied in any case by pure sweep jamming. It may be satisfied using multisweep jammig with not high signal power.

There are two different strategies for multisweep signal generation: linear frequency change from its minimum till maximum value which is analyzed in this paper and random frequency change while sweeping. Both these strategies are implemented in IRITEL jammer [19], [20]. This second strategy based on the earlier experience related to already implemented RCIED activation devices [7] may contribute to more reliable jamming. The subject of our future work will be analysis of random multisweep jamming and selection of optimum strategy for jamming frequency change. The special topic of interest could be application of multisweep jamming in the case of RCIED activation message signals transmission over mobile operators networks.

REFERENCES

- [1] A. GuLyÁS, „The Radio Controlled Improvised Explosive Device (RCIED) threat in Afghanistan“, AARMS, Vol. 12, No. 1, pp. 1-11., September 2013.
- [2] I. Overton, J. Dathan, C. Winter, J. Whittaker, R. Davies, H. Kaaman, „Improvised Explosive Device (IED) Monitor 2017“, Action on Armed Violence (AOAV), London, pp. 1-31, October 2017.
- [3] „Overview of Jammer System Design“, Technical Article, February 2012, pp. 1-2, <https://www.richardsonfpd.com/docs/rfpd/Overview-of-Jammer-System-Design.pdf>.
- [4] O. Alp, Ö. E. Kılıç, A. Ayvalik, Z. Savaş: „ATE Design and development for I-level maintenance and production line of RCIED Jammer Systems“, 2015 IEEE AUTOTESTCON, 2-5. November 2015, National Harbor, USA, DOI: [10.1109/AUTEST.2015.7356519](https://doi.org/10.1109/AUTEST.2015.7356519).
- [5] K. Lin, J. Dayton: „Game-Theoretic Models for Jamming Radio-Controlled Improvised Explosive Devices“, Military Operations Research, Vol. 16, No. 3, pp. 5-13, 2011., DOI: [10.2307/43943705](https://doi.org/10.2307/43943705).
- [6] K. Lin, R. G. McGrath: „Robust patrol strategies against attacks at dispersed heterogeneous locations“, International Journal of Operational Research, Vol. 30, No. 3, pp. 340-359., 2017., DOI: [10.1504/IJOR.2017.10007854](https://doi.org/10.1504/IJOR.2017.10007854).
- [7] J. A. Dayton: „Risk of Using Past to Predict Future: A Case Study of Jamming RCIEDs“, Master's Thesis, Naval Postgraduate School Monterey CA, 1st June 2009.

- [8] R. G. McGrath: „Patrol Policies Against Strategic Attackers at Dispersed Locations“, Proceedings of the 2015 Industrial and Systems Engineering Research Conference, 30th May – 2nd June 2015., Nashville, USA, pp. 1185-1194.
- [9] M. Perry, H. El-Amine: „Computational Efficiency in Multivariate Adversarial Risk Analysis Models“, Decision Analysis, Vol. 16, Issue 4, December 2019., pp. 239-333., <https://doi.org/10.1287/deca.2019.0394>.
- [10] R. G. McGrath: „Generating Robust Patrol Patterns Through Fictitious Play“, Proceedings of the 2017 Industrial and Systems Engineering Research Conference, 20th-23th May 2017., Pittsburgh, USA, pp. 338-343.
- [11] J. Mietzner, P. Nickel, A. Meusling, P. Loos, G. Bauch: „Responsive communications jamming against radio-controlled improvised explosive devices.“ IEEE Communications Magazine, Vol. 50, Issue 10, pp. 38-46, October 2012.
- [12] R. Poisel: „Modern Communications Jamming Principles and Techniques“, Second Edition, Artech House, Boston/London, 2011.
- [13] K. Wilgucki, R. Urban, G. Baranowski, P. Grądzki, P. Skarżyński: „Automated protection system against RCIED“, In Proc. Military Communication Institute (MCI), 2012.
- [14] Homeland Security Strategies GB LTD: „VIP-300T Covert IED Jammer – Trunk Mounted Version“, 2016., http://www.secintel.com/media/pdf/vip300T_CovertIEDJammer.pdf.
- [15] Phalanx, „Intelligent Safety Systems: New Hybrid RCIED Jammer Intelligent & Reactive Radio-controlled Designed to Prevent Improvised Explosive Devices“, <http://www.phalanxsafety.com/assets/phalanx-ried-jammer-rev5.pdf>.
- [16] Geospatial World: „Counter RCIED Systems“, July 2014, <https://www.geospatialworld.net/article/counter-rcied-systems/>.
- [17] Phantom Technologies LTD: „Tactical HF-UHF-VHF Jammer Very High Output Power – Model RCJ 5KW Output Power“, <https://phantom-technologies.com/wp-content/uploads/2017/12/RCJ-FM.pdf>, December 2017.
- [18] Elaman German Security Solutions: „Jammer – Principle of Operation“, <https://ht.transparencytoolkit.org/rcc-dev%5Cshare/Documentation/Gamma/ELAMAN/elamancat/Jammer/Jammer%20Principles%20of%20Operation.pdf>.
- [19] P. Petrović, N. Remenski, P. Jovanović, V. Tadić, B. Pavić, M. Mileusnić, B. Mišković, „WRJ 2004 Wideband Radio Jammer against RCIEDs“, tehničko rešenje – novi proizvod na projektu tehnološkog razvoja TR32051 pod nazivom „Razvoj i realizacija naredne generacije sistema, uređaja i softvera na bazi softverskog radija za radio i radarske mreže“, 2011., <http://www.iritel.com/images/pdf/wrj2004-e.pdf>.
- [20] M. Mileusnić, P. Petrović, B. Pavić, V. Marinković-Nedelicki, J. Glišović, A. Lebl, I. Marjanović, „The Radio Jammer Against Remote Controlled Improvised Explosive Devices“, 25th Telecommunications Forum (TELFOR), Belgrade, November 21-22th 2017, pp. 151-154, <https://ieeexplore.ieee.org/document/8249309>, ISBN 978-1-5386-3072-3.
- [21] A. Mpitzopoulos, D. Gavalas: „An effective defensive node against jamming attacks in sensor networks“, Security and Communications Networks, Vol. 2, 2009., pp. 145-163, DOI: [10.1002/sec.81](https://doi.org/10.1002/sec.81).
- [22] M. Mileusnić, B. Pavić, V. Marinković-Nedelicki, P. Petrović, D. Mitić, A. Lebl, „Analysis of Jamming Successfulness against RCIED Activation“, 5th International Conference IcETRAN 2018, Palić, June 11-14th 2018., Proceedings of Papers, pp. 1206-1211, ISBN 978-86-7466-752-1, paper awarded as the best one in the section Telecommunications.
- [23] M. Mileusnić, B. Pavić, V. Marinković-Nedelicki, P. Petrović, D. Mitić, A. Lebl, „Analysis of jamming successfulness against RCIED activation with the emphasis on sweep jamming“, *Facta Universitatis, Series Electronics and Energetics*, Vol. 32, No. 2, June 2019, <https://doi.org/10.2298/FUEE1902211M>, ISSN: 0353-3670, pp. 211-229., the extended and revised version of the paper from the IcETRAN 2018.
- [24] V. Marinković-Nedelicki, A. Lebl, M. Mileusnić, P. Petrović, „Combined Jamming in RCIED Activation Prevention“, 19th International Symposium INFOTEH-JAHORINA, March 18-20th 2020., pp. 1-6, DOI: [10.1109/INFOTEH48170.2020.9066329](https://doi.org/10.1109/INFOTEH48170.2020.9066329), ISBN 978-1-7281-4775-8.
- [25] B. Pavić, M. Mileusnić, V. Marinković-Nedelicki, P. Petrović, V. Matić, A. Lebl, „Software for control and supervision of the system for VIP persons protection from remote controlled explosive devices in extended frequency range (20MHz-6GHz)“, tehničko rešenje na projektu tehnološkog razvoja TR32051 pod nazivom „Razvoj i realizacija naredne generacije sistema, uređaja i softvera na bazi softverskog radija za radio i radarske mreže“, 2017., in Serbian.
- [26] V. Marinković-Nedelicki, A. Lebl, M. Mileusnić, P. Petrović, B. Pavić, „BER Calculation for Sweep Jamming of MPSK Modulated RCIED Activation Message Signals“, 18th International Symposium „INFOTEH Jahorina 2019“, Jahorina, 20-22. March 2019., ISBN: 978-1-5386-7073-6, pp. 1-6, DOI: [10.1109/INFOTEH.2019.8717747](https://doi.org/10.1109/INFOTEH.2019.8717747).
- [27] A. Lebl, M. Mileusnić, P. Petrović, B. Pavić, V. Marinković-Nedelicki, „Successful Sweep Jamming Rate Determination of MPSK Modulated RCIED Activation Message Signals“, International Journal of Electrical Engineering and Computing, Vol. 3, No. 2, December 2019., UDC 621.391:517.44:621.3.049.77, DOI 10.7251/IJEEC1902037L, pp. 37-44.

Application of 5G Channel Coding Techniques in Smart Grid: LDPC vs. Polar coding for Command Messaging

Mirjana Maksimović and Miodrag Forcan

Abstract— A reliable, scalable, secure, and cost-effective telecommunication and information exchange system is of immense importance in a Smart Grid (SG) vision. 5G, as a novel technology, promises to bring numerous benefits in the energy sector, mostly in increasing overall energy efficiency, reliability, quality of service and accelerating the SG development. Channel coding, as a fundamental building block in any communications system, plays a substantial role in the realization of fast communication with minimum errors during data transfer in an imperfect channel environment. In this paper command messaging in SG has been considered and the performance of 5G channel coding techniques, Low-Density Parity-Check (LDPC), and Polar codes, in terms of the Bit Error Ratio (BER) for different code rates, have been investigated. The simulation results confirm the superiority of Polar coding in the case of transmitting a typical command message from the base station to the Phasor Measurement Unit (PMU) device.

Index Terms—LDPC; Polar coding; 5G; Smart Grid; Command Message

I. INTRODUCTION

The number of smart devices increases continuously, resulting in the creation of the Internet of Things (IoT) network in which smart devices are connected via the Internet. Existing mobile networks need to be enhanced in terms of capacity, data rate, latency, and other performances in order to successfully respond to the increased usage of mobile and smart devices and diversification of novel application requirements. Hence, the development of the fifth generation of mobile communications, commonly called the 5G, has been motivated by the increased usage of mobile and other smart devices and demands for low latency, highly reliable, and highly safe communication networks [1].

5G has made enormous progress during the last few years and it is anticipated that during the 2020s tremendous growth in the required connectivity, traffic volume, and scope of application scenarios will occur [1]. 5G will support a new radio access technology called 5G-NR (new radio) and an enhanced core network called NGC (Next Generation Core) [2]. It is expected that 5G will encompass a lot more than

Mirjana Maksimović is with the Faculty of Electrical Engineering, University of East Sarajevo, Vuka Karadžića 30, 71123 East Sarajevo, Bosnia and Herzegovina (e-mail: mirjana.maksimovic@etf.ues.rs.ba).

Miodrag Forcan is with the Faculty of Electrical Engineering, University of East Sarajevo, Vuka Karadžića 30, 71123 East Sarajevo, Bosnia and Herzegovina (e-mail: miodrag.forcan@etf.ues.rs.ba).

previous generations of mobile communications, becoming a user-centric concept instead of being an operator-centric (3G) or the service-centric concept (4G). 5G, compared with 3G and 4G systems, can support applications characterized by large connection density, very high traffic volume, and very high mobility.

The focus of 5G-NR can be split into three categories based on different user requirements [1-3]:

- Enhanced mobile broadband (eMBB) – in this scenario, providing higher data rates and enhancing the user experience are required (for high-capacity and ultra-fast mobile communication),
- Massive Machine-Type Communication (mMTC) – the focus is on supporting a huge number of devices with low costs, enhanced coverage and low energy use (for industrial and IoT applications),
- Ultra-Reliable and Low-Latency Communication (URLLC) – communication in this scenario needs to be extremely reliable with very low latencies (mission-critical applications). These applications require sub-millisecond over-the-air latency with packet rate failure of 10^{-5} (error rates lower than 1 packet loss in 10^5 packets) [4, 5].

In order to satisfy the requirements of these application scenarios, 5G wireless networks demand networks' structural improvements in terms of transmission's reliability, system's security, and the quality of offered services. Networks' densification, larger bandwidth, increased spectral efficiency, and new air interface are subjects of intensive research in order to achieve the data rate and capacity for 5G [6]. To achieve high capacity performance in a km^2 , three important parameters should be improved [7]:

- A hundred times better data rates than previous generations,
- Less amount of latency (it should be 0.5 ms compared to 10 ms performed by 4G communication systems),
- A hundred times more connections (links).

The energy sector is one of the leading use cases where 5G technologies promise to bring numerous benefits. Increasing energy efficiency overall and accelerating the development of the Smart Grid (SG) are the predictions of how 5G will influence the energy sector [8]. However, the energy sector is quite challenging as it requires novel technologies to address a wide range of diverse requirements associated with different application scenarios. The expectations from 5G

communication network utilization in SG are to support an increasingly diverse set of novel and emerging services as well as their faster development. Massive connectivity from production to consumption, high data rate, low latency, flexible and optimal deployment, increased scalability, reduced power consumption, improved security and privacy, and cost-effectiveness are additional benefits that 5G promises [9].

Command messaging plays an important role in the case of a new SG. There are many examples of typical applications such as remote control of Smart Meters (SM), Circuit Breakers (CB), PMUs, and other application-specific Intelligent Electronic Devices (IED). The benefits of the CB remote control system in SG, among many other systems, are illustrated in [10-12]. The focus of this paper is to determine the transmission reliability of standard-defined command messages [13] to PMUs in the case of standard-adopted 5G channel coding techniques [14].

Since data transmission occurs in an imperfect channel environment where noise, fading, and interference are present, channel coding plays a substantial role in achieving a higher data rate to realize a fast communication with minimum errors during data transfer. In order to be used efficiently in the communication systems, the selected 5G channel code should have the ability to support a wide range of block lengths and code rates and have an excellent Block Error Rate (BLER) and Bit Error Rate (BER) performances.

This paper represents an attempt to select and implement appropriate channel coding techniques for command messaging in SG. Hence, the paper is organized as follows. An overview of 5G channel coding techniques is presented in Section 2. Section 3 shows the implementation of channel coding techniques in a specific Smart Grid use case – for sending command messages, as well as simulation results. Summary of the performed research and directions for future research are given in the Conclusion.

II. CHANNEL CODING

Regarding block lengths, short data bits are typically used in IoT applications while broadband data applications use long data bits. When it comes to different code rates, low coding rates have been practiced in rural areas due to the sparse distribution of base stations, while in urban regions, due to the ultra-dense population, high coding rates have been used. When channel code supports a wide range of data block lengths and data code rates, it is possible to avoid using wasteful data bits and utilization of code rate that causes signal imperfections. Usage of wasteful data and the undesirable code rate will result in unwanted data bits transfer, hence wasting more spectrum, which has a bandwidth, time duration, and energy. This will badly influence on throughput, latency, and capability of error correction. Therefore, the flexibility of the chosen code scheme is an important factor [7]. In addition to better flexibility, low computation complexity, low latency, low cost, and high reliability are also desired for the coding

scheme. Codes that show promising BER and BLER performances in a wide range of block lengths and coding rates are Low-Density Parity-Check (LDPC) codes and polar codes. Therefore, these codes are being considered for the 5G-NR physical layer. The channel coding, in this case, has been separated into channel coding of user information and channel coding of control information [1].

LDPC codes achieve a better result in case of data channels because they can efficiently support variable code rates, block lengths, and Hybrid Automatic Repeat Request (HARQ), with better decoding latency, throughput, and implementation complexity compared to other codes. On the other side, Polar codes are the most suitable for control channels because they offer the best error correction capability at the short messages used as control information while addressing a latency issue of successive cancellation decoding. Therefore, the 3rd Generation Partnership Project (3GPP) standardization has selected LDPC for uplink and downlink data channels and Polar codes for the uplink and downlink control channels, replacing the Turbo and Tail-Biting Convolutional Codes (TBCC) of LTE (Long Term Evolution), respectively [1, 15, 16]. More precisely, NR uses LDPC codes for user data which is transmitted on the Physical Downlink Shared Channel (PDSCH) and Physical Uplink Shared Channel (PUSCH). Polar codes are used for Uplink Control Information (UCI) transfer over the Physical Uplink Control Channel (PUCCH) or the PUSCH. In the downlink, Polar codes are used for encoding the Downlink Control Information (DCI) transmitted over the Physical Downlink Control Channel (PDCCH) and the payload in the Physical Broadcast Channel (PBCH) [1, 14, 17].

A. LDPC Codes

LDPC codes are efficient channel coding techniques that allow the correction of transmission errors. They were originally invented and presented by Gallager in 1963 [18] but have not been in use before 1996 when they were rediscovered by Mackay [19]. Mackay showed that the LDPC codes are linear block codes that can achieve empirical performance close to the Shannon limit for long words.

In general, LDPC codes are defined by a sparse parity check matrix that determines the transmission's performance. The theory of LDPC codes is related to graph theory and a parity check matrix is defined by a base graph along with a lifting size and cyclic shifts for the graph's edges. For NR, two base graphs are defined, along with eight sets of lifting sizes. In this way, a wide range of block lengths and code rates have been supported. The choice of the base graph depends on the size and code rate of the initial transmission [17, 20, 21].

Due to the sparsity of the parity check matrix, LDPC codes have relatively simple and practical decoding algorithms. Decoding is done by iteratively using the sum-product or using the belief propagation soft-decision decoder. Due to their excellent ability to attain performance near the Shannon limit, LDPC codes are currently being used in many communication systems such as DVB-S2 (satellite transmission, 10GBase-T Ethernet, 802.11n (Wi-Fi allowing

MIMO), 802.16e (Mobile WiMAX), etc. [6].

LDPC coding chain at the transmitter side for the 5G NR downlink shared transport channels contains following parts [17, 22-24]:

- CRC (Cyclic Redundancy Check) attachment to the transport block (payload for the physical layer) in order to provide error detection.
- Code block segmentation and code block CRC attachment - the transport block (including the 24 or 16 bit CRC) is segmented into multiple code blocks to reduce the complexity. Two LDPC base graphs are supported in the case of NR, one optimized for small transport blocks and one for larger transport blocks. After code block segmentation, each code block is appended with its own CRC and each code block is individually LDPC encoded.
- Channel coding using LDPC - In NR, new channel coding mechanisms are applied to enable error correction and error detection in the presence of noise, fading, and interference. Data channels use LDPC codes.
- Rate matching and code block concatenation – includes the stages of bit selection and interleaving defined for LDPC-encoded data and code block concatenation.

After these processing stages, the transport block is passed on the PDSCH for scrambling, modulation, layer mapping, and resource/antenna mapping. PDSCH supports QPSK, 16QAM, 64QAM, and 256QAM modulation schemes while PUSCH also supports pi/2-BPSK modulation in addition to those listed above for PDSCH.

At the receiver side, processing stages of the downlink shared channel correspond to those at the transmitter side.

- Rate recovery (rate dematching) - is performed on the receiver side to restore the encoded bit structure so that the LDPC decoding algorithm can decode the message. In this step, the inverse of the code block concatenation, bit interleaving, and bit selection stages have been performed.
- LDPC decoding – the LDPC decoder receives an LDPC encoded message that was transmitted over a channel. Due to noise presence, the received message values may differ from the message that was sent. LDPC code is designed to be able to correct errors and reconstruct the correct message from the received data. There are a variety of algorithms for decoding LDPC encoded messages: Belief propagation, Layered belief, Normalized min-sum, and Offset min-sum.
- Code block desegmentation and CRC decoding – in this step the input code block segments have been concatenated into one output data block. Any filler bits and type-24 bit CRC present in the input code block segments are removed. In other words, this process is the inverse of the LDPC code block segmentation and code block CRC attachment performed at the transmitter side.
- Transport block CRC decoding – as the final step, decoding, and removing CRC serves for message

verification at both the code-block and transport block levels. If there are no CRC errors, the transport block is being recovered and decoded with no errors.

As PUSCH is used for the transmission of uplink shared channel and layer 1/2 control information, each transport block in the uplink goes through the following processing stages [18, 19]:

- CRC attachment to the transport block
- Code block segmentation
- Channel coding of data and control information
- Rate matching and code block concatenation
- Multiplexing of data and control information - ensures that control and data information are mapped to different modulation symbols,
- Channel interleaver - implements a time-first mapping of control modulation symbols and frequency-first mapping of data modulation symbols onto the transmit waveform.

B. Polar Codes

Polar codes are one of the newest channel coding schemes introduced by Arikan [25] in 2009 and they are the first provably codes that arrive near Shannon's limits of capacity with low encoding and decoding complexities. As 5G systems require significant improvements in channel capacity, Polar codes are the promising technique because of the advantages they provide, the capacity they produce, and the absence of error floor. Polar codes are approved as the channel coding algorithm for 5G control channels where the information blocks are small compared to data transmission and HARQ is not used. Polar codes replace the used Convolutional Codes in LTE. The idea of Polar codes is to transform several instances of the original radio channel into a set of virtual channels that tend to have either high reliability or low reliability. This means that the channels are either noiseless or completely noisy and the transmission of the data (information bits) is performed via noiseless channel while the pure-noise channel transmits fixed (known by the transmitter and the receiver) symbols. Decoding can be performed in several ways, typically using successive cancellation and list decoding. Successive cancellation decoding is not well suitable for short-to-medium block lengths, but list decoding substantially improves the performance of polar codes at those block lengths [3, 20, 26]. Polar codes have a recursive structure with low complexity and were proven to achieve the channel capacity for long block lengths. Therefore, during the Polar code's design, a maximum number of bits should be considered. In NR, the Polar code has been designed to support 512 coded bits (prior to rate matching) in the downlink. It can be handled with up to 140 information bits, which provides a sufficient margin for future extensions [6, 7, 27].

In the case of polar coding in the downlink, a transport block goes through the processing stages of [1, 17, 23, 24, 26]:

- CRC attachment,
- CRC interleaver - with the help of interleaver, a CRC

block is not attached at the end of DCI block but distributed among the DCI bits. This assists potentially early termination in the PDCCH decoding process.

- Radio Network Temporary Identifier (RNTI) coding - a 16-bit identifier that enables the user equipment to determine if the message is intended for it.
- Channel coding – coding channel data with Polar codes.
- Rate matching - for Polar code rate matching is defined per coded block and consists of sub-block interleaving, bit selection, and bit interleaving. Channel interleaving is only used for PUCCH where it improves the polar code's error correction capability when employing higher-order modulation schemes for transmission over fading channels, while it is not employed for PDCCH and PBCH. Rate matching is performed after polar coding and before the bits are transmitted over the channel. Rate matching is about matching the length of information blocks (the number of bits) to the desired transmission rate. How these information blocks can be manipulated depends on their size after encoding, which can either lead to shortening, puncturing, or repetition of the coded bits to achieve the desired number of transmission bits.
- After polar coding and rate-matching, bits are scrambled, modulated using QPSK, and mapped to the resource elements used for the PDCCH

At the receiver side, processing stages of PDCCH corresponds to those at the transmitter side.

In the uplink, UCI has been coded using different coding techniques depending on UCI length. After adequate coding, rate-matching and bit-level interleaving are performed. The PUCCH uses sequence selection, BPSK, or QPSK depending on the PUCCH format and the number of bits with $\pi/2$ -BPSK available as a configurable option [17].

III. CHANNEL CODING OF COMMAND MESSAGE IN SMART GRID USE CASE

Standard PMU device consists of three main parts: measurement, phasor computation (assisted by Global Positioning System or GPS receiver), and communication. The communication part is used for streaming data in the standard-defined format. The main information to be transmitted is in the form of data messages consisting of calculated and GPS-based synchronized phasors. Data messages are transmitted uplink to Phasor Data Concentrators (PDC). However, downlink transmission of command messages from PDC is required to remotely control PMU data streaming. The typical PMU-based data collection network is shown in Fig.1.

For simulation purposes, an example of a command message that affects the behavior of the Phasor Measurement Unit (PMU) has been considered (Table I) [13]. The example presented in Table I causes a PMU to begin transmission of data messages. The information (payload) message length is 16 bytes or 128 bits. This or very similar type of command message can be used for remote control of other IED in SG.

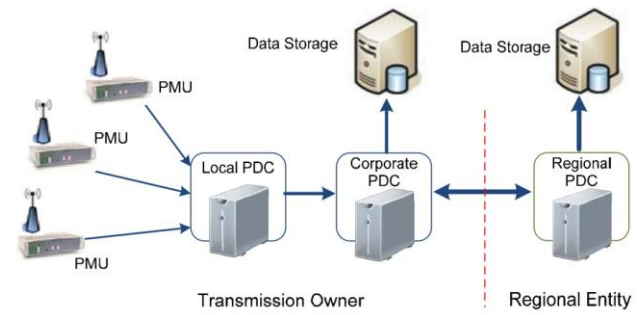


Fig. 1. Synchrophasor data collection network [13]

TABLE I
COMMAND MESSAGE EXAMPLE [13]

Field	Description	Example	Size (bytes)	Hexadecimal value
SYNC	Synchronization byte and version number	Command Message, version 1	2	AA 41
FRAMESIZE	Number of bytes in a frame	18	2	00 12
IDCODE	Data stream ID number, 16-bit integer, 1-65534	7734	2	1E 36
SOC	SOC time stamp	12:00 AM, 6.6.2006 = 1 149 591 600	4	44 85 60 30
FRACSEC	A fraction of second with Time quality.	No leap second pending or past, clock never locked, fractional time 0.77s	4	0F 0B BF D0
CMD	Defined commands are data on, data off, send header, send configuration, extended frame.	Turn on the data stream.	2	00 02
CHK	CRC-CCITT - 16-bit CRC calculated using the generating polynomial $X^{16} + X^{12} + X^5 + 1$.	-	2	CE 00

The command message under consideration is coded using LDPC and Polar coding techniques according to procedures recommended in the standard [14] and explained earlier in Section II. CRC part of the message is generated according to the same standard procedures. Code block segmentation is not required for short messages and thus it is not performed in simulations due to considered command message length. As the quality criterion of a channel code, BER of the coding schemes is plotted against the energy per bit to noise power spectral density ratio (E_b/N_0) for different code rates. MATLAB [23] is used to simulate the physical communication layer with LDPC and Polar codes and calculates the simulation results to BER vs. E_b/N_0 graphs (Fig. 2-4.). Command message transmission has been performed using QPSK over the Additive White Gaussian Noise (AWGN) channel. AWGN channel model variances are estimated from signal-to-noise ratio (SNR) values. The transmission parameters were set according to the 5G numerology. Each simulation was performed for 500 frames

and continued until the BER of 10^{-4} is achieved.

Figure 2. shows the LDPC coding of command message and obtained BER performances for variable code rates.

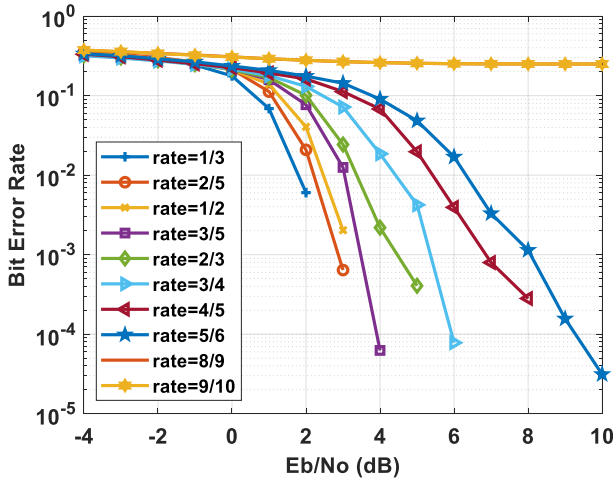


Fig. 2. LDPC - BER performance for variable code rates

BER performances for different code rates in case of Polar coding are given in Figure 3.

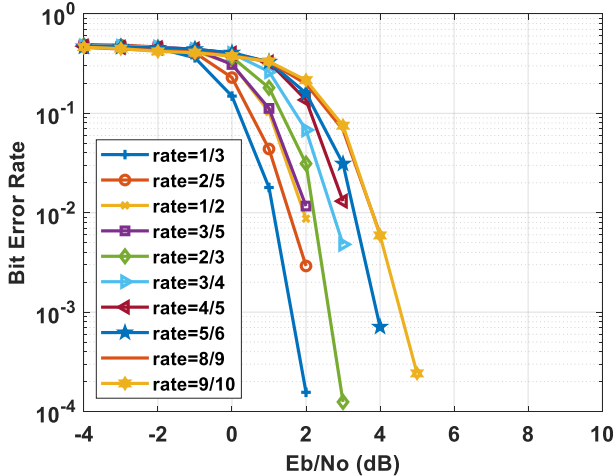


Fig. 3. Polar codes - BER performance for variable code rates

Figure 4 presents the comparative analysis of LDPC and Polar coding techniques in terms of the BER for several code rates. Rate matching function is set to enable BER analysis in the case of equal code rates for LDPC and Polar coded message.

All three figures (Fig. 2-4.) illustrate a typical curve - BER decreases with the increase of E_b/N_0 . The waterfall regions (regions where BER falls clearly after a certain E_b/N_0) for both coding schemes indicate that in the case of a Polar code application, the error correction requirements of BER of 10^{-4} can be achieved at lower E_b/N_0 , compared with LDPC code use. Another advantage of Polar codes over LDPC codes is a good error floor performance. The error floor region covers the region where performance flattens - BER does not fall as quickly as before. LDPC codes with good waterfall characteristics suffer most from the error floor problem. Fig. 4. clearly presents that Polar code outperforms the LDPC code

for all investigated code rates of $\{1/3, 1/2, 2/3, 5/6\}$, in case of transmitting the typical command message from base station to PMU device.

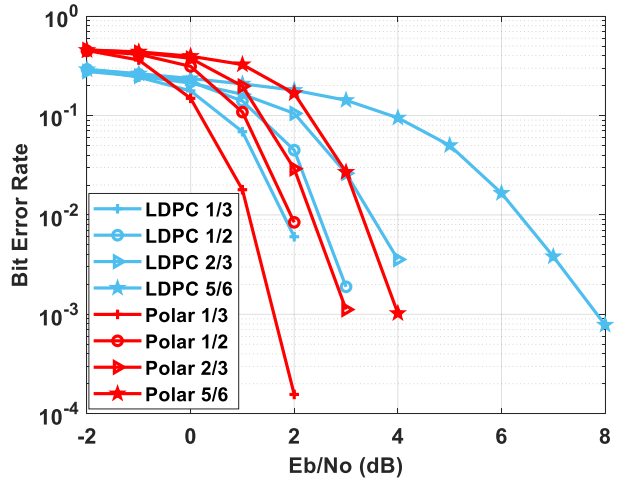


Fig. 4. BER performance for variable code rates: LDPC vs Polar coding

Simulation results confirm that Polar codes offer better error correction capabilities in comparison with LDPC codes in low BER area which is significant for transmitting short control messages. The use of Polar coding for command messaging in 5G-empowered SG applications has been justified according to error correction capability criterion.

IV. CONCLUSION

There is no doubt that 5G will completely revolutionize the entire energy sector. An immense number of smart devices deployed in the SG vision will require fast and secure data exchange. 5G channel coding techniques will play a major role in achieving fast communication with minimum errors in a variety of 5G-empowered applications. In order to demonstrate the selection of the appropriate channel coding scheme, the transfer of a typical command message from the base station to the PMU device has been investigated. The BER results obtained using QPSK for communication over AWGN, as a function of the E_b/N_0 shows that the Polar code achieves superior BER performance compared to the LDPC code in case of the command message transmission. Based on the results, Polar codes have been recommended for the use in control channels in 5G-based SG applications, over which short messages, such as command message, could be transmitted with lower BER.

Future work will be focused on selecting an appropriate channel coding scheme for the other types of messages used for the exchange of measurement data between power system equipment. The evaluation of the performances and complexity of the LDPC and Polar codes is a quite challenging task due to their dependency on the underlying hardware and the decoding algorithm. These issues will be also the focus of further research.

REFERENCES

- [1] Z. B. Kaykac Egilmez, L. Xiang, R. G. Maunder, and L. Hanzo, "The Development, Operation and Performance of the 5G Polar Codes," in

- [1] *IEEE Communications Surveys & Tutorials*, vol. 22, no. 1, pp. 96-122, Firstquarter 2020, doi: 10.1109/COMST.2019.2960746.
- [2] S. Z. Asif, *5G Mobile Communications Concepts and Technologies*, Taylor & Francis Group, LLC, 2019
- [3] T. Rosenqvist and J. Sloof, *Implementation and evaluation of Polar Codes in 5G*, The author(s) and Karlstad University, 2019, [Online]: <https://www.diva-portal.org/smash/get/diva2:1323867/FULLTEXT01.pdf>
- [4] *Ultra-Reliable Low-Latency Communication (URLLC) - Support for high reliability and low latency services like autonomous driving*, EventHelix, [Online]: <https://medium.com/5g-nr/ultra-reliable-low-latency-communication-urllc-9b2505e81579>
- [5] T. Fehrenbach, R. Datta, B. Göktepe, T. Wirth and C. Hellge, “URLLC Services in 5G Low Latency Enhancements for LTE”, 2018, [Online]: <https://www.groundai.com/project/urllc-services-in-5g-low-latency-enhancements-for-lte/2>
- [6] H. Niyagama Gamage, *Waveforms and Channel Coding for 5G*. University of Oulu, Faculty of Information Technology and Electrical Engineering, Department of Communications Engineering. Master's thesis, 63 p., 2016.
- [7] M. Dhuheir and S. Ozturk, “Polar Codes Applications for 5G Systems”, *Journal of Institute Of Science and Technology*, Volume 34, Issue 3, 2018.
- [8] *How will 5G revolutionise the world of energy and communications?*, Drax, [Online]: <https://www.drax.com/technology/how-will-5g-revolutionise-the-world-of-energy-and-communications/>
- [9] H. C. Leligou, T. Zahariadis, L. Sarakis, E. Tsampasis, A. Voulkidis, and T. E. Velivassaki, “Smart Grid: a demanding use case for 5G technologies.” 2018 IEEE International Conference on Pervasive Computing and Communications Workshops (PerCom Workshops), Athens, 2018, pp. 215-220, doi: 10.1109/PERCOMW.2018.8480296.
- [10] M. Forcan, and M. Maksimović, “Cloud-Fog-based approach for Smart Grid monitoring”, *Simulation Modelling Practice and Theory*, Volume 101, 2020, 101988, ISSN 1569-190X, <https://doi.org/10.1016/j.simpat.2019.101988>.
- [11] M. Forcan, and M. Maksimović, “Fog Computing-Based Communication Systems for Modern Smart Grids”, In *Fog Computing: Theory and Practice* (eds A. Zomaya, A. Abbas and S. Khan), Wiley 2020, pp.347-369, doi: 10.1002/9781119551713.ch13.
- [12] M. Forcan, M. Maksimović and J. Forcan, “Cloud-based Approach for Real-time Monitoring of Smart Grid Topology”, 5th Jubilee Virtual International Conference on Science, Technology and Management in Energy - eNergetics, pp. 47-54, 2019.
- [13] *IEEE Standard for Synchrophasor Data Transfer for Power Systems - IEEE Std C37.118.2™-2011*, IEEE Power & Energy Society, 2011.
- [14] *Multiplexing and channel coding*, 3GPP TS 38.212, Dec. 2019
- [15] Z.R.M. Hajiyat, A. Sali, M. Mokhtar, and F. Hashim, “Channel Coding Scheme for 5G Mobile Communication System for Short Length Message Transmission”, *Wireless Pers Commun* 106, 377–400, 2019, <https://doi.org/10.1007/s11277-019-06167-7>
- [16] J. H. Bae, A. Abotabl, H.-P. Lin, K.-B. Song and J. lee, “An overview of channel coding for 5G NR cellular communications”, *APSIPA Transactions on Signal and Information Processing*, vol. 8, e17, pp. 1-14, 2019
- [17] B. Bertenyi, S. Nagata, H. Kooropaty, X. Zhou, W. Chen, Y. Kim, X. Dai and X. Xu, “5G NR Radio Interface”, *Journal of ICT*, Vol. 6 1&2, 31–58. River Publishers. 2018, doi: 10.13052/jicts2245-800X.613
- [18] R.G. Gallager, *Low-Density Parity-Check Codes*. Cambridge, MA: MIT Press, 1963
- [19] D.J.C. MacKay, and R. M. Neal, “Near Shannon limit performance of low density parity check codes.” *Electron. Letters*, Vol.32, August 1996, 1645-1646 (reprinted with printing errors corrected in Vol.33, 457–458)
- [20] M. Sybis, K. Wesolowski, K. Jayasinghe, V. Venkatasubramanian, and V. Vukadinovic, “Channel Coding for Ultra-Reliable Low-Latency Communication in 5G Systems,” 2016 IEEE 84th Vehicular Technology Conference (VTC-Fall), Montreal, QC, 2016, pp. 1-5, doi: 10.1109/VTCFall.2016.7880930.
- [21] T. Strutz, “Low-Density Parity-Check codes— An introduction”, 2010-2014, 2016, [Online]: http://www1.hft-leipzig.de/strutz/Kanalcodierung/lpsc_introduction.pdf
- [22] X. Lin et al., “5G New Radio: Unveiling the Essentials of the Next Generation Wireless Access Technology,” in *IEEE Communications Standards Magazine*, vol. 3, no. 3, pp. 30-37, September 2019, doi: 10.1109/MCOMSTD.001.1800036.
- [23] Matlab R2019b, [Online]: https://www.mathworks.com/products/new_products/release2019b.html
- [24] *KT 5th Generation Radio Access; Physical Layer; Multiplexing and channel coding (Release 1)*. TS 5G.212 v2.3 (2016-9), KT PyeongChang 5G Special Interest Group (KT 5G-SIG); [Online]: https://m.corp.kt.com/data/kthome/business/kt5g/5G_212_v2.3.pdf
- [25] E. Arikan, “Channel polarization: A method for constructing capacity-achieving codes for symmetric binary-input memoryless channels.” *IEEE Transactions on Information Theory*, 55(7):3051–3073, July 2009. ISSN 0018-9448. doi:10.1109/TIT.2009.2021379.
- [26] E. Dahlman, S. Parkvall and J. Skold, *5G NR: The Next Generation Wireless Access Technology*, Elsevier, 2018

GPU-accelerated simulation environment for performance of relay signal adopting DF technique influenced by η - μ fading

Selena Vasić, Nenad Petrović, Stefan Panić, Dejan Milić, Suad Suljović

Abstract — In this paper, the performance of cellular communication system operating over η - μ fading channel, is considered. Using a Decode-and-Forward (DF) multi-hop relay system transmission performances can be enhanced. The closed-form expression for the outage probability (P_{out}) of the system has been derived. In the proposed system, the transmission time has been divided into two phases to be used by the decode and forward protocol. In the first phase, the source transmits its data whereas the relays and destination nodes are in receiving mode. In the second phase relay communicates to destination point by sending the recoded information. Moreover, we introduce a GPU-enabled simulation tool to illustrate how the derived expression within scenarios related to smart city mobile networks. According to the achieved results, leveraging GPU significantly accelerates fading calculation for this kind of analysis.

Index Terms— η - μ fading; Decode-and-Forward system; GPGPU; Cumulative distribution function (CDF); Outage probability (P_{out}); Smart city; Quality of Service (QoS).

I. INTRODUCTION

In cellular communications, on its path between transmitter and receiver, signal undergoes multiple degrading effects (such as fading, shadowing and interferences). Fading is one of the main causes of performance degradation of the receiver. The multipath (short-term) fading can be modeled with several distributions such as: Rayleigh, Rice, Nakagami- m , Weibull, η - μ or k - μ [1]. There are many different techniques engaged in mitigating fadding effects. Relay transmission has proven as practical communication technique providing efficient coverage in ad hoc and WLAN communication networks.

The impact of η - μ fading on wireless communication system performances is discussed in several papers. In [2], the first-order statistics for the distribution of η - μ and α - k - μ , eigenvalue functions and cumulative distribution functions are analysed. In [3], the outage probability of selection combining

Selena Vasić is with University Metropolitan, Faculty of Information Technologies, 63 Tadeuša Koščuška, 11000 Belgrade, Serbia, (e-mail: selena.vasic@metropolitan.ac.rs).

Nenad Petrović, Dejan Milić, and Suad Suljović are with Faculty of Electronic Engineering, University of Niš, 14 Aleksandra Medvedeva, 18000 Niš, Serbia, (e-mail: nenad.petrovic@elfak.ni.ac.rs, dejan.milic@elfak.ni.ac.rs, suadsara@gmail.com).

Stefan Panić is with University of Priština, Faculty of Natural Sciences and Mathematics, 29 Lole Ribara, 40000 Kosovska Mitrovica, Serbia, E-mail: stefanpnc@yahoo.com.

diversity receiver in the presence of η - μ short-term fading and Gama long-term fading is evaluated. Effective managing of radio environment assumes correct predictions and thorough description of the system's performance [4]. In order to cope with the increased demands in data rates in wireless networks, development of relay multi-hop transmission has been given significant attention. Multi-hop transmission is a communication technique that offers benefits in a wider coverage without involving high power on the transmitter side. Using spatial/multi-user diversions this approach facilitates communication through ad-hoc networks where nodes are able to communicate without central control. Multi-hop transmission is built on the concept where a mobile terminal transmits the signal between a base station (BS) and neighboring mobile stations (MS). We consider the case of a deep fading channel between the BS and the initial MS. As a result, source signals (S) on their way to destination (D) are transmitted over multiple paths [5].

Based on the complexity of the relay utilized there are two main types of multi-hop transmission systems: amplify-and-forward (non-regenerative) or decode-and-forward (regenerative) systems [6]. The first uses relays of a simpler design that are only able to amplify and forward the incoming signal without decoding it. They technically function as analog repeaters. On the other side, DF technique engages more complex relay that decodes the signal obtained from the source and then re-encodes it before the signal is sent to the destination. It regenerates the original information from the previous node before it retransmits the information to the next node [7]. In harshly affected channels, the relay takes more time to decode the received signal leading to a lack of efficiency and poor performance of the wireless telecommunication system [8]. The power of the transmitted signal at the relay can dominate the power of the useful signal at the relay. The strength of the emitted signal transmitted by relay using DF technique depends on the relay power constant c , while for $c > 1$ the signal is re-emitted with less power [9].

In this paper we consider a cellular communication system operating over η - μ fading channel. One of the statistical characteristics needed to evaluate the performance of the system operating in a fading environment is the system outage probability (P_{out}). It is needed in order to meet the requirements of Quality of Service (QoS). Once P_{out} is evaluated, it can be used in further calculations of the coverage of the observed cellular system. Within the coverage

area of the cellular system P_{out} is less than the predefined threshold. Also, it allows for evaluation of the minimum distance between two base stations such that a frequency area can be reused. The minimum distance between two base stations is co-channel interference (CCI) reduction factor and is used in the spectral analysis of the system [10]. It is also important to determine the model to select the area for frequency reuse. The outage probability can be obtained from the cumulative distribution function (CDF) of power $\eta\text{-}\mu$ random variables. Analytical and numerical results of this research can be used to design the optimal receiver for the cellular system operating over $\eta\text{-}\mu$ multipath fading channel.

II. MODEL OF SYSTEM

A model of regenerative relay system using DF technique is presented in Fig. 1. The system consists of source (S), relay (R) and receivers (D). Source-Relay link (S-R) is affected by $\eta_1\text{-}\mu_1$ fading with the power γ_1 . Link Relay- Destination (R-D) undergoes the influence of $\eta_2\text{-}\mu_2$ fading with the power γ_2 .

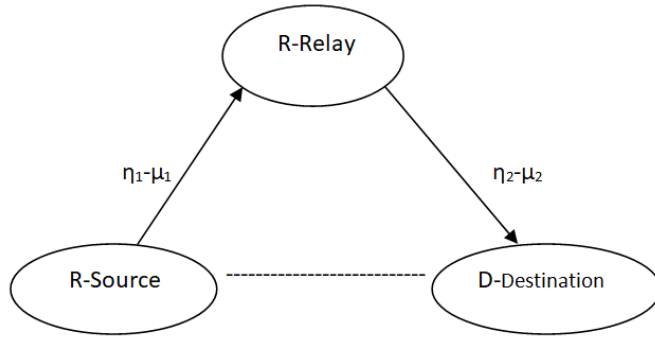


Fig. 1. Model of DF system under the influence of $\eta\text{-}\mu$ fading.

Multi-hop relaying technology is an effective solution in cellular and ad-hoc wireless communications systems. When engaging DF relay signal transmission, each transmission cycle has two stages: the one when the source S communicates with the relay and the destination point and the second when the relay decodes the signal from the source, re-encodes it and sends to the destination D.

In this paper, the value of the power constant of relay c is set to one. Using Mathematica and Origin software package the outage probability P_{out} of system will be first analytically derived and then presented graphically. The first order statistical parameters such as probability density function (PDF) and cumulative distribution function (CDF) of the signal affected by will be calculated. P_{out} is defined as the probability that the value of the SNR (signal-to-noise ratio) at reception is below the value of a predefined threshold (γ_{th}). Based on the obtained first- and second-order statistical characteristics at reception, analysis and performance evaluation of the entire wireless system without adoption of diversion techniques can be conducted [7].

The PDF of the signal x envelop modeled by $\eta\text{-}\mu$ fading, on either of the two links (S-R or R-D) can be written as [11]:

$$p_x(x) = \frac{4\sqrt{\pi}h^\mu x^{2\mu}}{\Gamma(\mu)H^{\mu-1/2}} \left(\frac{\mu}{\Omega} \right)^{\mu+1/2} e^{-\frac{2\mu h x^2}{\Omega}} I_{\mu-1/2} \left(\frac{2\mu H x^2}{\Omega} \right) \quad (1)$$

Here, x represents the instantaneous SNR, Ω is average SNR, μ is the number of clusters, H - is the parameter of the phase component, and h denotes fading parameter that describes the powers in phase. Furthermore, $I_v(\cdot)$ stands for modified Bessel function of the first kind, while $\Gamma(\cdot)$ stands for Gamma function. Variances of independent Gaussian processes in phase and quadrature, are random and in ratio defined by the following parameter: $\eta=E(X_{1i}^2)/E(X_{2i}^2)$.

Using the expression for modified Bessel function of the first kind: [12; 8.445]:

$$I_v(x) = \sum_{k=0}^{\infty} \frac{(x/2)^{v+2k}}{k! \Gamma(v+k+1)} \quad (2)$$

the expression (1) for signal's PDF, under the influence of $\eta\text{-}\mu$ fading becomes:

$$p_x(x) = \frac{4\sqrt{\pi}h^\mu}{\Gamma(\mu)} e^{-\frac{2\mu h x^2}{\Omega}} \sum_{i=0}^{+\infty} \frac{H^{2i} x^{4i+4\mu-1}}{\Gamma(i+\mu+1/2)i!} \left(\frac{\mu}{\Omega} \right)^{2i+2\mu} \quad (3)$$

By introducing the new parameter γ that describes the conversion of the signal strength to signal-to-noise ratio (SNR) we obtain the expression for the square of the instantaneous signal-to -noise value [13; 2.3]:

$$x^2 = \frac{\gamma}{w} \Omega, |J| = \frac{dx}{d\gamma} = \frac{1}{2\sqrt{\gamma}} \sqrt{\frac{\Omega}{w}} \quad (4)$$

In the above equation, w denotes the average SNR and J holds for Jacobian of the random variable transformation. Hence, the PDF of the instantaneous signal [13; 2.3] is:

$$p_\gamma(\gamma) = p_x(x)|J| = \frac{2\sqrt{\pi}h^\mu}{\Gamma(\mu)} e^{-\frac{2\mu h \gamma}{\bar{\gamma}}} \sum_{i=0}^{+\infty} \frac{H^{2i} \gamma^{2i+2\mu-1}}{\Gamma(i+\mu+1/2)i!} \left(\frac{\mu}{\bar{\gamma}} \right)^{2i+2\mu} \quad (5)$$

Furthermore, the cumulative distribution function (CDF) of the instantaneous SNR value [11] will be:

$$F_\gamma(\gamma) = \int_0^\gamma p(t)dt = \frac{\sqrt{\pi}}{\Gamma(\mu)} \sum_{i_1=0}^{\infty} \frac{H^{2i_1}}{2^{2i_1+2\mu-1} h^{2i_1+\mu}} \cdot \frac{1}{i_1! \Gamma(i_1+\mu+1/2)} \gamma^{\left(2i_1 + 2\mu, \frac{2\mu h}{\bar{\gamma}} \gamma \right)} \quad (6)$$

In the expression (6) γ (b, c) denotes a lower Gamma function. It can be represented by lower or complementary incomplete Gamma function $\Gamma(\alpha, x)$, and Gamma function $\Gamma(\cdot)$ [12; 8.356.3] as follows:

$$\gamma(n, x) = \Gamma(n) \left(1 - e^{-x} \sum_{k=0}^{n-1} \frac{x^k}{k!} \right) \quad (7)$$

Combining the last two expressions, the following form of the CDF of the SNR with $\eta\text{-}\mu$ distribution becomes:

$$F_\gamma(\gamma) = \frac{\sqrt{\pi}}{\Gamma(\mu)} \sum_{i_1=0}^{\infty} \frac{H^{2i_1} \Gamma(2i_1 + 2\mu)}{2^{2i_1+2\mu-1} h^{2i_1+\mu} i_1! \Gamma(i_1 + \mu + 1/2)} \cdot \left(1 - e^{-\frac{2\mu h}{\bar{\gamma}}} \sum_{i_2=0}^{2i_1+2\mu-1} \frac{1}{i_2!} \left(\frac{2\mu h}{\bar{\gamma}} \gamma \right)^{i_2} \right) \quad (8)$$

The outage probability of the system (P_{out}) for the observed DF relay signal transmission is given by [9; 2.34]:

$$P_{out} = \int_0^{+\infty} P_\mu \left[\gamma_1 \left(\frac{\gamma_{th} c}{\gamma_1 - \gamma_{th}} \middle| \gamma_2 \right) p_{\gamma_1}(\gamma_1) d\gamma_1 \right] = \int_0^{+\infty} F_{\eta-\mu} \left(\frac{\gamma_{th}(c + \gamma_2)}{\gamma_2} \right) p_{\eta-\mu}(\gamma_2) d\gamma_2 \quad (9)$$

In the above formula, the power constant of the DF relay is denoted as c . Combining the expressions (5) and (8) with the expression (9), we can obtain the expression for the P_{out} of a system at the receiver side:

$$P_{out} = \frac{\pi}{\Gamma^2(\mu)} \sum_{i_1=0}^{+\infty} \sum_{i_3=0}^{+\infty} \frac{H^{2i_1+2i_3} \Gamma(2i_1 + 2\mu)}{2^{2i_1+2\mu-2} \Gamma(i_1 + \mu + 1/2) \Gamma(i_3 + \mu + 1/2)} \cdot \frac{(\mu/\bar{\gamma})^{2i_3+2\mu}}{h^{2i_1} i_1! i_3!} \left[\int_0^{+\infty} \gamma_2^{2i_3+2\mu-1} e^{-\frac{2\mu h}{\bar{\gamma}} \gamma_2} d\gamma_2 - e^{-\frac{2\mu h \gamma_{th}}{\bar{\gamma}}} \sum_{i_2=0}^{2i_1+2\mu-1} \frac{1}{i_2!} \left(\frac{2\mu h \gamma_{th}}{\bar{\gamma}} \right)^{i_2} \int_0^{+\infty} \gamma_2^{2i_3-i_2+2\mu-1} (c + \gamma_2)^{i_2} e^{-\frac{2\mu h}{\bar{\gamma}} \gamma_2} e^{-\frac{2\mu h \gamma_{th}}{\bar{\gamma}}} d\gamma_2 \right]. \quad (10)$$

In Section III, Fig. 2 depicts the P_{out} on the receiver side (destination D), obtained from the expression (10). P_{out} is given in terms of the mean SNR, denoted by w . The parameters η and μ have been varied in order to observe their effect on the P_{out} .

III. NUMERICAL AND GRAPHICAL RESULTS

In order to observe the effect of fading severity, analytical results are presented graphically in the Fig. 2. The graph of the system P_{out} is obtained under the following conditions on the receiver side: $\mu_1=\mu_2=\mu$, $\eta_1=\eta_2=\eta$, $\gamma_{th1}=\gamma_{th2}=\gamma_{th}$, $\bar{\gamma}_1=\bar{\gamma}_2=\bar{\gamma}=w$.

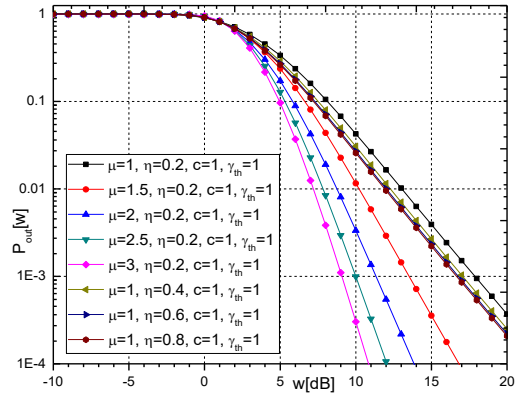


Fig. 2. P_{out} of system, for different values of parameters η and μ .

The outage probability of the system is given by the expression (10). With the increase of parameters μ and η , the P_{out} of system decreases for positive values of the mean SNR, (w in dB) and the system tends to increase its stability. Using program Mathematica, it is calculated that, for example, at $w=5$ dB, for the following values of parameters: $\mu=2$ ($c=\gamma_{th}=1$, $\eta=0.2$) the outage probability is: $P_{out}=17.22\%$, while for $\eta=0.6$ ($\mu=c=\gamma_{th}=1$,) it increases to $P_{out}=27.00\%$. Due to fact that outage probability can be calculated only with predefined numerical error (due to double infinite sum), around 40 summands were required to achieve precise calculation.

IV. SOFTWARE SIMULATION ENVIRONMENT

In this paper, we adopt the derived expression within a software environment which enables modeling and simulation of scenarios related to mobile networks in context of smart cities. The tool is run in web browser and developed relying on JavaScript¹ and HTML² on the front end, while Node.js³ is used for the back end. The implementation of these tools is built upon the previous work regarding the simulation of various aspects related to energy efficiency [14], autonomous vehicles [15], fog computing [16] and resource planning in smart cities [17]. In addition to previous work, Three.js⁴ is adopted in this paper to enable 3D graphics inside the web browser and aspects of mobile network modeling and simulation introduced. The layout of the web-based tool is displayed in Fig. 3. In given screenshot, the mobile network consumers are autonomous cars, while the antenna represents base station providing the mobile network service.

¹ <https://www.w3schools.com/js/>

² <https://www.w3schools.com/html/>

³ <https://nodejs.org/en/>

⁴ <https://threejs.org/>



Fig. 3. Screenshot of a web-based tool for modeling and simulation of smart city mobile network scenarios.

First, user creates a mobile network model using the graphical 3D environment run in a web browser. The aspects related to network infrastructure, terrain (obstacles), communication channel and service consumers are taken into account [18]. The value of Quality of Service (QoS) parameter is calculated based on P_{out} . The user-defined mobile network model together with QoS values is used as input of linear optimization process with respect to linear program presented in [18]. Finally, linear optimization process outputs the optimal base station configuration which can be further translated to Software Defined Radio (SDR) commands. In Fig. 4, an overview of the proposed modeling and simulation environment for network planning is given. However, in this paper, we focus on GPU-enabled fading calculation.

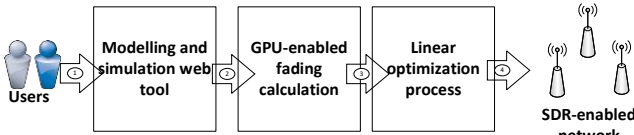


Fig. 4. Overview of software environment: 1-Drawing network model diagram 2-User-defined network model 3-QoS values 4-SDR commands

General-purpose GPU (GPGPU) programming has goal to speed-up the calculations processing huge streams of data in non-graphic applications relying on GPU. It has been approved as effective for fading effect calculation speed improvement [19]. In this paper, NVIDIA CUDA [20] is adopted for GPU-enabled calculation of P_{out} , which is further leveraged for QoS determination for a given location (l) at time point $t+1$, according to the formula:

$$Q_0 S_l(t+1) = Q_0 S_l(t)(1 - P_{out}) \quad (11)$$

The structure of CUDA kernel used for QoS calculation is illustrated as a pseudo-code in Fig. 5.

```

__global__ void qos_factor(Location* l, float* qos_new, float *qos_old)
{
    int tid = threadIdx.x + blockIdx.x * blockDim.x;
    while (tid < N)
    {
        qos_old[tid] = (1-Pout(l[tid]))*qos_old[tid];
        tid += blockDim.x * gridDim.x;
    }
}
  
```

Fig. 5. Pseudo-code of CUDA kernel for QoS factor determination.

According to the achieved results, the GPU-enabled calculation of QoS based on P_{out} , is around 54 times faster than equivalent task done on CPU using Origin and 28 times than our previous work from [21].

Finally, the linear optimization model's objective function [19] aims to minimize the energy consumption, distribution cost and quality of service for base stations, given as:

$$\text{minimize} \sum_{i \in \text{BaseStation}, j \in \text{Location}} x[i, j] e_cost[i] d_cost[i, j] qos_drop[i, j] \quad (12)$$

In expression (12), $x[i, j]$ is a decision variable, $e_cost[i]$ is energy consumption of a given $\text{BaseStation}[i]$, $d_cost[i, j]$ represents energy distribution cost at $\text{Location}[j]$, while $qos_drop[i, j]$ is a ratio between the maximum QoS parameter value and the estimate based on fading calculation for $\text{BaseStation}[i]$ at $\text{Location}[j]$.

V. CONCLUSION

In this paper, the performance of cellular communication system operating over $\eta\text{-}\mu$ fading channel has been considered. $\eta\text{-}\mu$ fading model contemplates a general non-line-of sight (NLOS) propagation scenario. By setting two shape parameters η and μ , this model includes some classical fading distributions as particular cases, e.g. Nakagami- q (Hoyt), One-Sided Gaussian, Rayleigh and Nakagami- m . The outage probability (P_{out}) exemplifies a key performance in cellular communications under fading effects. Considering the relevancy of $\eta\text{-}\mu$ fading channels, the obtained analytical expression for the P_{out} is of significant interest in analysis of channel performances. We have analyzed the transmission that engages the regenerative Decode-and-Forward (DF) relaying in a $\eta\text{-}\mu$ fading environment, without applying diversion techniques. Specifically, the outage probability P_{out} of the cellular relay telecommunication system has been considered. It is observed that an increase in parameter μ , (i.e. a decrease in the number of scattering clusters), leads to improved system performance. With increase of parameter μ , the probability density function becomes more narrow and tends toward a delta function at the position of the mean strength of the signal.

Furthermore, when μ tends to infinity, no-fading scenario is considered. In the observed relay transmission without combining, the outage probability depends mostly on the receiver sensitivity threshold. We have set the parameter c , that describes the amplification (the output power of the DF relay) to one. In addition, an illustration of the real-life scenario is achieved through introducing a web browser tool

for modeling and simulation of smart cities environment. The adoption of GPGPU significantly speeds up the fading effect calculation. To the best of authors' knowledge, similar analysis has not been presented in literature which signifies the contribution of this paper.

ACKNOWLEDGMENT

This work has been supported by the Ministry of Education, Science and Technological Development of the Republic of Serbia.

REFERENCES

- [1] David M.Jimenez and Jose F. Paris , "Outage Probability Analysis for η - μ Fading Channels", IEEE Communications letters, vol.14, no. 6, 2010.
- [2] P. Spalević, S. Panić, "Analysis of wireless transmission Improvement in specific propagation environments: Monograph", Kosovska Mitrovica, ISBN 978-86-80893-52-5, 2014.
- [3] Yacoub, M. D. (2007). The k - μ distribution and the η - μ distribution. *IEEE Communications Letters*, vol.9, no. 10, pp. 871-873.
- [4] W .C. Y. Lee, Mobile communications engineering: New York, Mc Graw-Hill, 2001.
- [5] M. Pätzold, Mobile Fading Channels Modelling, Analysis and Simulation. New York: John Wiley & Sons, 2nd ed. 2005.
- [6] B. Sunil and Nandana B. T., "Performance analysis and comparison of AF and DF relaying systems in Rayleigh fading channel considering poisson interference field," Inter. Conference on Innovations in Inf., Embedded and Communication Systems (ICIECS), Coimbatore, *ICIECS*, pp. 1-5, 2015, doi: 10.1109/ICIECS.2015.7192915.
- [7] J. Hu and N. C. Beaulieu, "Performance Analysis of Decode-and-Forward Relaying with Selection Combining", *IEEE Commun. Lett*, Vol. 11, No. 6, pp. 489-491, Jun. 2007.
- [8] K. Wannatrong, M. A. Hayat, Performance analysis of OSTBC with Hybrid Decode-Amplify and Forward relay network: Department of Electrical Engineering, Blekinge Institute of Technology Karlskrona, Sweden, September 2012.
- [9] S. N. Suljović, "Analysis of performance improvement in relay communication systems from the aspect of diversity combining techniques", Ph.D. dissertation, University of Niš, Faculty of Electronic Engineering, 2019.
- [10] M. Alouini and A. Goldsmith, "Area Spectral Efficiency of Cellular Mobile Radio Systems", *IEEE Transactions on Vehicular Technology*, ISSN: 0018-9545, vol. 48, no. 4, pp. 1047-1065, 1999.
- [11] G. V. Milovanović, S. Suljović, S. R. Panić, I. Kalčo, and M. H. Stefanović, "Efficient Numerical Methods for Analysis of Square Ratio of k - μ and η - μ Random Processes with Their Applications in Telecommunications", *Mathematical Problems in Engineering*, vol. 2018, Article ID 4967613, 9 pages, 2018.
- [12] I. S. Gradshteyn and I. M. Ryzhik, *Tables of Integrals, Series and Products* Academic. New York: 1980.
- [13] S. Panić, M. Stefanović, J. Anastasov and P. Spalević: Fading and Interference Mitigation in Wireless Communications, Taylor & Francis Publishing group, CRC Press, New York, USA, ISBN 978-14665-0841-5, 2013.
- [14] N. Petrović, Đ. Kocić, "Data-driven Framework for Energy-Efficient Smart Cities", *Serbian Journal of Electrical Engineering*, Vol. 17, No. 1, Feb. 2020, pp. 41-63, 2020. <https://doi.org/10.2298/SJEE2001041P>.
- [15] N. Petrović, Đ. Kocić, "Adopting linear optimization to support autonomous vehicles in smart city", *TELFOR* 2019, pp. 1-4, 2019. <https://doi.org/10.1109/TELFOR48224.2019.8971185>
- [16] N. Petrović, "Approach to Dynamic Adaptivity Simulation in Fog Computing Scenarios", *TELSIKS* 2019, pp. 58-61, 2019. <https://doi.org/10.1109/TELSIKS46999.2019.9002322>
- [17] N. Petrović, Dj. Kocic, "Framework for Efficient Resource Planning in Pandemic Crisis", *CIIT* 2020, pp. 1-6, 2020.
- [18] N. Petrović, S. Koničanin, D. Milić, S. Suljović, and S. Panić, "GPU-enabled Framework for Modelling, Simulation and Planning of Mobile Networks in Smart Cities", *ZINC* 2020, pp. 1-6, 2020, <https://doi.org/10.1109/ZINC50678.2020.9161773>
- [19] N. Petrović, S. Koničanin, D. Milić, S. Suljović, and S. Panić, "GPU-enabled Framework for Modelling, Simulation and Planning of Mobile Networks in Smart Cities", *ZINC* 2020, pp. 1-6, 2020, <https://doi.org/10.1109/ZINC50678.2020.9161773>
- [20] A. F. Abdelrakez et al., "A Novel Architecture using NVIDIA CUDA To speed up Simulation of Multi-Path Fast Fading Channels", pp. 1-5, 2009.
- [21] J. Sanders, E. Kandrot, *CUDA By Example: An Introduction to General-Purpose GPU Programming*, Addison-Wesley, 2011.
- [22] D. Milić, S. Suljović, N. Petrović, S. Koničanin, and S. Panić, "Software Environment for Performance of Relay Signal by DF Technique Influenced by k - μ Fading", *INFOTEH* 2020, pp. 1-4, 2020, <https://doi.org/10.1109/INFOTEH48170.2020.9066304>

Pozicioniranje u NLOS uslovima primjenom gravitacionog pretraživačkog algoritma

Stivo Lukić i Mirjana Simić

Apstrakt—Najveći problem u realizaciji lokacijskih usluga predstavlja pozicioniranje u uslovima blokade direktnе putanje između mobilne stanice MS (*Mobile Station*) i bazne stanice BS (*Base Station*), odnosno pozicioniranje u tzv. NLOS (*Non-Line of Sight*) propagacionom okruženju. U ovom radu prikazan je postupak poboljšanja tačnosti lociranja MS u čelijskim radio mrežama u NLOS uslovima, zasnovan na TOA (*Time of Arrival*) orijentisanom ML (*Maximum Likelihood*) estimatoru uz primjenu odabranog metaheurističkog metoda optimizacije.

Ključne reči—TOA metode; NLOS propagacija; ML estimator; metaheuristike; GSA algoritam.

I. UVOD

Kod višeputnog prostiranja radio talasa u čelijskim radio sistemima (*multipath propagation*), čest je slučaj da direktna talasna komponenta koja definiše LOS (*Line of Sight*) propagaciju, izostaje zbog opstrukcije od prepreka na prenosnom putu između predajnika i prijemnika. Pomenuti fenomen je poznat kao NLOS (*Non-Line of Sight*) transmisija radio signala i redovna je pojava u urbanom propagacionom okruženju. Ako se rastojanje između mobilne stanice MS (*Mobile Station*) i bazne stanice BS (*Base Station*) procjenjuje na osnovu vremena prispjeća referentnog radio signala za pozicioniranje TOA (*Time of Arrival*) u prijemnik MS ili BS, onda je isto proporcionalno izmjereno vremenskom kašnjenju direktnog talasa u odnosu na trenutak emitovanja signala sa predajnika BS ili MS (uz podrazumijevanu vremensku sinhronizaciju između MS i BS). Međutim, u NLOS okruženju, ne određuje se vremensko kašnjenje direktne komponente (*LOS path*), već neke druge, najčešće prve značajne primljene talasne komponente koja od ostalih NLOS komponenti ima i najmanje slabljenje (najveću snagu). Posljedica toga je uvijek pozitivna greška (*NLOS error*) u procjeni rastojanja između bazne stanice i mobilnog terminala (NLOS trajektorije uvijek su duže od direktnе), a time i veća greška u izračunatoj poziciji mobilnog korisnika [1]. Zbog toga su *TOA-based* metode pozicioniranja veoma osjetljive na NLOS propagaciju čiji doprinos unesene greške u određivanju lokacije MS može iznositi reda nekoliko stotina metara [2]. Iz navedenog razloga, NLOS se nameće kao glavni faktor degradacije performansi nekog sistema za pozicioniranje. Predmet istraživanja koji će biti razmotren u ovom radu jeste napredni mehanizam za eliminaciju NLOS grešaka mjerena

Stevo Lukić – MTEL a.d. Banja Luka, Vuka Karadžića 2, 78000 Banja Luka, Republika Srpska, BiH (e-mail: stevo.lukic@mtel.ba).

Mirjana Simić – Univerzitet u Beogradu, Bulevar Kralja Aleksandra 73, 11020 Beograd, Srbija (e-mail: mira@etf.rs).

rastojanja (*range estimation*), baziran na metaheurističkom konceptu optimizacije u varijanti 2D pozicioniranja sa mirujućom, odnosno statičnom MS.

II. ML ALGORITAM ZA NLOS SCENARIO

Pretpostavimo nešto ekstremnije uslove kada su zbog problema čujnosti za pozicioniranje dostupne samo četiri BS (uslov za cirkularnu lateraciju je da ih ima najmanje tri). Nepoznate koordinate MS neka su obilježene sa (x, y) , a poznate koordinate i -te BS sa (x_i, y_i) , $i = 1 \dots 4$. Tada se izraz za tačnu udaljenost između MS i i -te BS može napisati u sljedećem obliku:

$$d_i = \sqrt{(x - x_i)^2 + (y - y_i)^2}, \quad i = 1 \dots 4. \quad (1)$$

Mjerni model za slučaj totalnog NLOS scenarija u kome su putanje između MS i svih BS bez direktne optičke vidljivosti, postavlja se kako slijedi:

$$r_i = ct_i = d_i + b_i + n_i, \quad i = 1 \dots 4. \quad (2)$$

pri čemu je r_i "izmjerena" udaljenost između MS i i -te BS dobijena mjeranjem parametra TOA (t_i), c je brzina svjetlosti, n_i je standardni mjerni šum i -tog mjerjenja modelovan kao Gausova slučajna promjenjiva nulte srednje vrijednosti i varijanse σ_i^2 ($n_i \sim \text{Norm}(0, \sigma_i^2)$), dok je $(b_i > 0)$ pozitivna NLOS greška mjerjenja rastojanja nastala usled deficit-a direktne putanje između MS i i -te BS. NLOS greška pozicioniranja određena je kao eksponencijalna slučajna promjenjiva srednje vrijednosti λ_i i varijanse λ_i^2 sa funkcijom gustine vjerovatnoće [3]:

$$p_{NLOS}(b_i) = \begin{cases} \frac{1}{\lambda_i} \exp\left(-\frac{b_i}{\lambda_i}\right), & b_i > 0 \\ 0, & \text{inache} \end{cases}. \quad (3)$$

Generalno, parametri λ_i su neodređeni, a eventualno su im poznate donje i gornje granice.

Kao što je pokazano u [4], ML estimacija nepoznate lokacije MS svodi se na minimizaciju sljedeće ciljne funkcije:

$$F(\boldsymbol{\theta}, \boldsymbol{\lambda}) = \sum_{i=1}^4 (w_i(\boldsymbol{\lambda}) f_i(\boldsymbol{\theta}, \boldsymbol{\lambda}))^2. \quad (4)$$

gdje su nepoznate upravljačke promjenjive predstavljene sa komponentama lokacionog vektora $\boldsymbol{\theta} = [x \ y]^T$ i vektora srednjih vrijednosti NLOS grešaka $\boldsymbol{\lambda} = [\lambda_1 \dots \lambda_4]^T$.

Vrijednosti članova koji definišu odgovarajuće reziduale $w_i(\boldsymbol{\lambda})f_i(\boldsymbol{\theta}, \boldsymbol{\lambda})$ iznose respektivno:

$$w_i(\boldsymbol{\lambda}) = \frac{1}{\sqrt{\sigma_i^2 + \lambda_i^2}} \quad (5)$$

$$f_i(\boldsymbol{\theta}, \boldsymbol{\lambda}) = r_i - \lambda_i - d_i, \quad \text{za } i = 1 \dots 4. \quad (6)$$

pri čemu je poznati vektor "izmjerenih" udaljenosti okarakterisan kao $\mathbf{r} = [r_1 \dots r_4]^T$.

Pored činjenice da je NLOS greška rastojanja pozitivna, ona je u pravilu i mnogo veća od mjernog šuma, iz čega proizilaze sledeće relacije:

$$b_i > 0 \wedge b_i \gg n_i \Rightarrow r_i \geq d_i, \quad i = 1 \dots 4. \quad (7)$$

Ako se tome pridoda i dopunska restrikcija:

$$\lambda_i^L \leq \lambda_i \leq \lambda_i^U, \quad i = 1 \dots 4. \quad (8)$$

tada (4) postaje optimizacioni problem sa ograničenjima (*constrained optimization problem*). Gornji pojednostavljeni pristup podrazumijeva da parametri λ_i ne zavise od tačne udaljenosti između MS i i -te BS (konstantni su nezavisno od položaja MS). I pored toga, evidentno je da uz postojanje dvije nepoznate koordinate MS i četiri nepoznata parametra λ_i , rješavanje problema (4) postaje izuzetno otežano. Da bi se izbjegla takva situacija, polazi se od nešto strožijeg pristupa po kome su srednje vrijednosti NLOS grešaka λ_i direktno proporcionalne tačnom rastojanju (1) kao u [5]:

$$\lambda_i = kd_i. \quad (9)$$

pri čemu je k nepoznati faktor za koga su na osnovu izraza (8) poznate minimalna i maksimalna vrijednost:

$$k^L \leq k \leq k^U, \quad i = 1 \dots 4. \quad (10)$$

Konačno, ciljna funkcija (4) poprima sledeći oblik:

$$F(\boldsymbol{\theta}') = \sum_{i=1}^4 \frac{1}{(\sigma_i^2 + k^2 d_i^2)} [r_i - (k + 1)d_i]^2. \quad (11)$$

gdje je $\boldsymbol{\theta}' = [x \ y \ k]^T$ prošireni nepoznati lokacioni vektor, dok su udaljenosti d_i prethodno određene sa (1). Suprotno od očekivanog, broj nepoznatih parametara je smanjen za pola. Nakon primjene adekvatne metode optimizacije procjena faktora k se ignoriše, a usvaja željena procjena koordinata MS koja je konkretno i od interesa.

U geometrijskom smislu, idealan slučaj pozicioniranja podrazumijeva da se lokacija MS nalazi u presjeku četiri TOA kružnice koje su analitički predstavljene sa (1) i čiji se centri nalaze u dostupnim BS. Iz (2) se vidi da realna procjena rastojanja sadrži grešku usled prisustva Gausovog mjernog

šuma i NLOS propagacije. Posljedica toga je da presjek četiri kruga nije tačka, već zona preklopa konačne površine oblika cirkularnog četverougla sa vrhovima poznatih koordinata $V(V_x, V_y)$, $V_1(V_{1x}, V_{1y})$, $W_1(W_{1x}, W_{1y})$ i $W(W_x, W_y)$ u kojoj se teoretski može naći MS, kao što je to ilustrovano na Sl. 1. Uzimajući u obzir (7), funkcija cilja (11) dobija sledeća ograničenja kojima je i markirana prikazana presječna površina:

$$(x - x_i)^2 + (y - y_i)^2 \leq r_i^2, \quad i = 1 \dots 4. \quad (12)$$

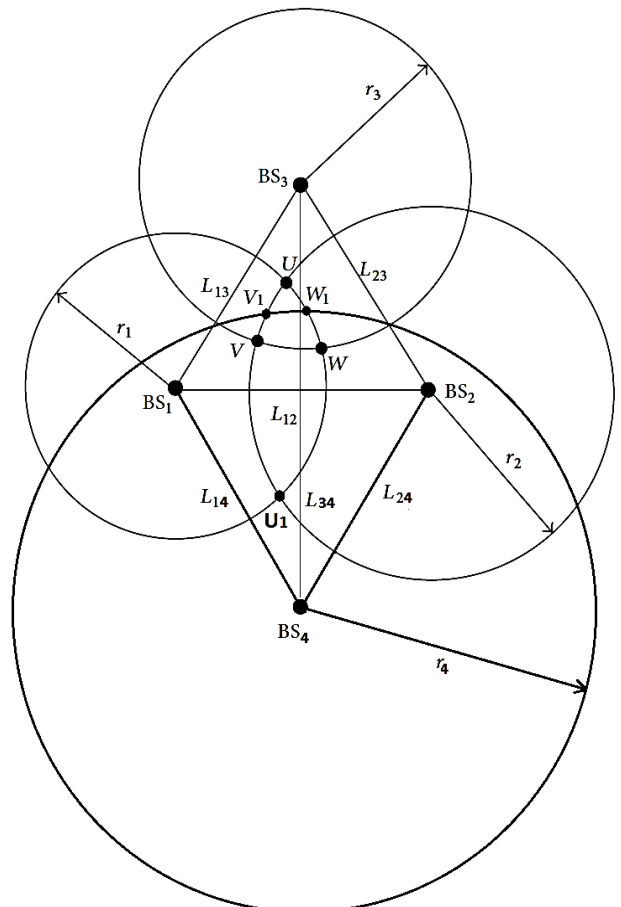
Dodatna ograničenja objektivne funkcije (11) odnose se na dozvoljene opsege upravljačkih promjenjivih. Imajući u vidu oznake sa Sl. 1., očigledno je da se koordinate MS mogu nalaziti unutar sledećih granica:

$$x_{\min} = \min\{V_x, V_{1x}, W_{1x}, W_x\}. \quad (13)$$

$$x_{\max} = \max\{V_x, V_{1x}, W_{1x}, W_x\}. \quad (14)$$

$$y_{\min} = \min\{V_y, V_{1y}, W_{1y}, W_y\}. \quad (15)$$

$$y_{\max} = \max\{V_y, V_{1y}, W_{1y}, W_y\}. \quad (16)$$



Sl. 1. Geometrijska konfiguracija TOA metode pozicioniranja sa 4 BS.

III. GRAVITACIONI PRETRAŽIVAČKI ALGORITAM

U inženjerskoj matematici postoji veliki broj metoda za uspješno rješavanje nelinearnih optimizacionih problema, odnosno minimizacije ciljne funkcije (11). Zbog svojih dobrih osobina, u ovom radu se koristi gravitacioni pretraživački algoritam GSA (*Gravitational Search Algorithm*), koji spada u savremene metaheurističke metode optimizacije. Glavna karakteristika ovih metoda je sukcesivno ponavljanje velikog broja operacija. Metaheuristike se mogu kvalifikovati kao uopšteni (nezavisan od problema) skup pravila koja se prilikom implementacije prilagođavaju svakom konkretnom problemu. Pri tome, performanse ovih metoda u dobroj mjeri zavise od pravilnog podešavanja odgovarajućih algoritamskih parametara [6]. Na žalost, za to podešavanje često ne postoje opšta pravila već se ono vrši na osnovu iskustva, odnosno principa "probaj-grijesi". U praksi se pokazalo da različite metaheurističke metode za relativno kratko vrijeme uspijevaju da pronađu dopustiva suboptimalna rješenja čak i za probleme složenije prirode, što je uticalo na njihovu široku primjenu zadnjih decenija. Osnovna prednost predloženih algoritama je njihova jednostavnost jer je metrika koja određuje kvalitet rješenja definisana preko algebarskih vrijednosti ciljne funkcije, što znači da za realizaciju ovih metoda nisu potrebne kompleksne derivacione procedure kao kod konvencionalnih gradijentnih postupaka. Nadalje, algoritmi su manje osjetljivi na izbor početnog rješenja, kao i na ograničenja ciljne funkcije. Nesumnjivo je da ovi algoritmi imaju veliki potencijal sa aspekta primjene na rješavanje optimizacionog problema određivanja lokacije korisnika u čelijskim radio mrežama [7].

Gravitacioni pretraživački algoritam GSA (*Gravitational Search Algorithm*) je relativno nova metaheuristika opisana u [8]. Kod GSA pretraživački agenti predstavljaju objekte čije se performanse izražavaju njihovim masama. Između objekata djeluju Njutnove privlačne gravitacione sile usled kojih se objekti globalno kreću ka objektima većih masa. Tokom procesa pretraživanja rješenja izračunavaju se mase objekata (na osnovu *fitness* vrijednosti ciljne funkcije), kao i njihova ubrzanja, brzine i pozicije tokom kretanja. Pozicija svake mase (agenta) u višedimenzionalnom prostoru pretraživanja predstavlja jedno rješenje problema. Posle izvjesnog vremena, svi objekti manjih masa biće privućeni od strane objekta najveće mase koji ujedno reprezentuje i optimalno rješenje problema minimizacije ciljne funkcije. Kao što je i uobičajeno, procedura startuje inicijalizacijom populacije agenata odnosno njihovih lokacija po principu slučajnog odabira unutar dopustivog prostora rješenja. U sistemu sa N mase (agenata), pozicija agenta i je definisana na sledeći način:

$$\mathbf{X}_i = [x_i^1, \dots x_i^k, \dots x_i^n], \quad i = 1 \dots N. \quad (17)$$

gdje je n dimenzija prostora pretraživanja, dok x_i^k označava poziciju agenta i u dimenziji k . Evaluacija najbolje i najgore *fitness* vrijednosti u tekućoj populaciji agenata $\text{best}(t)$ i $\text{worst}(t)$ respektivno, za problem minimizacije obavlja se kako slijedi:

$$\text{best}(t) = \min \text{fit}_i(t), \quad i = 1 \dots N. \quad (18)$$

$$\text{worst}(t) = \max \text{fit}_i(t), \quad i = 1 \dots N. \quad (19)$$

pri čemu $\text{fit}_i(t)$ predstavlja *fitness* vrijednost agenta i u trenutku (iteraciji) t . Inerciona masa i -tog agenta u iteraciji t , za svakog agenta se izračunava na osnovu sledećih izraza:

$$M_i(t) = \frac{m_i(t)}{\sum_{j=1}^N m_j(t)}. \quad (20)$$

$$m_i(t) = \frac{\text{fit}_i(t) - \text{worst}(t)}{\text{best}(t) - \text{worst}(t)}. \quad (21)$$

Ako se usvoji jednakost gravitacione i inercione mase, ukupna Njutnova gravitaciona sila koja djeluje na agenta i u dimenziji k u iteraciji t određuje se kao [8]:

$$F_i^k(t) = \sum_{j \in K_{\text{best}}, j \neq i} r_j G(t) \frac{M_i(t) M_j(t)}{R_{ij}(t) + \varepsilon} (x_j^k(t) - x_i^k(t)). \quad (22)$$

gdje je $G(t)$ gravitaciona konstanta u iteraciji t , $M_i(t)$ i $M_j(t)$ su mase agenata i i j , ε je mala konstanta i $R_{ij}(t)$ je Euklidска udaljenost između agenata i i j :

$$R_{ij}(t) = \|X_i(t), X_j(t)\|_2. \quad (23)$$

Gravitaciona konstanta je veoma važan faktor u implementaciji GSA jer se pomoću nje vrši kontrola preciznosti pretraživanja. S tim u vezi, gravitaciona konstanta se na početku algoritma postavlja na vrijednost G_0 koja tipično uzima vrijednost 100, da bi se onda smanjivala sa tekućom iteracijom t po eksponencijalnom zakonu:

$$G(t) = G_0 \exp(-\alpha \frac{t}{t_{\max}}). \quad (24)$$

pri čemu je α konstanta koju specificira korisnik i koja najčešće iznosi 20, a t_{\max} je maksimalan broj iteracija.

U (22) K_{best} predstavlja skup prvih K agenata sa najboljim *fitnessom*, najvećom masom (najvećom privlačnom silom) i najmanjom brzinom, dok je r_j slučajan broj u intervalu $[0,1]$. Ovaj skup se linearno smanjuje tokom vremena, počevši od vrijednosti N , tako da na kraju ostaje samo jedan agent. Parametri $G(t)$ i K_{best} definisani na prethodno opisani način uravnoteženo djeluju na procese globalnog i lokalnog pretraživanja prostora rješenja sa ciljem pronalaska globalnog optimuma. Shodno drugom Njutnovom zakonu kretanja, ubrzanje agenta i u iteraciji t , u dimenziji k se određuje kao količnik ukupne gravitacione sile koja djeluje na objekat i inercione mase:

$$a_i^k(t) = \frac{F_i^k(t)}{M_i(t)}. \quad (25)$$

Strategija pretraživanja po ovom konceptu se može opisati kao nalaženje sledeće brzine i pozicije agenta na osnovu njegove trenutne brzine, ubrzanja i pozicije [8]:

$$v_i^k(t+1) = r_i v_i^k(t) + a_i^k(t). \quad (26)$$

$$x_i^k(t+1) = x_i^k(t) + v_i^k(t+1). \quad (27)$$

gdje je kao i ranije r_i slučajan broj u intervalu $[0,1]$ koji se koristi da obezbijedi probabilistički karakter pretraživanja, x_i^k je pozicija agenta i u dimenziji k , v_i^k je brzina a a_i^k je ubrzanje agenta i u dimenziji k . Maksimalan broj iteracija t_{max} , veličina populacije N , početna vrijednost gravitacione konstante G_0 i vrijednost konstanti α i ε su kontrolni parametri kojima se utiče na performanse GSA algoritma.

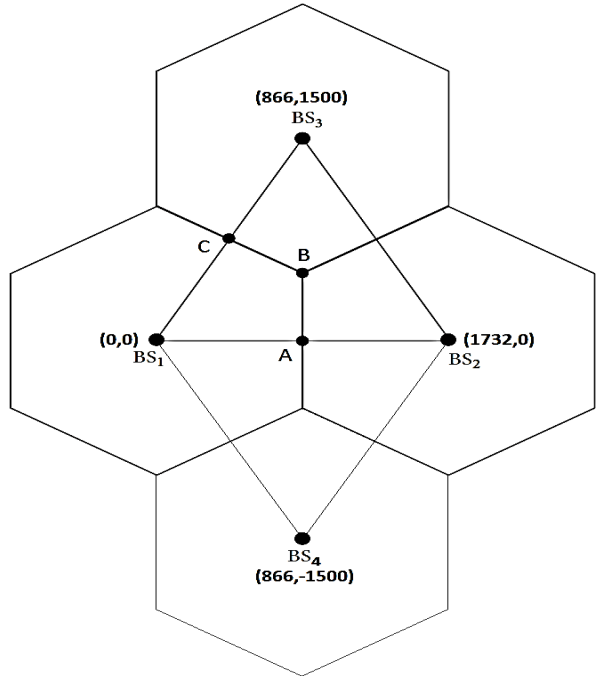
Postoje mnoge modifikacije standardnog GSA algoritma sa ciljem unapređenja sposobnosti lokalnog pretraživanja i globalne pretrage, kao i održavanja dobrog balansa između istih [9]. Efikasnost GSA algoritma može se povećati i hibridizacijom sa drugim metaheurističkim metodama kroz sinergiju i korišćenje njihovih najboljih karakteristika [10].

GSA algoritam se dobro pokazao kao metoda izbora za rješavanje problema lokalizacije u bežičnim senzorskim mrežama [11], kao i problema pronađaska optimalnih tokova snaga u elektroenergetskim distributivnim mrežama [12].

IV. REZULTATI SIMULACIJE

Simulacija je obavljena u makrocelularnom radio okruženju prikazanom na Sl. 2 kojeg čine četiri BS u simetričnoj geometrijskoj konstelaciji, tako da je uticaj parametra geometrijskog rasipanja preciznosti GDOP (*Geometric Dilution of Precision*) na tačnost pozicioniranja zanemarljiv. MS se može nalaziti u bilo kojoj tački oblasti ograničenoj sa tačkama BS1, A, B i C, u kojoj je zbog uticaja servisne BS1 izražen problem čujnosti sa udaljenijim BS. Jednostavnosti radi, uzeto je da između MS i servisne BS1 postoji LOS link ($\lambda_1 = 0$). Nasuprot tome, sa preostale tri BS ne postoji direktna optička vidljivost. Srednja vrijednost NLOS greške procijenjena je na 5% tačnih rastojanja. Standardna devijacija Gausovog mjernog šuma ista je za sve BS i iznosi 10 m. Koordinate dostupnih BS izražene u metrima postavljene su redom na vrijednosti LOS BS1 (0,0), NLOS BS2 (1732,0), NLOS BS3 (866,1500) i NLOS BS4 (866,-1500). Radijus heksagonalnih celija iznosi 1 km. Međutim, ovako postavljen simulacioni scenario ima i određena ograničenja. Naime, kada je distanca između MS i servisne BS1 malena, a istovremeno NLOS greška rastojanja "generisana" na ostalim BS izrazito velika, tada postoji mogućnost da TOA kružnica poluprečnika r_1 opisana oko servisne BS1 leži unutar preostale tri kružnice sa poluprečnicima r_2 , r_3 i r_4 . U tom slučaju predloženi algoritam ne bi bio primjenjiv. Prema tome, ako vrijede nejednačine $r_i > L_{1i} + r_1$ ($i = 2,3,4$), pri čemu je L_{1i} udaljenost servisne BS1 do susjednih BSi (Sl. 1), vrši se limitiranje iskačućih mjerena na iznos $r_i = L_{1i} + r_1$. Time je

zagarantovano da se bilo koje dvije TOA kružnice sijeku u najmanje jednoj tački čime je osigurana puna funkcionalnost algoritma [13].



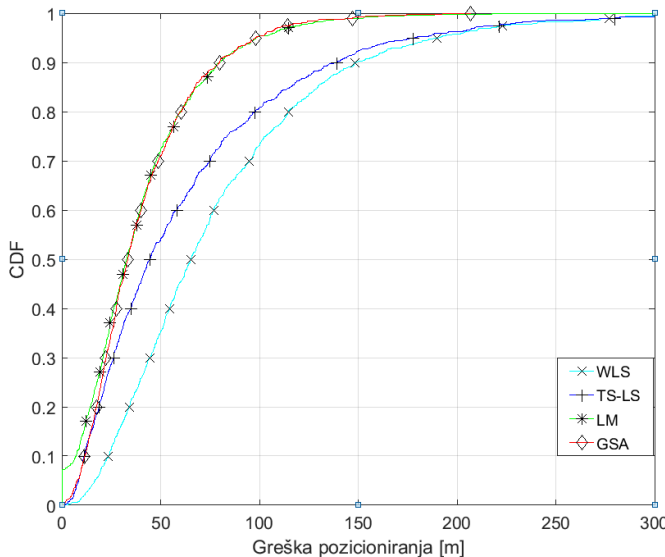
Sl. 2. Celularni sistem sa 4 BS.

Na bazi lokacione geometrije sa Sl. 2, izvršeno je ukupno 1000 nezavisnih TOA mjerena za različite položaje mirujuće MS za parametre propagacionog modela određenog sa (2), (3), (9) i (10). U Tabeli 1 prikazani su simulacioni parametri GSA algoritma.

TABELA I
PARAMETRI GSA ALGORITMA

Simulacioni parametar	GSA
Veličina populacije (N)	50
Dimenzija prostora pretraživanja (n)	3
Maksimalni broj iteracija (T)	100
Odnos srednje vrijednosti NLOS greške i udaljenosti (faktor k)	0.05
Minimalna vrijednost faktora k (k^L)	0.02
Maksimalna vrijednost faktora k (k^U)	0.10
Standardna devijacija Gausovog mjernog šuma (σ) [m]	10
Početna vrijednost gravitac. konstante (G_0)	100
Vrijednost konstante eksponencijalnog pada (α)	20

Inicijalna GSA populacija se smješta u oblast određenu sa (13)-(16). Predmetna procedura koristi tzv. kaznene (*penalty*) funkcije, čime se brzo odbacuju rješenja koja ne zadovoljavaju ograničenja (12). Veličina GSA populacije postavljena je na 50 agenata. Kao što je rečeno, početna vrijednost gravitacione konstante setuje se na vrijednost 100, a konstante eksponencijalnog pada na 20. Algoritam se zaustavlja nakon dostizanja maksimalnog broja od 100 GSA iteracija. Uspješnost GSA algoritma testirana je poređenjem sa klasičnim algoritmima pozicioniranja kao što su metod ponderisanih najmanjih kvadrata WLS (*Weighted Least Squares*) [14], iterativni algoritam najmanjih kvadrata zasnovan na Tejlorovom razvoju funkcija TS-LS (*Taylor-Series Least Squares Algorithm*) [5] i LM (*Levenberg-Marquardt*) gradijentni metod [15]. Na Sl. 3 prikazana je kumulativna funkcija raspodjele greške pozicioniranja CDF (*Cumulative Distribution Function*) za GSA i navedene komparativne algoritme.



Sl. 3. Kumulativna funkcija raspodjele greške pozicioniranja.

V. ZAKLJUČAK

Rezultati simulacione studije ukazuju da su performanse GSA algoritma po pitanju tačnosti pozicioniranja uporedive i neznatno bolje od LM gradijentnog algoritma koji se smatra standardom u problemima optimizacije. GSA algoritam je bolji od WLS i TS-LS algoritma. U 67% slučajeva tačnost pozicioniranja je ispod 50 m. Na osnovu naprijed iznijetih pokazatelja, kao i mogućnostima unapređenja osnovnog GSA algoritma kroz hibridizaciju sa ostalim metaheurističkim i egzaktnim metodama, isti može biti jedna od varijanti potencijalnog rješanja za TOA bazirane čelijske sisteme u NLOS situacijama.

LITERATURA

- [1] M. Simić, *Principi pozicioniranja u čelijskim radio sistemima*, Beograd, Srbija: Elektrotehnički fakultet, 2016.
- [2] M. I. Silventoinen, T. Rantalainen, "Mobile Station Emergency Locating in GSM," Proc. IEEE International Conference on Personal Wireless Communications, New Delhi, India, pp. 232-238, Febr., 1996.
- [3] L. J. Greenstein, V. Erceg, Y. S. Yeh, M. V. Clark, "A new path-gain/delay-spread propagation model for digital cellular channels," *IEEE Transaction on Vehicular Technology*, vol. 46, no. 2, pp. 477-484, May, 1997.
- [4] S. Lukić, M. Simić, "Eliminacija NLOS grešaka pozicioniranja u čelijskim radio mrežama primjenom ML estimatora sa ugradenim Levenberq-Marquardt algoritmom optimizacije," Zbornik radova 61. konferencije za ETRAN, Kladovo, Srbija, pp. TE 1.2. 1-6, Jun, 2017.
- [5] K. Yu, I. Sharp, Y. J. Guo, *Ground-based Wireless Positioning*, Chichester, England: John Wiley and Sons, 2009.
- [6] X.-S. Yang, *Nature-Inspired Optimization Algorithm*, London, England: Elsevier, 2014.
- [7] C. S. Chen, "A non-line-of-sight error mitigation method for location estimation," *International Journal of Distributed Sensor Networks*, vol. 13, no. 1, pp. 1-9, Jan., 2017.
- [8] E. Rashedi, H. Nezamabadi-pour, S. Saryazdi, "GSA: A Gravitational Search Algorithm," *Information Sciences*, vol. 179, no. 13, pp. 2232-2248, June, 2009.
- [9] S. Mirjalili, A. H. Gandomi, "Chaotic gravitational constants for the gravitational search algorithm," *Applied Soft Computing Journal*, vol. 53, pp. 407-419, 2017.
- [10] S. Mirjalili, S. Z. M. Hashim, "A new hybrid PSOGSA algorithm for function optimization," Proc. International Conference on Computer and Information Application, Tianjin, China, pp. 374-377, Dec., 2010.
- [11] R. Krishnaprabha, A. Gopakumar, "Performance of gravitational search algorithm in wireless sensor network localization," Proc. of 2014 IEEE National Conference on Communication, Signal Processing and Networking (NCCSN), Palakkad, India, pp. 1-6, Oct., 2014.
- [12] J. Radosavljević, M. Jevtić, N. Arsić, D. Klimenta, "Optimal power flow for distribution networks using gravitational search algorithm," *Electrical Engineering*, vol. 96, no. 4, pp. 335-345, July, 2014.
- [13] S. Venkatraman, J. Caffery Jr., H.-R. You, "A novel TOA location algorithm using LOS range estimation for NLOS environments," *IEEE Transactions on Vehicular Technology*, vol. 53, no. 5, pp. 1515-1524, Sept., 2004.
- [14] K. W. Cheung, H. C. So, W.-K. Ma, Y. T. Chan, "Least squares algorithm for Time of Arrival based mobile location," *IEEE Transactions on Signal Processing*, vol. 52, no. 4, pp. 1121-1130, April, 2004.
- [15] R. W. Ouyang, A. K. Wong, "An Enhanced TOA-based Wireless Location Estimation Algorithm for Dense NLOS Environments," Proc. IEEE Wireless Communications and Networking Conference, Budapest, Hungary, pp. 1-6, April, 2009.

ABSTRACT

The biggest problem in realization of location services is positioning in conditions of blocking the direct path between the mobile station (MS) and the base station (BS), or positioning in NLOS (Non-Line-Of-Sight) propagation environment. This paper presents the procedure for improving accuracy of MS locationing in cellular radio networks in NLOS conditions, based on the TOA (Time of Arrival) oriented Maximum Likelihood estimator using selected metaheuristic optimization method.

Positioning in NLOS conditions using gravitational search algorithm

Stevo Lukić and Mirjana Simić

Vremenska varijabilnost intenziteta električnog polja koje potiče od mikro LTE bazne stanice

Ivana Stojanović, Mladen Koprivica, Senior Member, IEEE, Nenad Stojanović,
Aleksandar Nešković, Senior Member, IEEE

Apstrakt—U radu je izvršena analiza promene intenziteta električnog polja koje potiče od mikro LTE (*Long Term Evolution*) bazne stанице, čije je merenje vršeno tokom sedam dana. Merenje je vršeno u frekvencijskom opsegu *downlink* smera komunikacije na centralnoj učestanosti od 1835 MHz. Realizacija intenzivnih merenja je izvršena u realnim uslovima rada mreže u *indoor* okruženju. Promene u intenzitetu električnog polja mogu se podeliti na dva perioda u toku jednog dana i to na period sa višim nivoima i češćom promenom intenziteta električnog polja (od 08:00 do 22:00 časova) i na period sa nižim nivoima i redim promenama u intenzitetu električnog polja (od 22:00 do 08:00 časova narednog dana). Razlike u intenzitetu električnog polja uočene su i između radnih dana (ponedeljak-petak) i neradnih dana (subota i nedelja). Izračunavanjem merne nesigurnosti odredena je vremenska varijabilnost intenziteta električnog polja. Izračunata merna nesigurnost koja je u opsegu od 1.71% do 11.26% pokazuje relativno malo odstupanje izmerenih vrednosti.

Ključne reči—Intenzitet električnog polja; LTE; mikro bazna stanica; *indoor* okruženje.

I. UVOD

ELEKTROMAGNETSKO polje nije nova pojava i postoji svuda oko nas u različitim oblicima. Prirodna i veštačka svetlost su takođe vidovi elektromagnetskog polja. Elektromagnetsko polje (*Electromagnetic Field*, EMF) može biti generisano od strane mobilnih telefona, baznih stanica, WiFi (*Wireless Fidelity*) uređaja, mikrotalasnih pećница, računara, raznih drugih telekomunikacionih uređaja i slično. Sva navedena zračenja dopiru do ljudskog tela i ostatka životne sredine. Deo tih zračenja se reflektuje, deo se apsorbuje, dok deo prolazi kroz ljudsko telo i druge objekte [1].

Bazne stanice mobilne telefonije svojim radom ne zagađuju životnu okolinu u konvencionalnom smislu, ali se kao i ostali radio i televizijski difuzni sistemi smatraju izvorima nejonizujuće radijacije. Iz tog razloga postoji potreba za merenjem takvih izvora radi provere usklađenosti sa normama

Ivana Stojanović – Telekom Srbija a.d., Bulevar umetnosti 16a, 11000 Beograd, Srbija i Elektrotehnički fakultet, Univerzitet u Beogradu, Bulevar kralja Aleksandra 73, 11120 Beograd, Srbija (e-mail: ivnvukanic@gmail.com).

Mladen Koprivica – Elektrotehnički fakultet, Univerzitet u Beogradu, Bulevar kralja Aleksandra 73, 11120 Beograd, Srbija (e-mail: kopra@etf.rs).

Nenad Stojanović – Vojna akademija, Univerzitet odbrane u Beogradu, Generala Pavla Jurišića Šturna 33, 11000 Beograd, Srbija (e-mail: nivzvk@hotmail.com).

Aleksandar Nešković – Elektrotehnički fakultet, Univerzitet u Beogradu, Bulevar kralja Aleksandra 73, 11120 Beograd, Srbija (e-mail: neshko@etf.rs).

kojima se ograničava uticaj na zdravlje ljudi.

Do sada su vršena brojna istraživanja o elektromagnetskom zračenju i njegovom uticaju na prirodnu sredinu. Rezultati izlaganja raznim telekomunikacionim signalima u toku 24 časa u školi i kući prikazani su u [2]. Mereni su intenziteti električnog polja za WiFi signale, signale mobilne telefonije, signale radio difuzije kao što su digitalna televizija i FM (*Frequency Modulation*) radio i signale koji potiču od DECT (*Digital European Cordless Telecommunications*) bežičnog fiksnog telefona. Merenja su vršena na pet lokacija u školama i pet lokacija u kućama. Rezultati su pokazali da najveće zračenje potiče od DECT telefona i WiFi uređaja, dok je nešto manje od signala mobilne telefonije, a najmanje od radio difuznih sistema. Pokazano je da zračenje zavisi od doba dana i količine korišćenja telekomunikacionih sistema u određenom periodu u toku tog doba dana. Analizirani su signali GSM (*Global System for Mobile Communications*), UMTS (*Universal Mobile Telecommunications Systems*) i LTE (*Long Term Evolution*) mobilnih tehnologija. Slično istraživanje vršeno je i u [3]. Vršeno je merenje i poređenje zračenja velikog broja telekomunikacionih signala. Merenja su vršena u urbanom okruženju, u glavnom gradu Švedske, Stokholmu, na više od 30 lokacija. Signali različitih tehnologija mobilne telefonije su imali nešto viši nivo električnog polja u odnosu na signale radio i televizijskih difuznih sistema i drugih telekomunikacionih sistema. Merenja su vršena u *outdoor* okruženju za razliku od merenja u [2], gde su merenja vršena u *indoor* okruženju.

Veliki broj različitih telekomunikacionih signala meren je u jednom sveobuhvatnom istraživanju u tri Evropske zemlje – Holandiji, Belgiji i Švedskoj, u različitim okruženjima i na velikom broju lokacija [4]. Merenja su vršena na 311 lokacija od čega je 68 bilo u *indoor* okruženju, a 243 u *outdoor* okruženju. Analizirane su merene vrednosti sa lokacija različite gustine naseljenosti i pokazano je da u *outdoor* okruženju najveći intenzitet električnog polja potiče od GSM baznih stanica, dok je u *indoor* okruženju to slučaj za DECT telefon.

Autori su u [5] upoređivali zračenja koja potiču od GSM i LTE baznih stanica. Pokazano je da je izlaganje elektromagnetskom zračenju, kada se posmatra gustina energetskog fluksa, tri puta niže kod LTE bazne stанице u odnosu na GSM baznu stanicu.

Istraživanja o uticaju zračenja koje potiče od mobilnog telefona koji se nalazi neposredno uz korisnika su takođe vršena. Utvrđeno je da je srednja vrednost intenziteta električnog polja koja potiče od LTE terminalnog uređaja

manja od 1% maksimalne izmerene vrednosti [6]. Istraživanje zračenja LTE mobilnih terminala vršeno je i u laboratorijskim uslovima. Ispitivano je na koji način utiče prag termičkog bola na mlade, zdrave osobe [7].

U ovom radu su prikazani rezultati merenja vremenske varijabilnosti intenziteta električnog polja u toku jedne sedmice, u frekvencijskom opsegu *downlink* smera komunikacije, koje potiče od mikro LTE bazne stanice. Analiza je izvršena kroz grafičke prikaze i izmerene i izračunate numeričke vrednosti.

U sekciji II rada date su osnovne karakteristike signala koji potiče od LTE bazne stanice. Sekcija III daje kratak pregled dosadašnjih dugoročnih merenja signala mobilne telefonije u Srbiji. U sekciji IV prikazana je merna oprema koja je korišćena i metodologija merenja. U sekciji V prikazani su najvažniji rezultati i njihova analiza. U sekciji VI dati su zaključci i mogući pravci budućeg istraživanja.

II. KARAKTERISTIKE LTE SIGNALA

Fizički sloj LTE signala u frekvencijskom opsegu *downlink* strane komunikacije zasniva se na OFDMA (*Orthogonal Frequency Division Multiple Access*) tehnologiji, koja dodeljuje radio resurse većem broju korisnika što za rezultat daje robusniji sistem sa povećanim kapacitetom. Multipleksiranjem korisničkih podataka malog protoka na širem kanalu postiže se povećanje kapaciteta telekomunikacionog kanala, dok se robusnost postiže raspoređivanjem korisničkog saobraćaja po učestanostima kako bi se izbegla uskopojasna interferencija i feding usled višestruke propagacije [8].

U vremenskom domenu, LTE transmisija je organizovana u radio frejmove dužine od po 10 ms. Ovakav frejm je podeljen na 10 podfrejmova dužine po 1 ms. Zatim se podfrejm deli na dva slota trajanja 0.5 ms svaki. A slot se sastoji od 7 ili 6 OFDM simbola, u zavisnosti da li se koristi normalni ili prošireni ciklični prefiks (*Cyclic Prefix*) [9].

Pored opšte poznatog kratkoročnog fedinga još nekoliko efekata ima uticaj na snagu elektromagnetskog polja u mobilnim mrežama. Najčešće spominjani efekti su: saobraćajno opterećenje, automatska regulacija snage i neprekidna transmisija. Ukupna predajna snaga bazne stanice zavisi direktno od broja i protoka aktivnih konekcija tj. od saobraćajnog opterećenja. Saobraćajno opterećenje baznih stanica varira i zavisi od: doba dana, dana u nedelji, tarifnog profila koji se koristi, lokacije bazne stanice... Mobilni operateri konfigurišu bazne stanice tako da pod određenim okolnostima zadovoljavaju saobraćajne potrebe u takozvanom satu najvećeg opterećenja („*busy hour*“ – period od 60 minuta tokom 24 sata kada dolazi do maksimalnog saobraćajnog opterećenja).

III. RANIJA DUGOROČNA MERENJA SIGNALA MOBILNE TELEFONIJE U SRBIJI

Vršeno je merenje varijabilnosti intenziteta električnog polja u frekvencijskom opsegu *downlink* smera komunikacije kod GSM 900 MHz, DCS 1800 MHz (*Digital Communication*

System) i UMTS 2100 MHz baznih stanica u urbanom delu Beograda, koje je proizašlo iz projekta LEXNET (*Low-EMF Exposure Future Networks*) [10].

U [11] su prikazani rezultati dobijeni dugoročnim merenjem varijabilnosti intenziteta električnog polja koje potiče od GSM baznih stanica. Merenja su vršena u urbanom delu Beograda na sedam različitih lokacija i to pet u *indoor* i dva u *outdoor* okruženju. Dobijeni rezultati su pokazali da se dan može podeliti na dva perioda. Prvi period predstavlja interval od 09:00 do 23:00 časova kada je viši intenzitet električnog polja i drugi period od 23:00 do 09:00 časova narednog dana kada je niži intenzitet električnog polja. Takođe je uočeno da je nivo električnog polja nešto niži bio u toku vikenda u odnosu na radne dane. Vrednosti izmerenog intenziteta električnog polja bile su u intervalu od 0.022 V/m do 0.042 V/m. Raspodela izmerenih vrednosti veoma je bliska normalnoj raspodeli. Prilikom izračunavanja merne nesigurnosti, vršeno je usrednjavanje izmerenih vrednosti u nekoliko vremenskih intervala. Dobijeni rezultati merne nesigurnosti bili su u opsegu od 3.57% do 12.11%. Sa povećanjem intervala usrednjavanja smanjivala se vrednost merne nesigurnosti.

Uporedna analiza dugoročnog merenja intenziteta električnog polja koje potiče od GSM, DCS i UMTS baznih stanica izvršena je u [12]. Merenja su takođe vršena u urbanom delu Beograda na sedam različitih lokacija. Pet lokacija je bilo u *indoor* i dva u *outdoor* okruženju. Kao i u [11], dva perioda u toku dana su se izdvojila. Opseg izmerenih vrednosti intenziteta električnog polja koje potiče od DCS bazne stanice je od 0.06 V/m do 0.11 V/m, kod UMTS taj opseg je od 0.03 V/m do 0.09 V/m, dok je kod GSM opseg isti kao u [11]. Raspodela izmerenih vrednosti kod UMTS sistema je bliska *log-normalnoj* raspodeli, za razliku od GSM i DCS sistema kod kojih ta raspodela teži normalnoj. Kod UMTS sistema, značajno veći broj izmerenih vrednosti intenziteta električnog polja ima niže vrednosti iz izmerenog opsega, za razliku od GSM i DCS sistema. I u ovom slučaju je prilikom izračunavanja merne nesigurnosti vršeno usrednjavanje izmerenih vrednosti u nekoliko vremenskih intervala. Za GSM tehnologiju merna nesigurnost je bila u opsegu od 4.04% do 12.11%, za DCS tehnologiju od 2.71% do 7.92% i za UMTS tehnologiju od 4.69% do 14.69%. Sa povećanjem intervala usrednjavanja smanjivala se vrednost merne nesigurnosti za sve tri analizirane tehnologije. Dobijeni rezultati su očekivani jer se GSM koristi uglavnom za prenos govora, a retko za prenos podataka, DCS se inače retko koristi, a kada se koristi uglavnom je u pitanju govorni servis. UMTS tehnologija se u trenutku merenja uglavnom koristi za prenos podataka, a ređe za prenos govora, što se odrazilo na veću varijabilnost intenziteta električnog polja.

IV. MERNA TEHNOLOGIJA

Prilikom merenja varijabilnosti intenziteta električnog polja korišćen je *Rohde&Schwarz* (RS) EMF merni sistem koji se nalazi u okviru Laboratorije za radio-komunikacije Elektrotehničkog fakulteta, Univerziteta u Beogradu. Merni

sistem se sastoji od spektralnog analizatora *Rohde&Schwarz* FSH6 i izotropne merne sonde *Rohde&Schwarz* TS-EMF. Koristi se za pretraživanje radio-frekveničkog spektra u opsegu od 30 MHz do 3 GHz. Prilikom merenja, spektralni analizator i izotropna merna sonda su postavljeni u prizemlju zgrade Elektrotehničkog fakulteta tokom sedam dana, što predstavlja tipično urbano *indoor* okruženje. Za potrebe merenja korišćena je infrastruktura preduzeća za telekomunikacije "Telekom Srbija" a.d.. Merni sistem je prikazan na slici 1.



Sl. 1. Korišćena merna oprema *Rohde&Schwarz* EMF

Na mernoj lokaciji se nalazi 12 kros-polarizovanih antena, od kojih su četiri antene preko kojih je realizovan GSM servis, četiri antene preko kojih je realizovan UMTS servis i četiri antene preko kojih je realizovan LTE servis. Merenja su sprovedena u opsegu u kome rade LTE bazne stanice za *downlink* smer komunikacije. Rezultati su beleženi na svake četiri sekunde uz pomoć softvera *White Tigress Baby - Measurements*, razvijenog u okviru Laboratorije za radio-komunikacije. Na spektralnom analizatoru su bile podešene sledeće vrednosti parametara prilikom merenja:

- centralna frekvencija – 1835 MHz,
- širina opsega (*resolution bandwidth*) – 1 MHz i
- vreme prebrisavanja (*sweep time*) – 100 ms.

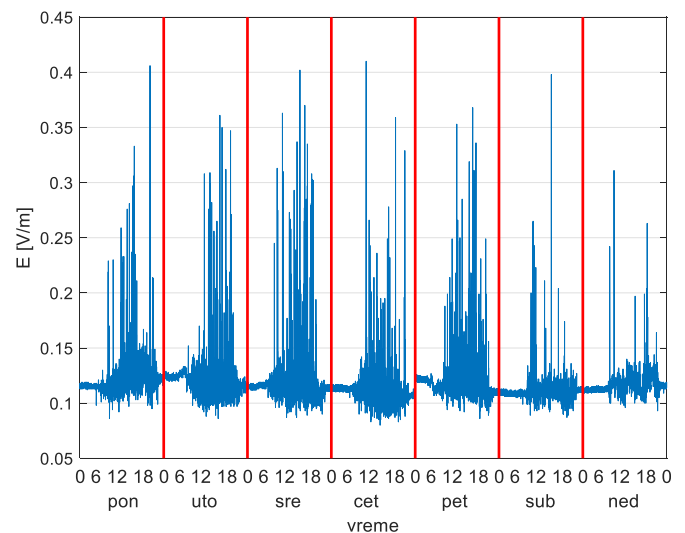
Merni sistem meri sve tri prostorne komponente električnog polja (E_x , E_y i E_z) istovremeno i kao rezultat daje vrednost ukupnog intenziteta električnog polja.

V. REZULTATI MERENJA

Rezultati dobijeni merenjem intenziteta električnog polja tokom sedam dana prikazani su grafički na slici 2. Sa slike se mogu uočiti dva različita perioda u toku svakog dana ako se posmatra razlika u jačini električnog polja. Prvi periodi imaju veće intenzitete i karakteristični su za dnevni deo dana, dok drugi periodi imaju manji intenzitet električnog polja i karakteristični su za noć. Periodi sa povećanim intenzitetom električnog polja mogu se nazvati aktivni sati, dok se periodi

sa smanjenim intenzitetom mogu nazvati neaktivni sati. Promene u intenzitetu električnog polja počinju da se javljaju oko 08:00 časova porastom nivoa, dok je sledeća promena u intenzitetu zabeležena oko 22:00 časova kada dolazi do pada intenziteta električnog polja, pa je tako za aktivan deo dana izabran period od 08:00-22:00 časova, dok je za neaktivan deo dana izabran period od 22:00-08:00 časova narednog dana. Promene vrednosti intenziteta električnog polja slične su za svaki dan, uz neznatne razlike tokom vikenda (subota i nedelja) kada je bilo manje varijacija u odnosu na radne dane (ponedeljak – petak) i kada su vrednosti jačine električnog polja bile niže. Izdvojeni periodi odgovaraju radnom vremenu Elektrotehničkog fakulteta, Univerziteta u Beogradu.

Merjenje je početo u petak u ponoć i trajalo je sedam dana. Sa slike 2 se može uočiti mali nesklad u vrednostima intenziteta električnog polja u ponoć između četvrtka i petka koji se javlja upravo zbog početka i završetka merenja.



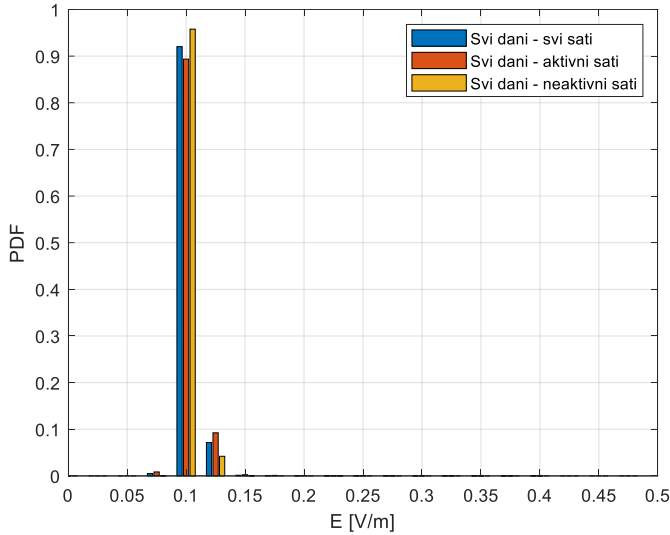
Sl. 2. Vremenska varijabilnost intenziteta električnog polja LTE signala u frekveničkom opsegu *downlink* smera komunikacije

Za potrebe dalje analize, na osnovu uočenih razlika kod radnih dana u nedelji i vikenda i aktivnih i neaktivnih sati, izvršena je podela rezultata na šest različitih kategorija i to:

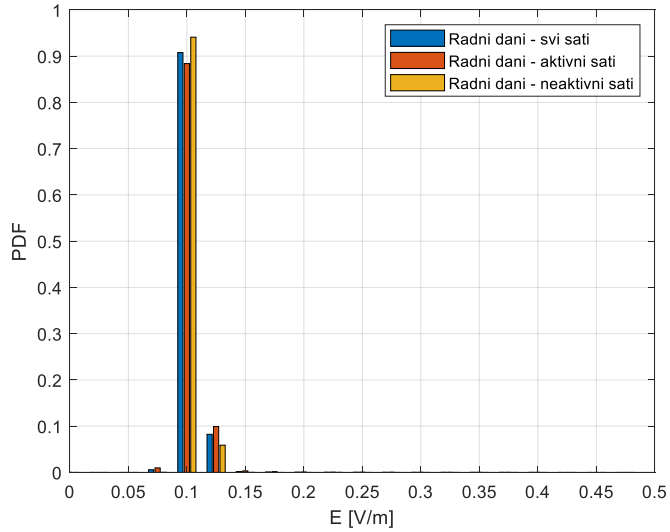
- svi dani – svi sati,
- svi dani – aktivni sati,
- svi dani – neaktivni sati,
- radni dani – svi sati,
- radni dani – aktivni sati,
- radni dani – neaktivni sati.

Na slici 3 prikazana je funkcija gustine verovatnoće intenziteta električnog polja za tri kategorije kada se razmatra svih sedam dana tokom kojih su vršena merenja. Sa slike se može uočiti da je najveći broj izmerenih vrednosti intenziteta električnog polja u intervalu od 0.1-0.15 V/m. Jako je mali broj izmerenih vrednosti intenziteta električnog polja u intervalu od 0.15-0.45 V/m i gotovo da se ne uočavaju na slici 3, dok se na slici 2 jasno uočavaju. Sa slike 3 se može uočiti da je kod nižih vrednosti intenziteta električnog polja veći

broj izmerenih vrednosti tokom neaktivnih sati (žuti stupci), dok je kod aktivnih sati obrnuto (crveni stupci). Vrednosti intenziteta električnog polja, koje su prikazane plavim stupcima, odnose se na sve sate i sve dane i imaju vrednosti između rezultata dobijenih posmatranjem samo aktivnih ili samo neaktivnih sati. Izmerene vrednosti iz opsega od 0.1-0.15 V/m predstavljaju preko 98% svih izmerenih vrednosti intenziteta električnog polja.



Sl. 3. Funkcija gustine verovatnoće intenziteta električnog polja za sve dane



Sl. 4. Funkcija gustine verovatnoće intenziteta električnog polja za radne dane (ponedeljak – petak)

Slični rezultati dobijeni su i kada su posmatrane tri kategorije kod kojih su analizirani samo radni dani, što je kroz funkciju gustine verovatnoće intenziteta električnog polja prikazano na slici 4. Poređenjem sa rezultatima dobijenim za sve dane, ilustrovanim na slici 3, uočava se blago povećanje broja izmerenih vrednosti sa većim intenzitetom električnog polja. Kako se LTE mobilna tehnologija u trenutku merenja koristila isključivo za prenos podataka, uočava se da je zbog

velikih brzina prenosa veoma kratko vreme emisije signala u *downlink* smeru komunikacije, pa je stoga registrovan mali broj izmerenih većih vrednosti intenziteta električnog polja.

Velika većina izmerenih vrednosti električnog polja ima niske nivoje, kada se posmatra opseg svih izmerenih vrednosti, koje potiču od LTE bazne stanice (0.05-0.45 V/m). Ipak, te vrednosti su nešto više u odnosu na vrednosti izmerene u [11] i [12] kod GSM, DCS i UMTS tehnologije.

Merna nesigurnost je parametar koji se pridružuje rezultatu merenja i koji karakteriše disperziju vrednosti koje se mogu se s razlogom pripisati mernoj veličini [13]. Merna nesigurnost je korišćena u daljoj analizi izmerenih rezultata.

Merna nesigurnost se može odrediti statističkom analizom velikog broja izmerenih vrednosti [13, 14]. Za potrebe određivanja merne nesigurnosti, potrebno je najpre odrediti srednju vrednost prema izrazu:

$$E_{sr} = \frac{1}{N} \sum_{i=1}^N E_{mer_i} \quad (1)$$

gde je sa E_{mer_i} označena i -ta izmerena vrednost, a sa N broj izvršenih merenja. Dalje je potrebno odrediti standardnu devijaciju prema izrazu:

$$\sigma(E_{sr}) = \sqrt{\frac{1}{N-1} \sum_{i=1}^N (E_{mer_i} - E_{sr})^2}. \quad (2)$$

Konačno, merna nesigurnost u procentima se dobija kao odnos standardne devijacije i srednje vrednosti:

$$u_{mn} (\%) = \frac{\sigma(E_{sr})}{E_{sr}} \cdot 100. \quad (3)$$

U tabeli I prikazane su vrednosti merne nesigurnosti u procentima za određene vremenske intervale. Merna nesigurnost je izračunata za svaki dan u nedelji posebno, za sve radne dane (ponedeljak – petak), neradne dane, odnosno dane vikenda (subota i nedelja) i za svih sedam dana. Za svaki navedeni period izdvojeni su rezultati za sve sate, aktivne sate i neaktivne sate.

Dobijene vrednosti za sve vremenske periode su u opsegu od 1.71-11.26%. Najmanja merna nesigurnost dobijena je u toku neaktivnih sati u subotu (1.71%), dok je najveća merna nesigurnost dobijena u sredu u toku aktivnih sati (11.26%).

Posmatrajući sve sate u analiziranim vremenskim intervalima, izračunata je merna nesigurnost u opsegu od 4.86-8.76%. Najmanja merna nesigurnost dobijena je za subotu (4.86%), a najveća za sredu (8.76%). Kod aktivnih sati, merna nesigurnost je u opsegu od 5.30-11.26%. Najveća vrednost dobijena je za sredu (11.26%), a najmanja za nedelju (5.30%). Kod neaktivnih sati, zbog značajnog smanjenja varijacije intenziteta električnog polja, opseg vrednosti merne nesigurnosti je od 1.71-4.64%. Najmanja vrednost merne nesigurnosti od 1.71% dobijena je za subotu, dok je najveća

vrednost od 4.64% dobijena kada se analizira svih sedam dana tokom kojih je meren intenzitet električnog polja. Ako se posmatraju pojedinačni dani kod neaktivnih sati, najveća merna nesigurnost dobijena je za petak – 4.59%, i ta vrednost je manja od maksimalne za 0.05%.

Uočava se da je merna nesigurnost veća kod aktivnih sati nego kod neaktivnih za sve razmatrane vremenske intervale. Takođe, kod svih vremenskih intervala, merna nesigurnost za sve sate je između aktivnih i neaktivnih sati, što je i očekivano. Vrednosti merne nesigurnosti izračunate za subotu i nedelju, tj. za neradne dane, su znatno manje u odnosu na radne dane, posmatrano bilo pojedinačno, bilo za sve radne dane skupa. To važi i za aktivne i za neaktivne sate, ali je kod neaktivnih sati ta razlika znatno manja, što je i očekivano jer je mikro bazna stanica namenjena za opsluživanje korisnika koji se nalaze unutar zgrade Elektrotehničkog fakulteta.

TABELA I
MERNA NESIGURNOST IZRAŽENA U PROCENTIMA ZA ODREĐENE VREMENSKE INTERVALE

Vremenski interval	Svi sati	Aktivni sati	Neaktivni sati
Ponedeljak	6.92	7.96	2.83
Utorak	7.53	8.80	3.21
Sreda	8.76	11.26	2.32
Četvrtak	6.80	8.56	2.74
Petak	7.53	9.02	4.59
Subota	4.86	6.11	1.71
Nedelja	5.07	5.30	2.01
Radni dani	8.07	9.85	4.52
Neradni dani	5.80	6.86	2.58
Svi dani	7.61	9.13	4.64

TABELA II
SREDNJE I MAKSIMALNE VREDNOSTI INTENZITETA ELEKTRIČNOG POLJA
IZRAŽENE U V/M ZA ODREĐENE VREMENSKE INTERVALE

Vremenski interval	Svi sati		Aktivni sati		Neaktivni sati	
	Srednja vrednost	Maksimalna vrednost	Srednja vrednost	Maksimalna vrednost	Srednja vrednost	Maksimalna vrednost
Ponedeljak	0.1192	0.4060	0.1217	0.4060	0.1157	0.1300
Utorak	0.1181	0.3610	0.1151	0.3610	0.1224	0.1520
Sreda	0.1152	0.4020	0.1154	0.4020	0.1147	0.2450
Četvrtak	0.1097	0.4100	0.1088	0.4100	0.1111	0.1260
Petak	0.1162	0.3680	0.1166	0.3680	0.1157	0.1270
Subota	0.1093	0.3980	0.1098	0.3980	0.1084	0.1270
Nedelja	0.1160	0.3110	0.1186	0.3110	0.1123	0.2420
Radni dani	0.1157	0.4100	0.1155	0.4100	0.1159	0.2450
Neradni dani	0.1126	0.3980	0.1142	0.3980	0.1104	0.2420
Svi dani	0.1148	0.4100	0.1151	0.4100	0.1143	0.2450

U tabeli II prikazani su uporedni rezultati srednjih vrednosti i maksimalnih vrednosti intenziteta električnog polja po danima u nedelji, radnim danima, neradnim danima i tokom čitave nedelje. Takođe su razmatrani, aktivni sati, neaktivni sati i svi sati.

Srednje vrednosti intenziteta električnog polja su vrlo slične za sve razmatrane periode i iznose oko 0.11 V/m kada se posmatraju svi sati. Najveća srednja vrednost dobijena je za ponedeljak (0.1192 V/m), a najmanja za subotu (0.1093 V/m). Očekivano je da manje vrednosti budu za dane vikenda, ali je za četvrtak dobijena nešto niža srednja vrednost (0.1097 V/m) u odnosu na nedelju (0.1160 V/m). Kada se posmatraju maksimalne izmerene vrednosti one su u opsegu od 0.3110 V/m (nedelja) do 0.4100 V/m (četvrtak), što su vrednosti znatno veće od izračunatih srednjih vrednosti.

Kada se posmatraju samo aktivni sati, izračunate srednje vrednosti su nešto više u odnosu na to kada se posmatraju svi sati. Srednje vrednosti su u opsegu od 0.1088-0.1217 V/m. Maksimalne vrednosti u toku aktivnih sati se poklapaju sa maksimalnim vrednostima kod svih sati, što znači da su sve maksimalne vrednosti intenziteta električnog polja izmerene u toku aktivnih sati što je i očekivano.

Maksimalne vrednosti intenziteta električnog polja u toku neaktivnih sati zнатно су niže od maksimalnih vrednosti izmerenih u toku aktivnih sati. Srednje vrednosti tokom neaktivnih sati su za njansu niže od srednjih vrednosti tokom aktivnih sati, uz odstupanja koja su se javila u utorak i četvrtak, kao i kada se posmatraju svi radni dani gde su srednje vrednosti neaktivnih sati bile više od srednjih vrednosti aktivnih sati. Opseg srednjih vrednosti intenziteta električnog polja je od 0.1084 V/m (subota) do 0.1224 V/m (utorak). Opseg maksimalnih izmerenih vrednosti intenziteta električnog polja u toku neaktivnih sati je od 0.1260 V/m (četvrtak) do 0.2450 V/m (sreda).

Iako nije očekivano da pojedine srednje vrednosti za neaktivne sate budu veće od vrednosti kod aktivnih sati iz tabele II, gledajući grafik sa slike 2, uočavaju se značajnije promene u intenzitetu električnog polja čije vrednosti padaju i ispod vrednosti koja je konstantnija tokom neaktivnih sati, gde se može pronaći odgovor na neočekivan rezultat.

VI. ZAKLJUČAK

U radu je izvršeno merenje i analiza vremenske varijabilnosti intenziteta električnog polja koje potiče od mikro LTE 1800 MHz bazne stanice u toku jedne sedmice. Merenje je vršeno neprekidno tokom sedam dana u urbanom delu Beograda. Za merenje je korišćena merna oprema Rohde&Schwarz EMF.

Rezultati merenja su pokazali da se mogu izdvojiti dva različita perioda u toku dana. Jedan period se odnosi na vreme između 08:00-22:00 časova, kada su viši nivoi i češće varijacije intenziteta električnog polja. Drugi period je u intervalu od 22:00-08:00 časova sledećeg dana i tada su niži nivoi i smanjene su na minimum promene u intenzitetu električnog polja. Uočeno je i smanjenje emisije i varijacije intenziteta električnog polja u dane vikenda.

Zbog velike brzine prenosa podataka kraće su emisije signala sa višim nivoom zračenja. Zato je 98% svih izmerenih vrednosti intenziteta električnog polja u intervalu od 0.1-0.15 V/m, u čiji opseg ulaze i izračunate srednje vrednosti po danima u nedelji.

Računanjem merne nesigurnosti utvrđena su odstupanja od vrednosti koje se opravdano mogu uzeti za rezultat merenja. Izračunata merna nesigurnost koja je u opsegu od 1.71% do 11.26% pokazuje relativno malo odstupanje izmerenih vrednosti. Najmanja merna nesigurnost dobijena je u toku neaktivnih sati za subotu (1.71%) kada je bilo najmanje varijacija u intenzitetu električnog polja, dok je najveća merna nesigurnost dobijena za sredu u toku aktivnih sati (11.26%) kada su varijacije intenziteta električnog polja bile najčešće.

U budućem istraživanju potrebno je vršiti dugoročnija merenja promene intenziteta električnog polja na različitim lokacijama, vremenskim uslovima i u različitim okruženjima. Potrebno je voditi računa o broju korisnika koje opslužuje LTE bazna stanica u datom trenutku. Takođe, u narednom periodu planirano je merenje zračenja terminalnih uređaja povezanih na LTE baznu stanicu i njihov uticaj na ljude u okruženje.

LITERATURA

- [1] M. K. L. Alhasnawi, S. Abdulla, D. Fatseas, R. G. Addie, "Spectral density constraints on wireless communication," *Heliyon*, vol. 6, no. 5, e03979, 2020.
- [2] L. Verloock, W. Joseph, F. Goeminne, L. Martens, M. Verlaek, K. Constandt, "Temporal 24-hour assessment of radio frequency exposure in schools and homes," *Measurement* 56, pp. 50-57, 2014.
- [3] W. Joseph, L. Verloock, F. Goeminne, G. Vermeeren, L. Martens, "Assessment of general public exposure to LTE and RF sources present in an urban environment," *Bioelectromagnetics*, vol. 31, no. 7, pp. 576-579, 2010.
- [4] W. Joseph, L. Verloock, F. Goeminne, G. Vermeeren, L. Martens, "Assessment of RF exposures from emerging wireless communication technologies in different environments," *Health Physics*, vol. 102, no. 2, pp. 161-172, 2012.
- [5] M. Y. Zvezdina, Y. A. Shokova, O. Y. Nazarova, H. T. A. Al-Ali, G. H. A. Al-Farhan, "Visualization of electromagnetic exposure near LTE antennae," IOP Conference Series: Earth and Environmental Science, 115.1: 012037, 2018.
- [6] P. Joshi, D. Colombi, B. Thors, L. E. Larsson, C. Törnevik, "Output power levels of 4G user equipment and implications on realistic RF EMF exposure assessments," *IEEE Access* 5, pp. 4545-4550, 2017.
- [7] Z. Vecsei, G. Thuróczy, I. Hernádi, "The effect of a single 30-min long term evolution mobile phone-like exposure on thermal pain threshold of young healthy volunteers," *International journal of environmental research and public health*, vol. 15, no. 9, 1849, 2018.
- [8] I. Stojanović, M. Koprivica, N. Stojanović, A. Nešković, "Analysis of the impact of network architecture on signal quality in LTE technology," *Serbian Journal of Electrical Engineering*, vol. 17, no. 1, pp. 95-109, 2020.
- [9] E. Lunca, C. Damian, A. Salceanu, "EMF exposure measurements on 4G/LTE mobile communication networks," International Conference and Exposition on Electrical and Power Engineering, Iasi, Romania, pp. 545-548, October 16-18, 2014.
- [10] M. Tesanovic, E. Conil, A. De Domenico, R. Agüero, F. Freudenstein, L. M. Correia, S. Bories, L. Martens, P. M. Wiedemann, J. Wiart, "Wireless networks and EMF—paving the way for low-EMF networks of the future: the LEXNET project," *IEEE Vehicular Technology Magazine*, vol. 9, no. 2, pp. 20-28, 2014.
- [11] M. Koprivica, M. Petrić, M. Popović, J. Milinković, S. Nikšić, A. Nešković, "Long-term variability of electromagnetic field strength for GSM 900MHz downlink band in Belgrade urban area," 22nd Telecommunications Forum TELFOR, Belgrade, Serbia, pp. 9-12, November 25-27, 2014.
- [12] M. Koprivica, M. Petrić, M. Popović, J. Milinković, A. Nešković, "Empirical analysis of electric field strength long-term variability for GSM/DCS/UMTS downlink band," *Telfor Journal*, vol. 8, no. 2, pp. 87-92, 2016.
- [13] Joint Committee for Guides in Metrology (BIPM, IEC, IFCC, ILAC, ISO, IUPAC, IUPAP and OIML), "JCGM 100:2008, Evaluation of measurement data – Guide to the Expression of Uncertainty in Measurement", 2008.
- [14] G. Basso, "Uncertainty in the measurement of electromagnetic field with isotropic broadband sensor and selective E&H field analyzer", NARDA Safety Solutions, 2009.

ABSTRACT

The paper analyzes the variability of the electric field strength originating from the micro LTE base station. Measurement of the electric field strength was performed during seven days. The measurement was performed in the frequency range of the downlink direction of communication at the central frequency of 1835 MHz. Intensive measurements were performed in real network conditions in indoor environment. Variability of electric field strength can be divided into two periods in one day, a period with higher levels and more frequent changes in electric field strength (from 08:00 AM to 10:00 PM) and a period with lower levels and less frequent changes in electric field strength (from 10:00 PM to 08:00 AM the next day). Differences in the electric field strength were also observed during working days (Monday-Friday) in relation to non-working days (Saturday and Sunday). The time variability of the electric field strength was determined by calculating the measurement uncertainty. The obtained measurement uncertainty, which is in the range from 1.71% to 11.26%, shows a relatively small deviation of the measured values.

Long-Term Variability of Electric Field Strength Originating from Micro LTE Base Station

Ivana Stojanović, Mladen Koprivica, Nenad Stojanović,
Aleksandar Nešković

Verovatnoća prekida komunikacije u hibridnom RF - PLC/VLC sistemu

Jelena Anastasov, *Student Member, IEEE*, Dejan Milić, *Member, IEEE*, Daniela Milović i Nenad Milošević

Apstrakt— U ovom radu razmatra se hibridni sistem za prenos informacija do krajnjeg korisnika u zatvorenom prostoru. Prenos se obavlja preko kooperativnog linka sa DF (decode-and-forward) relejem koji povezuje PLC (power line communication) i VLC (visible light communication) deonice. Kao back-up link koristi se bežični RF kanal. Korisnik, primenom SC kombinovanja (selection combining) bira link koji mu omogućava bolji kvalitet signala. U radu je analizirana verovatnoća prekida i uticaj parametra PLC, VLC i RF deonica na performanse ovakvog sistema. Detaljnije, razmatran je uticaj pozicije LED lampe (visina, ugao zračenja), uticaj odnosa srednjih snaga signala i šuma sa svim deonicama, dubine fedinga radio kanala i vrednosti praga prekida na verovatnoću prekida komunikacije u posmatranom sistemu.

Ključne reči—verovatnoća prekida; PLC link; VLC link; DF relej; RF link; selepciono kombinovanje.

I. UVOD

Prenos informacija u eri razvoja IoT (Internet of Things) je od izuzetne važnosti. Veliki broj uređaja u pametnim kućama, zgradama, saobraćajnoj infrastrukturi, kao i veliki broj senzora i upravljačkih sistema zahteva sigurnu komunikaciju kroz različite medijume u cilju sveobuhvatne pokrivenosti [1]. Pored najrasprostranjenijeg bežičnog RF (radio frequency) prenosa, koriste se i PLC (power line communication) tehnologija kao i bežične optičke komunikacije kod kojih se optički signali prostiru kroz slobodni prostor i koje se mogu podeliti na FSO (free space optical) i VLC (visible light communication).

PLC tehnologija se aktivno izučava poslednjih decenija jer je efikasna i ekonomično isplativa. Razlog je postojanje rasprostranjene elektroenergetske infrastrukture preko koje se vrši prenos informacija [2]. PLC se koristi u zatvorenim prostorijama, ali i za povezivanje udaljenih komunikacionih čvorova. Komunikacija se obavlja preko dalekovoda, tako da PLC predstavlja žičanu komunikaciju što ukazuje na povećanu sigurnost prenosa u poređenju sa bežičnim sistemima. S druge strane VLC tehnologija koristi svetlosne diode koje služe ne samo za osvetljavanje prostorije već i za

komunikaciju [3]. VLC emituje informacije u vidljivom delu spektra, tako da predstavlja odličnu alternativu RF prenosu kod koga je spektar maksimalno eksploatisan. VLC prenos nudi prednosti visoke sigurnosti i kapaciteta uz ekološki prihvatljive standarde [4].

VLC sistem treba biti povezan sa spoljnom mrežom što je moguće izvršiti primenom RF [5] ili FSO [6] tehnologije. Međutim, najperspektivnije rešenje povezivanja VLC pristupne tačke sa spoljnom baznom stanicom je preko elektroenergetskih kablova kojima se istovremeno vrši napajanje LED osvetljenja i prenos informacija velikom brzinom [7]. Implementacija releja između PLC i VLC deonice doprinosi poboljšanju performansi sistema.

U radu [8], autori su razmatrali kooperativni PLC/VLC sistem sa AF (amplify-and-forward) relejem i odredili kapacitet posmatranog sistema. Analitički izrazi za kapacitet i verovatnoću prekida sistema sa kaskadnom vezom PLC i VLC linka koji su povezani preko DF (decode-and-forward) releja izvedeni su u [9]. U radu [10], prikazana je analiza performansi kooperativnog PLC/VLC sistema sa više LED lampi i više korisnika, pri čemu se korišćenjem selekcione metode kombinovanja (selection combining-SC) bira korisnik koji učestvuje u komunikaciji.

U ovom radu razmatra se sistem u kome se jedan korisnik nalazi u zatvorenom prostoru i informacije prima preko VLC linka koji je preko DF releja povezan sa PLC linkom, pri čemu korisnik informacije može primati tu istu informaciju i preko standardnog RF linka. Procenjujući kvalitet signala prenešenog preko PLC/VLC linka i RF linka, primenom SC kombinovanja, korisnik odlučuje koji deo sistema za prenos informacija će koristiti. U radu je izведен je izraz za verovatnoću prekida razmatranog sistema i analiziran je uticaj parametara svih prenosnih kanala u sistemu na vrednosti verovatnoće prekida komunikacije.

Ukratko, rad je strukturiran po poglavljima na sledeći način. U drugom poglavlju dat je opis modela sistema koji je korišćen u analizi. U trećem poglavlju su detaljno opisani komunikacioni kanali ovog sistema. U četvrtom poglavlju, izведен je izraz za izračunavanje verovatnoće prekida. Numerički rezultati i diskusija dobijenih rezultata prikazana je u petom poglavlju rada. U poslednjem poglavlju dati su osnovni zaključci prikazane analize.

II. MODEL SISTEMA

Razmatran je hibridni asimetrični RF - dual-hop kooperativni PLC/VLC sistem. Kao što je prikazano na slici

Jelena Anastasov – Elektronski fakultet, Univerzitet u Nišu, Aleksandra Medvedeva 14, 18115 Niš, Srbija, (e-mail: jelena.anastasov@elfak.ni.ac.rs).

Dejan Milić – Elektronski fakultet, Univerzitet u Nišu, Aleksandra Medvedeva 14, 18115 Niš, Srbija, (e-mail: dejan.milic@elfak.ni.ac.rs).

Daniela Milović – Elektronski fakultet, Univerzitet u Nišu, Aleksandra Medvedeva 14, 18115 Niš, Srbija, (e-mail: daniela.milovic@elfak.ni.ac.rs).

Nenad Milošević – Elektronski fakultet, Univerzitet u Nišu, Aleksandra Medvedeva 14, 18115 Niš, Srbija, (e-mail: nenad.milosevic@elfak.ni.ac.rs).

1, komunikacioni izvor prenosi signal do VLC LED lampe putem PLC deonice. Lampa je povezana sa PLC-om uz pomoć DF releja koji dekodira signale sa PLC veze i ponovo šalje dekodiranu verziju originalnog signala putem VLC deonice do prijemnika. Signali koji se prenose od izvora do releja, prolaze kroz nekoliko tačaka diskontinuiteta, brojne spojeve kablova za napajanje itd. [2]. Zbog toga, pored originalnog do releja stiže i skup zakasnelyih kopija signala što ukazuje na postojanje fedinga. PLC kanal je takođe izložen uticaju različitih aditivnih šumova. Relej prima signal r_{PLC} oblika [9], [10]

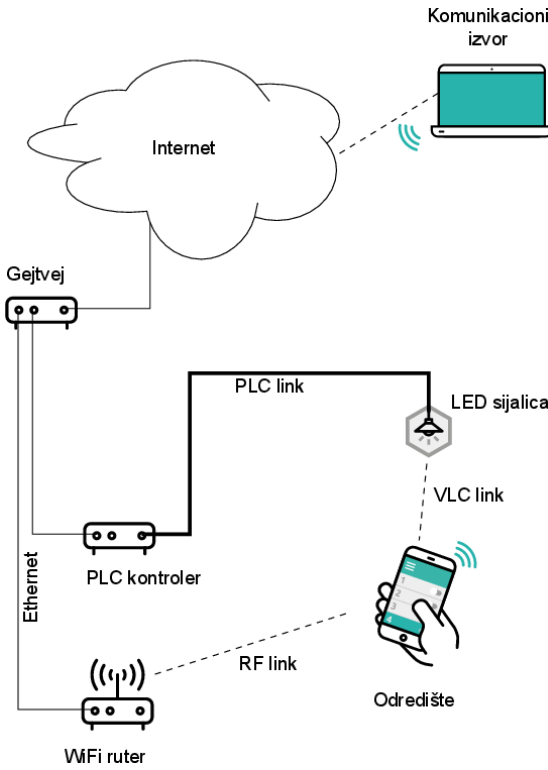
$$r_{PLC} = h_{PLC}i + n_{PLC}, \quad (1)$$

gde je i izvorni informacioni signal, h_{PLC} trenutna vrednost fedinga, a n_{PLC} ukupni trenutni šum u PLC kanalu.

Relej dekodira primljene podatke i prosleđuje ih na VLC link kao [9], [10]

$$r_{VLC} = h_{VLC}\hat{i} + n_{VLC}, \quad (2)$$

gde je \hat{i} dekodirana verzija izvornog signala, h_{VLC} trenutna vrednost amplitude i n_{VLC} trenutna vrednost šuma u VLC kanalu. Preko VLC linka signal stiže do odredišne tačke tj. do korisnika.



Slika1. Model komunikacionog sistema

Sa druge strane, ista informacija se šalje i putem antene RF predajnika, radio kanalom u kojem takođe postoji feding. Signal koji stiže do odredišta je sledećeg oblika

$$r_{RF} = h_{RF}i + n_{RF}, \quad (3)$$

gde je h_{RF} trenutna vrednost fedinga u RF kanalu, a n_{RF} trenutna vrednost aditivnog šuma.

Korisnik tj. prijemnik sadrži dve prijemne antene (fotodetektor i RF antenu) i koristi metodu SC kombinovanja ekstrahući poslatu informaciju, biranjem veće vrednosti

trenutnog odnosa snage signala i snage šuma (SNR-signal to noise ratio).

III. MODELI KOMUNIKACIONIH KANALA

A. PLC komunikacioni kanal

U PLC kanalu postoji efekat fedinga tako da se, trenutna vrednost amplitude kanala, h_{PLC} , modeluje se lognormalnom raspodelom [11], tj. funkcija gustine verovatnoće (PDF-probability density function) promenljive h_{PLC} , može se predstaviti kao

$$f_{h_{PLC}}(h) = \frac{1}{h\sqrt{2\pi\sigma^2}} e^{-\frac{(\ln h - \mu)^2}{2\sigma^2}}, \quad (4)$$

gde μ predstavlja srednju vrednost a σ^2 varijansu veličine h_{PLC} . Ukupni šum u PLC kanalu je zbir pozadinskog i impulsnog šuma $n_{PLC} = n_I + n_{bn}$. PDF trenutne vrednosti ukupnog šuma ima sledeći oblik [9]-[11]

$$f_{n_{PLC}}(n) = P_1 \frac{1}{\sqrt{2\pi\sigma_G^2}} e^{-\frac{n^2}{2\sigma_G^2}} + P_2 \frac{1}{\sqrt{2\pi\sigma_G^2(1+\chi)}} e^{-\frac{n^2}{2\sigma_G^2(1+\chi)}}, \quad (5)$$

gde je $P_1 = (1 - \lambda T)$ i $P_2 = \lambda T$. Parametrom λ se definiše učestanost pojavljivanja impulsnog šuma u toku vremena T , a λT predstavlja verovatnoću pojavljivanja impulsnog šuma u kanalu. Parametar σ_G^2 predstavlja snagu pozadinskog šuma, a χ odnos snaga impulsnog i pozadinskog šuma.

Trenutna vrednost SNR-a u PLC kanalu se definiše kao

$$\gamma_{PLC} = \frac{E_b |h_{PLC}|^2}{\sigma_G^2 (1 + \chi)}, \text{ a PDF trenutnog SNR-a na sledeći način}$$

[10]

$$f_{\gamma_{PLC}}(\gamma) = (1 - \lambda T) \frac{1}{\sqrt{2\pi\sigma_0^2 \gamma}} e^{-\frac{(\ln \gamma - \mu_0)^2}{2\sigma_0^2}} + \lambda T \frac{1}{\sqrt{2\pi\sigma_1^2 \gamma}} e^{-\frac{(\ln \gamma - \mu_1)^2}{2\sigma_1^2}}, \quad (6)$$

gde je $\mu_0 = 2\mu + \ln \bar{\gamma}_{pB}$, $\mu_1 = 2\mu + \ln \bar{\gamma}_{pl}$ i $\sigma_0 = \sigma_1 = 2\mu$.

Kako bi pojednostavili analizu i izveli izraze u zatvorenom obliku, koristićemo aproksimaciju lognormalne raspodele u Gama raspodelu, detaljno opisanu u [12], tako da se PDF trenutnog SNR-a može napisati u sledećem obliku

$$f_{\gamma_{PLC}}(\gamma) = (1 - \lambda T) \left(\frac{m_b}{\Omega_b} \right)^{m_b} \frac{\gamma^{m_b-1}}{\Gamma(m_b)} e^{-\frac{\gamma m_b}{\Omega_b}} + \lambda T \left(\frac{m_i}{\Omega_i} \right)^{m_i} \frac{\gamma^{m_i-1}}{\Gamma(m_i)} e^{-\frac{\gamma m_i}{\Omega_i}}, \quad (7)$$

gde je $\Gamma(\cdot)$ Gamma funkcija definisana kao $\Gamma(z) = \int_0^\infty t^{z-1} \exp(-t) dt$ [13, (8.3107.1)], a m_b i m_i parametri

oštine efekta senke Gama raspodele fedinga, i Ω_b i Ω_i vrednosti srednjeg SNR-a. Veze između parametara lognormalne i Gama raspodele se mogu naći u radu [12].

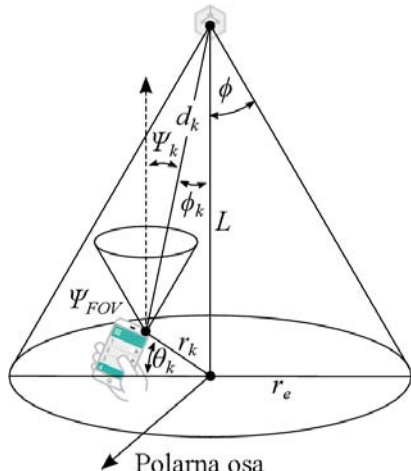
Integraljenjem prethodne jednačine i korišćenjem relacije [14, (8.4.16)], izведен je i izraz za izračunavanje kumulativne funkcije raspodele (cumulative distribution function-CDF) trenutnog SNR-a u PLC kanalu, na sledeći način

$$F_{\gamma_{PLC}}(\gamma) = (1 - \lambda T) \frac{1}{\Gamma(m_b)} G_{1,2}^{1,1} \left(\frac{m_b \gamma}{\Omega_b} \middle| m_b, 0 \right), \\ + \lambda T \frac{1}{\Gamma(m_i)} G_{1,2}^{1,1} \left(\frac{m_i \gamma}{\Omega_i} \middle| m_i, 0 \right), \quad (8)$$

gde je $G_{p,q}^{m,n} \left(z \middle| \begin{matrix} a_1, \dots, a_p \\ b_1, \dots, b_q \end{matrix} \right)$, Meijer-ova G funkcija [13, (9.301⁷)].

B. VLC komunikacioni kanal

Parametri modela VLC kanala predstavljeni su na slici 2. LED sijalica se nalazi na visini L i pokriva površinu kruga maksimalnog poluprečnika r_e .



Sl. 2. Model VLC komunikacionog kanala

Položaj korisnika je slučajna veličina, koji se u polarnom koordinatnom sistemu određuje uglom θ_k i poluprečnikom r_k . Euklidsko rastojanje između LED osvetljenja i korisnika je $d_k = (r_k^2 + L^2)^{1/2}$. Važi Lambertov zakon $z = -1/\log_2(\cos(\phi))$, gde je ϕ ugao zračenja LED sijalice. Parametrom Ψ_{FOV} je označeno vidno polje prijemnika. Upadni ugao i ugao zračenja korisnika označeni su kao ψ_k i ϕ_k , respektivno, pri čemu je $\cos(\psi_k) = \cos(\phi_k) = L/d$. Pojačanje kanala LOS (line-of-sight) linka između LED-a i korisnika je

$$h_{VLC} = \frac{\Xi(z+1)L^{z+1}}{(r_k^2 + L^2)^{\frac{z+3}{2}}}, \quad (9)$$

pri čemu je $\Xi = AR_p U(\psi_k)g(\psi_k)/2\pi$ konstanta za konkretni sistem, A površina detektora, R_p responsivnost fotodetektora, $U(\psi_k)$ pojačanje optičkog filtra i $g(\psi_k)$ optički koncentrator [15].

Kako je položaj korisnika slučajna veličina sa uniformnom raspodelom po krugu poluprečnika r_e , funkcija gustine verovatnoće pojačanja kanala je [15]

$$f_{h_{VLC}}(h) = \frac{2}{r_e^2(z+3)} (\Xi(z+1)L^{z+1})^{\frac{2}{z+3}} h^{-\frac{2}{z+3}-1} \quad (10)$$

PDF trenutnog SNR-a, $\gamma_{VLC} = \bar{\gamma}_{VLC} h^2$, je [10]

$$f_{\gamma_{VLC}}(\gamma) = \frac{\bar{\gamma}_{VLC}^{z+3}}{r_e^2(z+3)} (\Xi(z+1)L^{z+1})^{\frac{2}{z+3}} \gamma^{-\frac{z+4}{z+3}}, \quad (11)$$

za $\gamma \in [\lambda_{\min}, \lambda_{\max}]$, gde je $\lambda_{\min} = \frac{\bar{\gamma}_{VLC}(\Xi(z+1)L^{z+1})^2}{L^{2(z+3)}}$ i $\lambda_{\max} = \frac{\bar{\gamma}_{VLC}(\Xi(z+1)L^{z+1})^2}{(r_e^2 + L^2)^{(z+3)}} \quad$ i $\bar{\gamma}_{VLC} = \frac{\rho^2 P_{opt}^2}{N_0 B}$. Optička snaga je označena sa P_{opt} , N_0 je spektralna gustina šuma, B je propusni opseg i ρ je koeficijent električno-optičke konverzije.

Kumulativna funkcija raspodele se može dobiti, integraljenjem (10) u granicama $\gamma \in [\lambda_{\min}, \lambda_{\max}]$, u obliku

$$F_{\gamma_{VLC}}(\gamma) = \frac{-1}{r_e^2} (\Xi(z+1)L^{z+1})^{\frac{2}{z+3}} \left(\frac{\gamma}{\bar{\gamma}_{VLC}} \right)^{-\frac{1}{z+3}} + \left(1 + \frac{L^2}{r_e^2} \right). \quad (12)$$

C. RF komunikacioni kanal

Prepostavili smo da se feding u RF kanalu može modelovati Nakagami- m raspodelom, tako da je PDF trenutnog SNR-a RF linka, γ_{RF} , sledećeg oblika [12]

$$f_{\gamma_{RF}}(\gamma) = \frac{m^m}{\bar{\gamma}_{RF}^m \Gamma(m)} \gamma^{m-1} \exp\left(-\frac{m\gamma}{\bar{\gamma}_{RF}^m}\right), \quad (13)$$

pri čemu je $\bar{\gamma} = E[r^2]$ srednja vrednost SNR-a, a m Nakagami parametar koji opisuje dubinu fedinga ($m \geq 0.5$).

Odgovarajući CDF trenutnog SNR-a je

$$F_{\gamma_{RF}}(\gamma) = 1 - \frac{\Gamma\left(m, \frac{m\gamma}{\bar{\gamma}_{RF}^m}\right)}{\Gamma(m)}, \quad (14)$$

gde $\Gamma(.,.)$ predstavlja nekompletну Gamma funkciju definisanu kao $\Gamma(\alpha, x) = \int_x^\infty t^{\alpha-1} \exp(-t) dt$ [13, (8.350.2⁷)].

IV. VEROVATNOĆA PREKIDA KOMUNIKACIJE U SISTEMU

U sistemu sa DF relejem, vrednost ekvivalentnog SNR-a se definiše kao $\gamma_{eq} = \min(\gamma_{PLC}, \gamma_{VLC})$, a funkcija gustine verovatnoće izračunava pomoću formule

$$f_{\gamma_{eq}}(\gamma) = f_{\gamma_{PLC}}(\gamma)(1 - F_{\gamma_{VLC}}(\gamma)) + f_{\gamma_{VLC}}(\gamma)(1 - F_{\gamma_{PLC}}(\gamma)). \quad (15)$$

Nadalje, CDF trenutne vrednosti SNR-a PLC/VLC linka se računa kao

$$F_{\gamma_{eq}}(\gamma) = F_{\gamma_{PLC}}(\gamma) + F_{\gamma_{VLC}}(\gamma) - F_{\gamma_{PLC}}(\gamma)F_{\gamma_{VLC}}(\gamma). \quad (16)$$

S obzirom na to da prijemna tačka koristi metodu SC kombinovanja, krajnja vrednost trenutnog SNR-a se izračunava kao $\gamma_{end} = \max(\gamma_{eq}, \gamma_{RF})$, tako da je lako izračunati verovatnoću prekida komunikacije posmatranog sistema na sledeći način

$$P_{out}(\gamma_{th}) = F_{\gamma_{eq}}(\gamma_{th})F_{\gamma_{RF}}(\gamma_{th}), \quad (17)$$

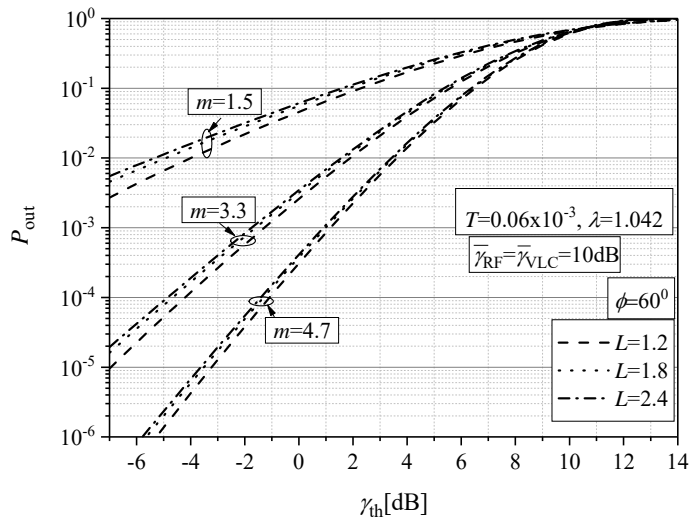
gde je γ_{th} prag prekida koji se odabira sa stanovišta kvaliteta prijema. Zamenom (8) i (12) u (15), a zatim zamenom (15) i (14) u (17) može se izračunati verovatnoća prekida za definisane parametre sistema.

V. NUMERIČKI REZULTATI

U ovo delu rada, prikazani su numerički rezultati dobijeni na osnovu analitičkog izraza za izračunavanje verovatnoće prekida, tj. na osnovu jednačine (17). Rezultati su dobijeni u softverskom paketu *Mathematica®*, u kome je i ugrađena, specijalna, Meijer-ova G funkcija.

Neki od parametara PLC-VLC linka su fiksirani u analizi na svim slikama i to: $m_b=0.6$, $m_t=2$, $A=0.1m$, $R_p=0.4A/W$, $U(\psi_k)=g(\psi_k)=7dB$.

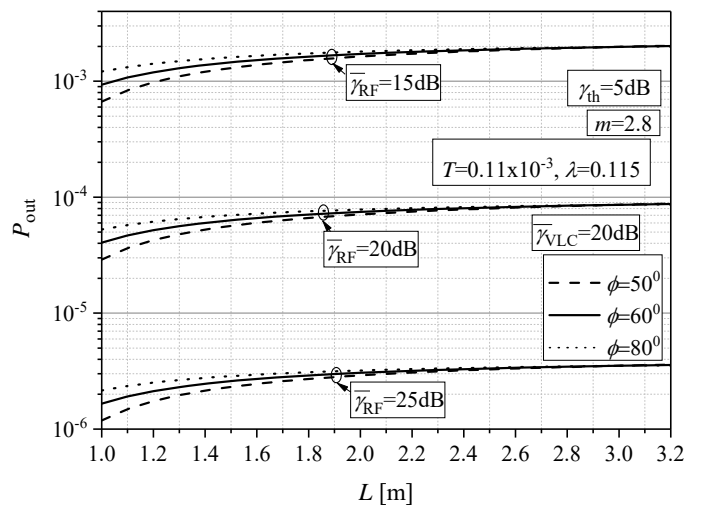
Na slici 3., prikazana je verovatnoća prekida komunikacije u posmatranom sistemu u funkciji od praga prekida za različite vrednosti dubine feedinga u radio kanalu. Takođe razmatran je i uticaj položaja tj. visine instalirane LED sijalice za konstantnu vrednost parametra m . Sa slike se može uočiti da su za niže vrednosti praga prekida i verovatnoće prekida niže. U sistemu sa radio kanalom u dubljem feedingu, performanse su generalno lošije, tako da su verovatnoće prekida najveće za slučaj kada je $m=1.5$. Uticaj promene visine na kojoj se nalazi LED sijalica je nešto očigledniji kada je RF kanal u dubokom feedingu. S obzirom na to da je LED sijalica instalirana na manjim visinama, bliža korisniku a samim tim i LOS komponenta jača, verovatnoće prekida komunikacije u sistemu su u tom slučaju niže.



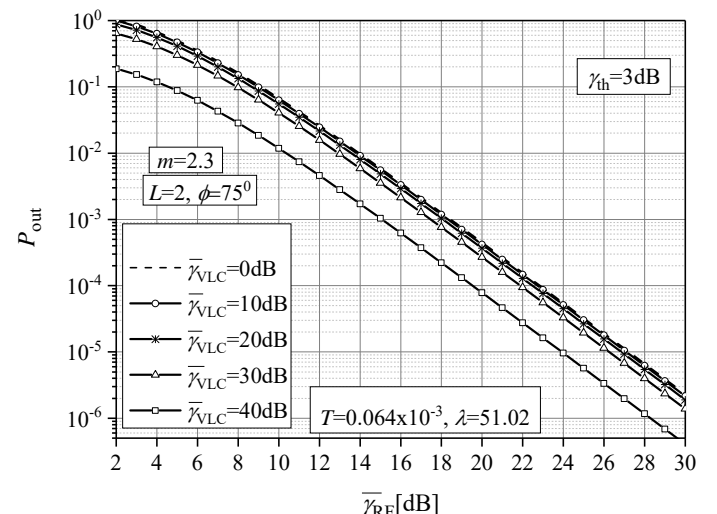
Sl. 3. Verovatnoća prekida u zavisnosti od praga prekida za različite dubine Nakagami- m feedinga

Na slici 4 data je verovatnoća prekida u funkciji visine LED sijalice za različite uglove zračenja i različite vrednosti srednje snage SNR-a na RF deonici. Povećanjem srednjeg SNR-a Nakagami- m feeding kanala dolazi do poboljšanja performansi sistema, tj. do smanjenja verovatnoće prekida. Nakon neke izvesne visine instaliranja LED lampe na plafonu, dalje povećanje u visini nema uticaja na vrednost verovatnoće prekida tj. ta vrednost ostaje konstantna za bilo koju vrednost $\bar{\gamma}_{RF}$. Što je ugao zračenja LED lampe manji, to je jačina LOS komponente signala veća, a samim tim i verovatnoća prekida na tom linku i u celokupnom sistemu niža.

Na slici 5., analiziran je uticaj srednjeg SNR-a RF i VLC linka na verovatnoću prekida komunikacije u posmatranom sistemu. Može se uočiti da se povećanjem srednjeg SNR-a na VLC deonici i/ili povećanjem srednjeg SNR-a u Nakagami- m kanalu, vrednosti verovatnoće prekida znatno smanjuju.



Sl. 4. Verovatnoća prekida u zavisnosti od visine LED sijalice za različite uglove zračenja



Sl. 5. Verovatnoća prekida u zavisnosti od srednjeg SNR-a RF deonice za različite vrednosti srednjeg SNR-a VLC deonice

VI. ZAKLJUČAK

U ovom radu prikazana je analiza verovatnoće prekida u hibridnom komunikacionom sistemu u kojem se ista informacija nezavisno šalje RF linkom u prisustvu Nakagami- m fedinga i kooperativnim VLC/PLC linkom do prijemne antene sa SC kombajnerom.

Na osnovu dobijenih numeričkih rezultata može se zaključiti da najveći uticaj na smanjenje verovatnoće prekida ima povećanje srednjeg SNR-a na bilo kojoj od prenosnih deonica u sistemu. Značajan uticaj ima i dubina fedinga u radio kanalu (povećanje parametra m Nakagami- m fedinga). Smanjenje ugla zračenja ili visine LED lampe u odnosu na poziciju korisnika, smanjuje verovatnoću prekida, a povećanje visine posle neke izvesne vrednosti nema uticaj na dalju promenu verovatnoće prekida.

Dalji pravac istraživanja u ovoj oblasti bi bio na temu poboljšanja bezbednosti komunikacije na fizičkom nivou analiziranog telekomunikacionog sistema u slučaju jednog ili više prisluskivača.

ZAHVALNICA

Ovaj rad je podržan od strane Ministarstva prosvete, nauke i tehnološkog razvoja Republike Srbije.

LITERATURA

- [1] J. A. Stankovic, "Research directions for the Internet of Things," *IEEE Internet Things J.*, vol. 1, no. 1, pp. 3-9, Feb. 2014.
- [2] S. Mudrievskyi "Power line communications: state of the art in research, development and application," *AEU – Int J Electron Commun.* Vol. 68, no. 7, pp. 575-577, 2014.
- [3] S. Sheoran, P. Garg, and P. K. Sharma, "Interference mitigation technique with coverage improvement in indoor VLC system," *Trans. Emerg. Telecommun. Technol.*, vol. 30, no. 2, p. e3511, Feb. 2019.
- [4] Z. Ghassemlooy, L. N. Alves, S. Zvanovec, and M. Khalighi, *Visible Light Communications: Theory and Applications*, 1st ed. Boca Raton, FL, USA: CRC Press, 2017.
- [5] D. A. Basnayaka and H. Haas, "Design and analysis of a hybrid radio frequency and visible light communication system," *IEEE Trans. Commun.*, vol. 65, no. 10, pp. 4334–4347, Oct. 2017.
- [6] A. Gupta, N. Sharma, P. Garg, and M. S. Alouini, "Cascaded FSO-VLC communication system," *IEEE Wireless Commun. Lett.*, vol. 6, pp. 810–813, Dec. 2017.
- [7] X. Ma, J. Gao, F. Yang, W. Ding, H. Yang, and J. Song, "Integrated power line and visible light communication system compatible with multi-service transmission," *IET Commun.*, vol. 11, no. 1, pp. 104–111, Jan. 2017.
- [8] W. Gheth, K. M. Rabie, B. Adebisi, M. Ijaz, G. Harris, "Performance Analysis of Integrated Power-Line/Visible-Light Communication Systems with AF Relaying," 2018 IEEE Global Communications Conference (GLOBECOM), Abu Dhabi, United Arab Emirates, United Arab Emirates, 9-13 Dec. 2018.
- [9] W. Gheth, K. M. Rabie, B. Adebisi, M. Ijaz, G. Harris, "On the Performance of DF-based Power-Line/Visible-Light Communication Systems," 2018 International Conference on Signal Processing and Information Security (ICSPIS), DUBAI, United Arab Emirates, United Arab Emirates, 7-8 Nov. 2018.
- [10] M. Jani, P. Garg, A. Gupta, "Performance Analysis of a Co-Operative PLC/VLC System with Multiple Access Points for Indoor Broadcasting," *AEU International Journal of Electronics and Communications*, vol. 103, pp. 64-73, May 2019.
- [11] Y. H. Ma, P. L. So, E. Gunawan, "Performance analysis of OFDM systems for broadband power line communications under impulsive noise and multipath effects," *IEEE Trans. Power Del.*, vol. 20, no. 2, pp. 674–682, Apr. 2005.
- [12] I. M. Kostic, "Analytical approach to performance analysis for channel subject to shadowing and fading," *IEE P-Commun.*, vol. 152, no. 6, pp. 821-827, 9 Dec. 2005.
- [13] I. S. Gradshteyn, I. M. Ryzhik, *Table of Integrals, Series, and Products*. 6th ed., New York: Academic, 2000.
- [14] A. P. Prudnikov, Y. A. Bryčkov, O. I. Marichev, and G. G. Gould, *Integrals and Series. Volume 3, More Special Functions*, 1st ed. Amsterdam, The Netherlands: Gordon Breach Sci., 1986.
- [15] T. Komine and M. Nakagawa, "Fundamental analysis for visible-light communication system using LED lights," *IEEE Trans. on Consum. Electron.*, vol. 50, no. 1, pp. 100-107, Feb. 2004.

ABSTRACT

In this paper, a hybrid communication system with an end-user node for indoor broadcasting is considered. A cooperative power line communication (PLC) and visible light communication (VLC) links, connected by the decode-and-forward (DF) relay, are used for a signal transmission. As a back-up, an independent RF wireless channel is also used for transmission of the same signal. A user node's receiver utilizes selection combining (SC) method to choose a branch with higher signal quality. In this work, the outage probability is analysed and the impact of various PLC, VLC and RF link parameters on the system performance are assumed. In more details, the impact of LED lamp's position (the distance and the semi-angle), the average signal-to-noise-ratio (SNR) of the PLC, VLC or RF link, fading severity and the outage threshold impacts on the outage probability of the system under consideration is investigated.

Outage probability analysis of a hybrid RF – VLC/PLC communication system

Jelena Anastasov, Dejan Milić, Daniela Milović, Nenad Milošević